DYNAMICS AND CHARACTERIZATION OF MEMBRANE FOULING IN A LONG REVERSE OSMOSIS MEMBRANE CHANNEL

TAY KWEE GUAN

NATIONAL UNIVERSITY OF SINGAPORE

2006

DYNAMICS AND CHARACTERIZATION OF MEMBRANE FOULING IN A LONG REVERSE OSMOSIS MEMBRANE CHANNEL

TAY KWEE GUAN

(*B. Eng (Hons)***,** *NUS***)**

A THESIS SUBMITTED

FOR THE DEGREE OF DOCTOR OF PHILOSOPHY

DEPARTMENT OF CIVIL ENGINEERING

NATIONAL UNIVERSITY OF SINGAPORE

2006

ACKNOWLEDGEMENT

I would like to express my sincere gratitude to my supervisor Associate Professor Song Lianfa for his guidance on this research and invaluable advice on looking at life and work.

Special thanks to Professor Ong Say Leong for encouraging me to take the big step forward in taking up the doctoral degree, and to the members of my PhD committee, Associate Professor Hu Jiangyong and Associate Professor Liu Wen-Tso.

Sincere thanks to my colleagues and the staff of Environmental Engineering Laboratory, especially Mr Chandrasegaran, for their kind assistance and advice, and to my final project students, Meryl Lan, Lim Huiling, See Lilin, Tan Wee Tat and Louis Tanudjaja for their valuable contribution in this study.

Finally, I would like to dedicate this thesis to my wonderful parents, Mr Tay Swee Chuen and Madam Ng Chor. I would not have been able to continue this research without their understanding and strong encouragement. I also appreciate support from all my good friends.

To my dear friend in Heaven, Jimmy, this is also for you.

TABLE OF CONTENTS

SUMMARY

Reverse osmosis (RO) is becoming increasingly popular in water reclamation and wastewater treatment because of its high permeate quality and reducing costs. The single most critical problem that exists in all RO processes is membrane fouling, a process of foulant accumulation on the membrane surface that deteriorates membrane performance and shortens membrane lifespan. The impact of fouling is enormous as the costs related to fouling mitigation (feed water pretreatment and membrane cleaning) can be staggeringly over 20% of the total operating cost! This does not include the down-time economic loss due to cleaning and membrane replacement when membranes are irreversibly fouled. Hence efficient mitigation or minimization of membrane fouling is a key factor to increase the competitive edge of RO over conventional separation processes in water reclamation and wastewater treatment.

Fouling alleviation and control is seriously hindered by ineffective fouling characterization. Fouling characterization refers to the ascertainment of fouling behavior in the RO processes through quantification of feed water fouling strength and prediction of fouling development. It is well known that the most widely used SDI (Silt Density Index) is not a good indicator of the fouling strength of feed water to RO processes. The use of 0.45μm microfiltration membranes in the determination of SDI cannot capture the smaller foulants, which are arguably the more potent foulants to RO membranes. In addition, there is no established quantitative relationship between the SDI and the fouling behavior in RO processes. As a result, the SDI cannot be used to quantitatively predict and assess fouling development in full-scale RO processes, and

is certainly unable to indicate the effectiveness of feed water pretreatments. For decades, fouling in full-scale RO processes has been tracked or indicated with the average permeate flux, which is based on the fundamental membrane transfer theories. Unfortunately, the membrane transfer theories cannot reasonably explain the recent observations of flux decline in the RO processes of highly permeable membranes after an initial period of constant average permeate flux at steady operating conditions. It also cannot account for the shortened duration of the fully restored average permeate flux after each membrane cleaning. All this evidence demonstrates that membrane fouling in RO processes is a very complex phenomenon that cannot be fully delineated with simple membrane transfer theories. Hence the overall objective of this study is to develop an effective fouling characterization method that includes effective measurement of fouling in full-scale RO processes under any operating conditions and accurate quantification of feed water fouling strength for reliable prediction of membrane fouling.

The study began with a systematic investigation into the behavior of permeate flux in a long RO membrane channel. In this research, the long membrane channel refers to the membrane channel commonly used in full-scale RO processes, which is made up of several membrane elements connected in series. The length of the membrane channel can range from 5m to 7m in a single pressure vessel. It was shown that a long channel with highly permeable RO membranes should not and could not be treated as a homogeneous system because the key operating parameters (e.g. crossflow velocity, salt concentration, and permeate flux) varied substantially along the membrane channel. When the membrane channel was treated as a heterogeneous system, it was found that the linear relationship between the permeate flux and the driving pressure

was not valid over the entire pressure range. There was a characteristic pressure of a long membrane channel. While the permeate flux was controlled by the well known membrane transfer principle (linear relationship) for driving pressures lower than the characteristic pressure, it was restricted by the thermodynamic limit (thermodynamic equilibrium) of the system for driving pressures greater than the characteristic pressure. One important finding of a RO process under thermodynamic equilibrium restriction was that the average permeate flux was insensitive to the increase in membrane resistance.

A new fouling strength indicator, termed the fouling potential, was proposed for the fouling strength of feed water. The fouling potential could be easily determined with a crossflow RO membrane cell under conditions similar to the designed working conditions for the RO processes. Because of the use of an RO membrane in the measurement, all possible foulants to the RO membranes would be captured and would contribute to the fouling potential. Experiments showed that the newly defined fouling potential was linearly related to the foulant concentration and was independent from membrane resistance, driving pressure, or other operating parameters. More importantly, the fouling potential could be readily used to predict fouling development in RO processes.

Fouling development in a long membrane channel could be well predicted by incorporating the proposed fouling potential of feed water into the model for the performance of the system. The model was able to trace the increase in resistance along the membrane channel due to accumulation of foulants with time and predict the

corresponding average permeate flux of the channel. Simulations of fouling development in a long membrane channel revealed an interesting behavior of the average permeate flux. Under certain conditions (thermodynamic equilibrium restriction), the average permeate flux remained constant for an initial period of operation before the decline in flux could be observed. The behavior had been reported in the literature and was verified with fouling experiments on a 4 meter long membrane channel in this research study. This interesting behavior highlighted that the decline in the average permeate flux could not be used as an effective indicator of membrane fouling in a long membrane channel that could be potentially operated under thermodynamic equilibrium regime.

A more effective fouling characterization method was developed to overcome the inadequacy of using average permeate flux to track fouling in full-scale RO processes. The central idea of the new characterization method was based on the intrinsic feature of membrane fouling: the total membrane resistance would increase with membrane fouling. With the new fouling characterization method, fouling development in a long membrane channel could be accurately quantified even when no obvious flux decline was observed in the process. Furthermore, the characterization method could also be used for more accurate assessment of the effectiveness of membrane cleaning.

A related topic on channel blockage with the foulants captured by the spacers in the feed channel of spiral-wound membrane modules was also investigated. This type of fouling reduced the effective cross-sectional area of the feed channel and increased the differential pressure across the feed channel length. The information obtained from

this topic can add another dimension to our knowledge on membrane fouling in real membrane processes.

NOMENCLATURE

A	Cross-sectional area of feed channel, m^2
A_0	Cross-sectional area of a clean spiral-wound module, m^2
c	Salt concentration, mg/L
c_0	Feed salt concentration, mg/L
c_b	Salt concentration in bulk solution, mg/L
c_e	Concentrate concentration, mg/L
c_m	Salt concentration on membrane surface, mg/L
c_{f0}	Feed foulant concentration, mg/L
c_w	Salt concentration in permeate water, mg/L
C	Dimensionless salt concentration
C_e	Dimensionless concentrate concentration
D	Diffusion coefficient
D_h	Hydraulic diameter, m
f_{os}	Osmotic coefficient, Pa·L/mg
F	Filtration coefficient, Pa^{-1}
h	Feed channel height at location x and time t
H	Height of clean feed channel, m
I	Total foulant flux, mg/s
I_0	Total foulant flux entering the feed channel at $x = 0$, mg/s
I_f	Fouling index
$j_\perp$	Particle flux in the direction perpendicular to the membrane surface, m/s
J_s	Solute flux, m/s
J_w	Water flux, m/s

k	Capture coefficient, m^{-1}
k_0	Capture coefficient of clean channel, m^{-1}
k_f	Fouling potential, $Pa \cdot s/m^2$
k_m	Mass transfer coefficient
k_s	Membrane permeability for solute
k_w	Membrane permeability for water
L	Length of feed channel, m
M	Mass of foulant per unit area, g/m^2
Q_0	Feed flow rate, m^3/s
Q_e	Concentrate flow rate, m^3/s
R_f	Resistance of fouling layer, $Pa \cdot s/m$
R_m	Total membrane resistance, $Pa \cdot s/m$
R_{m0}	Clean membrane resistance, $Pa \cdot s/m$
r	Permeate recovery
r^2	Linear correlation coefficient
r_{rej}	Salt rejection
r_s	Specific resistance of the fouling layer, $Pa \cdot s/m^2$
t	Time
u	Crossflow velocity, m/s
u_0	Feed crossflow velocity, m/s
v	Permeate flux, m/s
v_0	Permeate flux of clean membrane, m/s
$\bar{v}$	Average permeate flux, m/s
w	Width of the feed channel, m
X	Dimensionless distance from channel entrance

y	Direction perpendicular to the bulk flow

Greek

Δc	Salt concentration difference across membrane, mg/L
Δp	Driving pressure, Pa
ΔP	Dimensionless driving pressure, Pa
Δp^*	Characteristic pressure, Pa
Δp_0	Initial driving pressure, Pa
Δp_d	Differential pressure, Pa
$\Delta \pi$	Osmotic pressure difference across membrane, Pa
ΔR_f	Resistance of the fouling layer, Pa·s/m
α	Correcting factor for the capture coefficient
ξ	Dummy variable
λ	Friction coefficient
η	Water viscosity
ρ	Density of fouling layer, kg/m^3
ρ_w	Density of the feed water, kg/m^3
$\prod_0$	Dimensionless osmotic pressure
π_0	Osmotic pressure, Pa

Subscript

t	Time

LIST OF TABLES

LIST OF FIGURES

Chapter 1

INTRODUCTION

1.1 Background

The historic development of high flux cellulose acetate reverse osmosis (RO) membrane by Loeb and Sourirajan in 1960s (Glater 1998) was an important milestone in the history of RO processes. It signified the beginning of RO as a commercially viable separation technology on industrial-scale or full-scale. The breakthrough in membrane technology generated much excitement and demand for a deeper understanding of the RO separation processes. Today RO is widely used for separation and concentration of solutes in many fields, such as chemical and biomedical industry, food and beverage processing, and water and wastewater treatment (Hajeeh and Chaudhuri 2000; Riley 1991; Wiesner and Chellam 1999; Vedavyasan 2000). The most common uses of RO membranes are in the seawater desalination and water reclamation industries. There are estimated 12,500 desalination plants around the world, supplying 20 million cubic metres per day or 1% of world's production of drinking water. The market in this field is expected to reach US$70 billion in the next 10 years (Martin-Lagardette 2000; Matsuura 2001).

The increasing acceptance of RO technology in seawater desalination and water reclamation is no coincidence. Although water covers some 70% of the planet's surface, according to recent WMO / UNESCO estimates, less than 0.3% of the global water resources consists of accessible freshwater. Much of the world's water resources (98%) are in the form of seawater, with the remainder locked in the polar caps and

glaciers (Samson and Charrier 1997). The persistent problem of water shortages is made worse with diminishing fresh water supply, water pollution and increasing water demand from industrialization and growing population. Together with more stringent water quality requirements by the regulating bodies, these two major driving factors (Mallevialle *et al*. 1996; AWWA 1999; Bremere *et al*. 2001) make RO an attractive process in water treatment and reclamation. In addition, RO has many advantages over conventional separation processes such as distillation and other physical operations. For example, RO is more economically attractive than distillation in water desalination since it involves no phase transition during the separation process (Mulder 1996). In a study by the California Coastal Commission (Pantell 1993), the energy consumption in terms of electricity used by RO was only about one-third that of distillation. RO does not require clarification tanks and disinfection units, hence it usually requires less space and is easy to operate (Mulder 1996; Elarde and Bergman 2001). Compared to conventional separation processes, RO produces less sludge as it seldom involves the use of chemicals such as coagulants or polymers (Winters 1987; Bryne 1995).

RO technology is playing a key role in water reclamation and seawater desalination to secure water supply in Singapore. In Singapore, water is a scarce and valuable resource that is limited by resource, space and political constraints. Singapore consumes around 1.14 billion litres (300 million gallons) of water daily and this amount is expected to grow by one-third in 10 years (News in *Membrane Technology* 2004(3), page 2). To cope with the rising water demand due to rapid economic expansion and high population growth, water reclamation and seawater desalination have become the inevitable means to complement the current fresh water sources. Several NEWater Factories (NEWater is the name given to the reinvented potable

water) have been built in Singapore to reclaim clean water from treated municipal wastewater using RO technology (Qin *et al.* 2004). Current NEWater production is about 10,000 m^3/d and is expected to make up 15 % of the country's water supply by 2010. Singapore also looks into the sea for additional water supply. Seawater, which accounts for 98% of global water resources, is probably the only water source that can satisfy our ever-increasing demand of water supply. The country's water supply is further increased with the completion of a 136,000 m^3/day seawater RO desalination plant (Industrial News in *Filtration & Separation* 2003, page 8) in the western part of the island.

Despite the attractive attributes of RO, the separation process is plagued by the single most critical problem – membrane fouling (Mulder 1996; Saad 1999; Bryne 1995; Song and Elimelech 1995). Fouling is the accumulation of contaminants or foulants on the membrane surface, which leads to the reduction of water production, deterioration of product water quality and shortened membrane lifespan (Nicolaisen 2002). In extreme cases, uncontrollable fouling can cause complete failure of the whole RO plant (Kaakinen and Moody 1985). Aptly described by Mulhern (Mulhern 1995) as the "cancer" in RO processes, membrane fouling is not preventable as it readily occurs in all RO processes. However, the rate of fouling can be greatly reduced if effective pre-treatment is installed upstream of the RO membrane system. Performance of severely fouled membranes can be restored to great extent, although not completely, if they undergo effective membrane cleanings. However, the costs associated with fouling control and membrane cleaning represent a significant proportion of the total operating cost. Studies have shown that pretreatment of feed water and membrane cleaning can

constitute as high as 20% each of the total operating costs (Durham *et al.* 2002; Van der Bruggen and Vandecasteele 2002; Dudley *et al.* 2000).

The success of full-scale RO processes is very much dependent on the effectiveness of fouling control and membrane cleaning. To reduce the overall operating cost, there is a trend towards operating RO processes at a high recovery (Wilf and Klinko 2001; Rautenbach *et al.* 2000; Kurihara *et al.* 2001). This modern approach to RO operation, which was regarded as not economically viable in early RO processes because of high energy demand, is now technically feasible in purifying low salinity feed water with the recent technological advances in producing more permeable RO membranes. The use of highly permeable RO membranes, however, can lead to a phenomenon known as hydraulic imbalance. In a long pressure vessel containing several highly permeable RO membrane modules connected in series, the permeate would be mainly produced in the first few membrane modules, while the contribution from the last few membrane modules is very limited (Wilf 1997; Nemeth 1998).

The success of fouling control and alleviation relies heavily on the effectiveness of fouling characterization, which involves quantification of feed water fouling strength and prediction of fouling development in a long membrane channel. In this research work, a long membrane channel is defined as the membrane channel that is made up of several membrane elements connected in series in a single pressure vessel and can range from 5m to 7m (Bryne 1995; Wilf 1997). This arrangement of membrane elements is commonly found in full-scale RO processes. The fouling strength of feed water can be used to evaluate pretreatment efficiency and to predict fouling behavior in the full-scale RO processes. The fouling strength of feed water is commonly

represented with Silt Density Index (SDI) and Modified Fouling Index (MFI) (Bryne 1995; Brauns *et al.* 2002; Mulder 1996). These tests involve filtering the feed water through a 0.45μm microfiltration membrane at constant pressure in a dead-end filtration device. In many full-scale RO plants, feed water is required to satisfy a limiting SDI or MFI before entering the RO membrane system. Fouling in full-scale RO processes is customarily measured by the decline in the average permeate flux (Saad 1999; Rico and Arias 2001). This practice is based on the assumption that the permeate flux is inversely proportional to the membrane resistance (Lonsdale *et al.* 1965; Mason and Lonsdale 1990; Soltanieh and Gill 1981). The use of permeate flux as an indicator of fouling has been demonstrated or verified by numerous laboratory tests and some full-scale installations (Desai 1977; Larson *et al*. 1983; Van Gauwbergen and Baeyens 1998; Koyuncu *et al.* 2001) and has been the cornerstone of most, if not all, design practices of full-scale RO water and wastewater treatments since 1960s.

Pilot tests are usually conducted for observation of fouling development in the full-scale RO processes to generate the needed design parameters in fouling mitigation and control. The duration of pilot test may last months or over a year to obtain the meaningful information. Because pilot tests are usually costly and time-consuming, only limited operating scenarios can be tested and evaluated. Hence the information obtained for fouling characterization is quite limited and incomplete.

1.2 Problem Statement

Fouling control is crucial to the success of RO membrane processes in water and wastewater treatment. The two necessary prerequisites for successful fouling control

are: (1) accurate determination of the fouling strength of feed water and (2) the ability to use the feed water fouling strength to predict fouling development in the full-scale RO processes.

The commonly used fouling indices (e.g. SDI) are well known to have limitations with respect to their usefulness for indicating the fouling strength of feed water to RO membranes. The most notable limitation is their inability to measure all possible foulants to RO membranes. Therefore these fouling indices cannot be directly used to predict fouling behavior in full-scale RO processes. Another problem is the lack of theories or models for fouling development in full-scale RO processes. When highly permeable RO membranes are used, the average permeate flux is often insensitive to membrane fouling in an initial period of operation. This behavior cannot be reasonably explained within the framework of the conventional membrane filtration theories. To compensate for the inadequacy of the current fouling characterization practices, full-scale pilot tests are necessary for a better understanding of fouling characteristics under the designed operating conditions. However these costly pilot tests are time-consuming and can only be conducted for a limited number of operating scenarios.

Therefore, there is an urgent need for a more effective fouling characterization method. It is desirable to have an inclusive fouling index that can capture all possible foulants in feed water to RO membranes. The fouling index or parameter should be determined conveniently in a small laboratory membrane setup and should provide an accurate estimate of the fouling strength of feed water. Fouling development in full-scale RO processes with highly permeable membranes needs to be systematically characterized. A link between membrane fouling in a full-scale RO plant and the fouling strength of

feed water determined from laboratory tests is highly demanded. Pilot tests will be significantly reduced or eliminated with the implementation of the new fouling characterization method.

1.3 Research Objectives

The overall objective of this thesis is to develop a comprehensive fouling characterization method that can effectively reflect and accurately quantify membrane fouling in full-scale RO processes. To achieve the overall objective, this study undertakes the following tasks:

a. To study the behavior of average permeate flux in a long RO membrane channel;
b. To investigate fouling characteristics in a long RO membrane channel;
c. To propose a more accurate quantification method for feed water fouling potential and;
d. To develop an operational characterization technique to effectively reflect membrane fouling in full-scale RO processes.

The ultimate goal of this study was to provide a fast and reliable fouling characterization for full-scale RO processes to replace or reduce the dependence on pilot tests. As is shown in Fig. 1.1, the fouling strength of feed water and the operating conditions of the membrane system are the two key factors for fouling development in the full-scale RO processes. Currently, the combined effect of the two factors is accurately determined in full-scale pilot tests. Unfortunately, these expensive tests usually take at least a few months and can only cover limited operating scenarios.

With the development of a more effective fouling characterization method, it will be possible to obtain a reliable fouling characterization of full-scale RO processes in a few hours or days, depending on the time required to determine the feed water fouling strength with the laboratory membrane device.

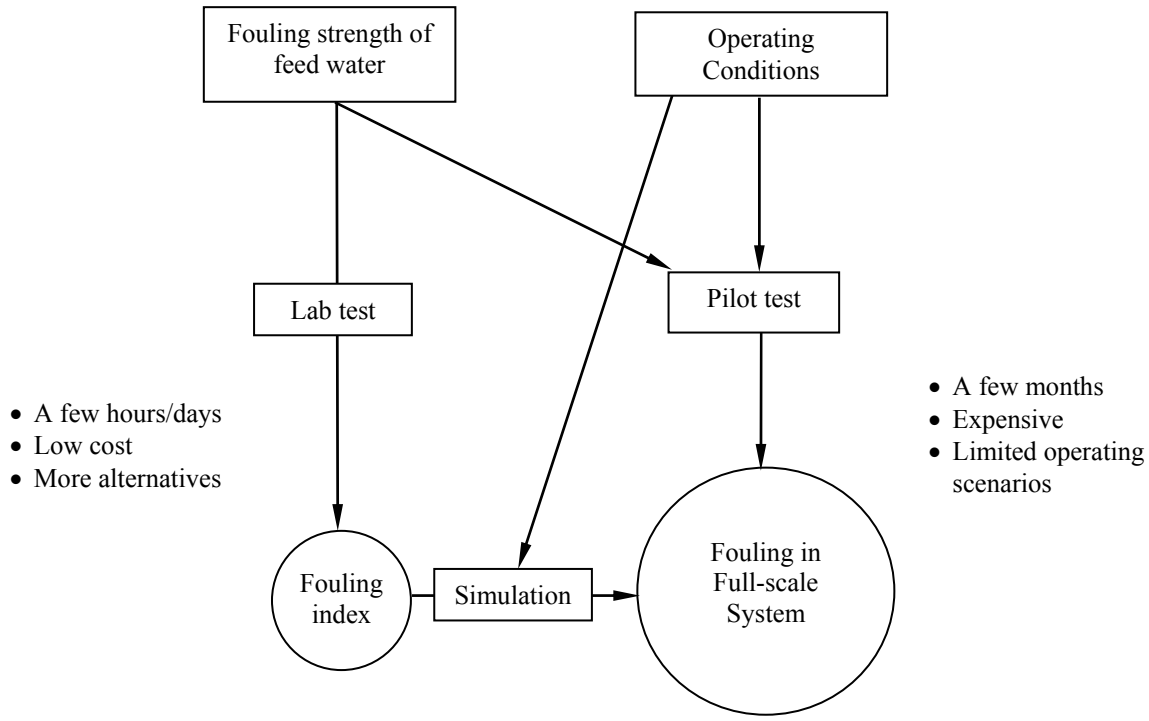

Figure 1.1. Comparison of the new characterization method and pilot test

1.4 Organization of Thesis

This thesis is divided into the following chapters, each defining a specific area of study that leads to the achievement of the overall objective.

Chapter 2 – Literature Review

This chapter provides a comprehensive review on membrane processes, transport models and membrane fouling. Discussions focus mainly on full-scale RO processes with long membrane channels.

Chapter 3 – The Behavior of Permeate Flux in a Long RO Membrane Channel

The behavior of permeate flux in a long RO membrane channel is described in this chapter. The non-linear dependence of average permeate flux on driving pressure in a long membrane channel was simulated and verified experimentally with a 4m long membrane channel in the laboratory. Flux-controlling mechanisms were delineated and discussed.

Chapter 4 – Feed Water Fouling Strength Quantification

A new fouling potential indicator was proposed to quantify the fouling strength of feed water. The proposed fouling potential indicator could measure all possible foulants in feed water to RO membranes. The linear relationship between fouling indicator and foulant concentration, and the independence of fouling indicator from other operating parameters were verified experimentally with a laboratory-scale crossflow RO membrane cell.

Chapter 5 – Fouling Development and Quantification in a Long Membrane Channel

This chapter describes fouling development in a long RO membrane channel. The inadequacy of the average permeate flux to reflect membrane fouling in full-scale RO processes is discussed and verified experimentally with a 4m long membrane channel in the laboratory. More accurate fouling indices directly related to the total membrane resistance are presented.

Chapter 6 – Development of Differential Pressure in a Spiral-Wound Membrane Channel

The increase in differential pressure across the length of membrane channel due to foulant capture by feed spacers is described in this chapter. The

differential pressure was found to be affected by channel height and the capture rate of foulants.

Chapter 2

LITERATURE REVIEW

2.1 Membranes and Membrane Processes

2.1.1 Chronology of Membrane Development

Membranes were already used as the media for filtration in the 19th and early 20th centuries. Back then, membranes had no industrial or commercial uses, but were used as a laboratory tool to develop physical and chemical theories (Baker 2000). No significant membrane industry existed because membrane filtration was seen as too unreliable, slow, unselective and expensive. A breakthrough came in early 1960s when Loeb-Sourirajan developed defect free, high flux, anisotropic cellulose acetate (CA) RO membranes which were able to produce fluxes 10 times higher than any membrane available at that time. With the achievement of such high flux, the potential for desalting seawater at the industrial level was seen possible. The period from the 1960s to 1980s saw significant changes in membrane technology. Membrane production processes such as interfacial polymerization and multi-layer composite casting and coating were developed to produce high performance composite membranes, which were thinner, had higher salt rejection and water production rates. Today, advances in membrane technologies have rapidly enlarged our capabilities to restructure production processes and to protect the environment and public health. Membrane technologies play increasingly important roles as unit operations for resource recovery, pollution prevention, and energy production, as well as environmental monitoring and quality control. They are also key component technologies of fuel cells and bioseparation applications. The membrane technologies markets have grown rapidly in

the last two decades. The worldwide sales of membrane technologies rose from US$363 million in 1987 to more than US$1 billion ten years later. Approximately 40% of membrane sales is destined for water and wastewater treatment applications; food and beverage processing combined with pharmaceuticals and medical applications account for another 40% of sales; and the use of membranes in chemical and industrial gas production is growing. This broad range of applications and projected sales is targeted to reach US$1.5 billion by 2002 (Wiesner and Chellam 1999).

2.1.2 Membrane Definition and Process Classification

In the book *Diffusion and Membrane Technology*, Tuwiner (Tuwiner 1962) defined membrane as "a barrier, usually thin, which separates two fluids. May be intended as a seal or formulated to be semi-permeable, i.e. permit transfer of some component and not of others or, at least to possess transfer properties which are selective". Although there is no exact definition of a membrane, the above description adequately defines the physical structure and macroscopic function of a membrane, which is commonly recognized as a selective semi-permeable barrier between two phases (Soltanieh and Gill 1981; Mulder 1996; Aptel and Buckley 1996). Membranes can be classified according to different mechanisms of separation, physical morphology and materials (Aptel and Buckley 1996). In water and wastewater treatment, organic polymeric membranes are the most common types of membranes used. Among the organic polymeric materials, the two most important materials are cellulose acetate (CA) and polyamide (PA) (AWWA 1999; Baker 2000). CA membranes are low in cost and are hydrophilic. They have good resistance against chlorine and have very smooth surfaces. However they can only operate within a small pH range ($4 \leq pH \leq 7$) as they

hydrolyze easily. They have low upper operational temperature limits and do not have good rejection properties with organics. PA membranes, on the other hand, have higher water flux and a higher range of operating temperatures. They reject organics well and resist membrane compaction. However they are hydrophobic and sensitive to the presence of chlorine. The wide diversification of membrane types is not required in this research study and will not be further discussed.

Table 2.1. Some membrane processes and their driving forces

Membrane Process	Driving Force
Microfiltration	Pressure
Nanofiltration	Pressure
Reverse osmosis	Pressure
Gas separation	Pressure
Pervaporation	Pressure
Osmosis	Concentration
Electrodialysis	Concentration
Membrane distillation	Temperature/pressure

Membrane processes may achieve separation under different driving forces; some examples are presented in Table 2.1. In pressure-driven membrane processes, pressure is applied to drive the solvent through the membrane, while other molecules and particles are retained in various extents depending on the pore size distribution of the membrane. Examples of pressure-driven membrane processes are microfiltration, ultrafiltration, nanofiltration and reverse osmosis. These membrane processes are differentiated according to the pore size, which is related to the size of retained particles. However, the issue of presence of pores in RO membranes remains debatable, as the mechanism for separation in RO is entirely different from other pressure-driven

membrane processes. The membrane structure, pore size and separating mechanism of the pressure-driven membrane processes are shown in Table 2.2.

Table 2.2. Classification of pressure-driven membrane processes

Membrane Process	Membrane Structure	Pore Size	Separating Mechanism
Microfiltration	Macropores	0.05 – 1.0 μm	Sieving
Ultrafiltration	Mesopores	0.002 – 0.1 μm	Sieving
Nanofiltration	Micropores	0.001 – 0.01 μm	Sieving + solution-diffusion
Reverse osmosis	Dense	0.1 – 1.5 nm	Solution-diffusion

Sieving Mechanism. Sieving mechanism works on the difference of molecular size between the solute and solvent. It assumes the pore size of the membrane to be between the molecular size of the larger solute and smaller solvent so that solute can be retained at the membrane-solution interface, while solvent passes through the membrane.

Solution-diffusion Mechanism. RO membrane is generally considered as a dense layer without the pores commonly found in MF and UF. The solution-diffusion mechanism is the centerpiece of one of the popular theories used to describe the separation associated with RO membranes. It assumes that both the solvent and solute dissolve on the homogenous non-porous membrane surface, before being transported across the membrane by diffusion in an uncoupled manner. Separation takes place

when the membrane has a higher solubility and diffusivity for the solvent as compared to the solute.

2.1.3 Basic Membrane Transport Theory for RO Processes

Reverse Osmosis (RO), also known as hyperfiltration, is an innovative separation technology that has the capability to separate the smallest particles such as ions from the water. Because of the dense structure of the RO membranes, a much higher pressure has to be applied in order to overcome the osmotic pressure and high membrane resistance to produce substantial amount of water.

There are two general independent approaches in deriving membrane transport models for RO processes (Soltanieh and Gill 1981). The first one is based on non-equilibrium or irreversible thermodynamics, where the membrane is treated as a black box in which relatively slow processes are taking place near equilibrium. Information on the mechanism of transport is not needed in this method, which is useful when flow coupling exists between various species that are transported through the membrane. The second approach assumes that some mechanisms of transport and fluxes are related to the forces present in the system. In this method, the physicochemical properties of the membrane and solution, such as membrane porosity, solubility of solute and solvent, and solute and solvent diffusivity, are considered in the derivation of the membrane transport model. The theoretical models currently in use for describing RO transport are given below:

a. From irreversible thermodynamics (IT):
    i. Kedem-Katchalsky model
    ii. Spiegler-Kedem model

b. Frictional models

c. Solution-diffusion model

d. Solution-diffusion-imperfection model

e. Diffusion-viscous flow model (highly-porous model)

f. Finely-porous model

g. Preferential adsorption-capillary flow model

The transport models above will not be elaborated in this study as they are covered in detail in the literature (Soltanieh and Gill 1981; Mason and Lonsdale 1990; Mulder 1996). Although there are several differences between these transport models, such as different predictions concerning transport coefficients, selectivity at the membrane surfaces and interaction of solute and solvent within the membranes, they are equivalent in the sense that they end up with the same transport equations. It is commonly accepted that the driving forces for water and solute transports are different. Water is primarily driven through the RO membrane by a hydraulic pressure difference, while solute transport across the membrane is driven primarily by the concentration difference. The water flux and solute flux passing through the RO membrane are given respectively by

$$J_w = k_w(\Delta p - \Delta \pi) \tag{2.1}$$

$$J_s = k_s \Delta c \tag{2.2}$$

where J_w is the water flux, k_w is the membrane permeability coefficient for water, Δp is the driving pressure, $\Delta \pi$ is the osmotic pressure difference across the membrane, J_s is the solute flux, k_s is the membrane permeability coefficient for salt and Δc is the salt concentration difference across the membrane. Osmotic pressure can be calculated

with the Van't Hoff equation if the solution contains only single solute. When the solution contains multiple salts, osmotic pressure is generally estimated with the following expression (Bryne 1995).

$$\Delta\pi = 68.95\Delta c \tag{2.3}$$

Eq. (2.1) has been demonstrated or verified by numerous laboratory tests and some full-scale installations (Koyuncu *et al.* 2001; Lonsdale *et al.* 1965; Van Gauwbergen and Baeyens 1998; Pietsch *et al*. 1998). Although the expression was first developed in 1960s, it remains the cornerstone of all design practices of full-scale RO processes for water and wastewater treatments.

2.1.4 Concentration Polarization

Concentration polarization (CP) is a phenomenon in which the solute or particle concentration in the vicinity of the membrane surface is higher than that in the bulk solution (Song and Elimelech 1995). The occurrence of CP is due to the different permeabilities of the membrane for various components of the solution suspension and limited mixing near the membrane surface. CP increases the membrane resistance and consequently reduces the permeate flux across the membrane. The high surface concentration also induces solute transport through the membrane, which is dependent on the concentration difference across the membrane, and affects the quality of the permeate water. For the past two decades, numerous theories have been developed to understand CP and to predict the permeate rate in crossflow filtration. A representative model is the gel-layer model, which was used directly to interpret experimental data in ultrafiltration. Another popular theory to describe CP is the osmotic-pressure model.

However this model has been shown to be fundamentally equivalent to gel-layer model (Wijmans *et al*. 1985).

The gel-layer theory evaluates permeate flux by assuming fixed surface particle concentration and uses a mass transfer coefficient from theories of convective heat transfer to impermeable surfaces. If the solute is completely retained by the membrane, the permeate flux increases with pressure until the gel concentration is reached. Further increase in pressure results in the compaction of the gel layer just above the membrane surface and increase in resistance across the gel layer such that the permeate flux remains a constant-limiting flux. The limiting flux in this model is described as

$$v = k_m \ln\left(\frac{c_m}{c_b}\right) \tag{2.4}$$

where c_m is the concentration on membrane surface or gel concentration, c_b is the bulk solution concentration and k_m is the mass transfer coefficient. Eq. (2.4) is the basic equation for CP and c_m/c_b is known as the concentration polarization modulus (Mulder 1996). However, the gel-polarization model at most can only be treated as a semi-empirical model because the adoption of the mass transfer coefficient k_m from heat transfer to membrane separation has not been theoretically proven.

The osmotic-pressure model regards the limiting flux as the result of the increased osmotic counter-pressure produced by the high concentration of the rejected solute near the membrane surface. One of the osmotic pressure models is the Spiegler-Kedem solution-diffusion model (Sablani *et al*. 2001). The model has the similar conceptual problems as the gel-layer model. Wall particle concentration must be estimated from

certain empirical relationships or simplified assumptions. This is why empirical expressions are often used to predict permeate flux in RO system. Furthermore, this model is not applicable to microfiltration and ultrafiltration as osmotic pressure in these cases is negligible.

A new theory for CP was developed by Song and Elimelech (Song and Elimelech 1995) based on the hydrodynamics and thermodynamics of particles in suspension. In this theory, the extent of CP and the behavior of permeate flux are characterized by a dimensionless filtration number. When the filtration number is smaller than the critical value, a polarization layer exists directly over the membrane surface and the wall concentration is determined by pressure and temperature. At higher filtration number, a cake layer of retained particles forms between the membrane surface and CP layer. The thickness of the cake, rather than the concentration in the cake layer, will change with the applied pressure.

From Eq. (2.4), we can see that higher permeate flux can be achieved by increasing the mass transfer coefficient. Hence in spiral-wound membrane modules, feed spacers are provided to promote mixing and consequently to increase the mass transfer coefficient. However, the effect of CP on RO performance and the effectiveness of feed spacers to reduce CP in RO processes remain in dispute. Recently, Zhou and her coworkers (Zhou *et al.* 2005) demonstrated that the vertical concentration polarization effect on the filtration performance was less critical than that of the salt accumulation along the membrane channel (longitudinal concentration polarization). In their study, a macroscopic method to investigate CP in a spiral-wound membrane channel with spacers was developed for describing the performance of a long membrane channel.

The extent of CP is represented by a polarization factor and the effectiveness of feed spacers is quantified with a hydraulic dispersion coefficient. It is demonstrated through numerical simulations that the effect of CP on spiral-wound membrane modules is negligible if the feed concentration is very low, or when the hydraulic dispersion coefficient is greater than eight times of the salt diffusion coefficient. The depolarization effect of the spacers in the membrane channel is also strongly supported by the good fit between the experimental measurements and numerical simulations with the model developed in their study.

2.1.5 Full-Scale RO Processes

The most common configuration of RO membranes in full-scale water production facilities is the spiral-wound membrane module (Bryne 1995; Sablanl *et al*. 2002; Schwinge *et al.* 2004). Spiral-wound modules are widely used because they can provide more membrane surface area with compact packing. It is also less prone to membrane fouling and offer better cleaning efficiency. A spiral-wound module, shown in Fig. 2.1, is constructed by rolling several sheets of RO membranes, with plastic screens commonly known as feed spacers in between the membrane sheets, around a central permeate tube. The feed spacers provide mechanical support to the entire module structure and the voids created by the feed spacers between the membrane sheets define the feed channel. In addition, the feed spacers are designed as turbulence promoters to enhance mass transfer near the membrane surface and reduce the potential of membrane fouling. Feed water is supplied into the feed channel from one side of the module. Water passes through the membrane under pressure and is collected in the central permeate tube. The concentrate flows out from the other side of the module.

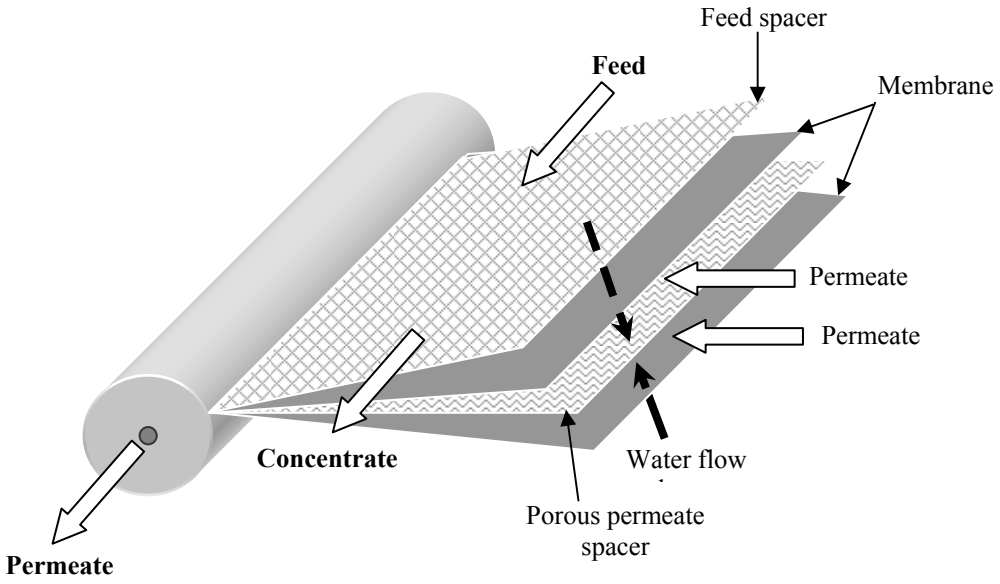

Figure 2.1. Cutaway view of a spiral-wound membrane module

In full-scale RO processes, several spiral-wound membrane modules (usually 5-7 modules) are laid in series in a pressure vessel to form a long membrane channel, as shown in Fig. 2.2. A number of these pressure vessels are connected or arranged in parallel or in series to form single-stage or multi-stage process. In multi-stage RO design, concentrate from one stage of RO membranes is fed into the succeeding stage to achieve a higher recovery. Depending on the recovery, the number of pressure vessels in the succeeding stage is selected so that the feed crossflow velocity is kept constant. An example of a two-stage RO full-scale system is schematically shown in Fig. 2.3. There are two basic methods that can be used in the RO process, namely, single-pass system and recirculation system. The choice of which system to adopt and arrangement of the pressure vessels is based on the extent of separation required and the production costs.

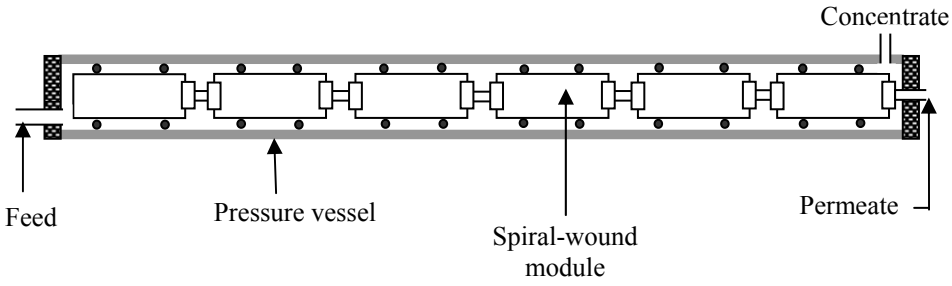

Figure 2.2. Cross section of a pressure vessel with 6 spiral-wound membrane modules connected in series

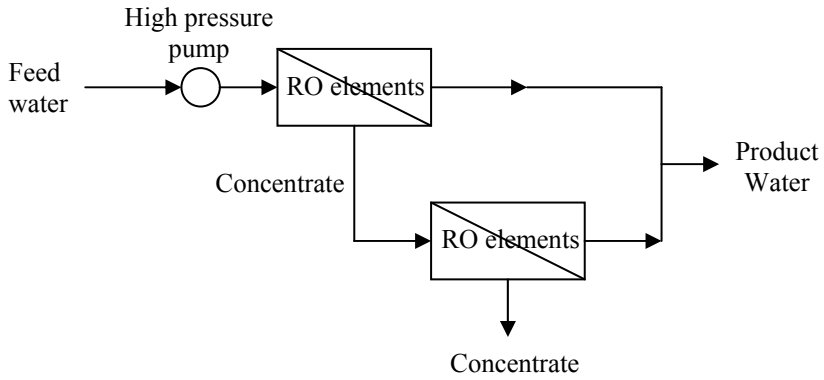

Figure 2.3. A schematic two-stage RO membrane system

A full-scale RO plant is an expensive investment, with high start-up and maintenance cost. Hence it is vital to identify, design and control the key operating parameters that affect the plant's profitability. Permeate recovery is an important parameter that has a significant effect on the investment and operating cost (Wilf and Klinko 2001). Higher recovery is directly translated into an increase in profit and a lower cost associated with a smaller downstream treatment train. Higher recovery is usually achieved by increasing the membrane surface area, which includes connecting several membrane modules in series and employing multi-stage configurations. The ease of operating at high recovery has been aided by the advent of highly permeable RO membranes, such

as the ultra-low pressure RO membranes that are capable of producing high recovery at relatively lower pressures. It has been documented that recovery could be driven to as high as 85% for brackish water (Almulla *et al.* 2002) and 60% for seawater (Kurihara *et al.* 2001; Wilf and Klinko 2001). However, the use of higher recovery is often limited by scaling, osmotic pressure (energy demand) and increase in permeate salinity (Rautenbach *et al.* 2000; Wilf and Klinko 2001). Therefore high recovery is most suitable for feed water with low salinity such as wastewater and brackish water.

The push to higher recovery, especially with the highly permeable RO membranes, can lead to the problem of hydraulic imbalance (Wilf 1997; Nemeth 1998), where high permeate flux is produced in the first few membrane modules, while little or no flux is produced in the last few modules in a pressure vessel. The problem arises when high specific flux from the first few membrane modules increases the salt concentration dramatically downstream along the membrane channel. The increase in the osmotic pressure, together with the frictional pressure loss, reduces the net driving pressure in the last few membrane modules. Hydraulic imbalance also increases permeate salinity and the possibility of membrane fouling. In order to resolve this problem, Wilf (Wilf 1997) suggested the use of membrane modules of lower permeability in the lead positions followed by the highly permeable membrane modules. Although such an arrangement provides a more uniform flux distribution along the membrane channel and reduces the permeate salinity, it signals that the highly permeable RO membranes cannot be fully utilized with conventional process design protocols.

Extensive efforts have been made in the past two decades to develop fundamental theories that relate performance of RO processes to membrane properties and

operating conditions (Soltanieh and Gill 1981; Mason and Lonsdale 1990). It is generally accepted that at any point on a RO membrane, permeate flux is proportional to driving pressure and salt transfer is proportional to concentration difference across the membrane (Slater and Brooks 1992). In the early days of full-scale RO processes, high driving pressures had to be used to overcome the high resistance of the RO membranes in order to obtain the desired permeate flux or recovery (Strathmann 1981; Marinas and Selleck 1992). Although the osmotic pressure of the liquid increased along the membrane channel, the changes in the net driving pressure were negligible because the driving pressure was predominantly high. The whole RO process could be reasonably approximated with a completely mixed reactor or homogeneous system, and changes in operating parameters such as salt concentration and driving pressure could be neglected (Mulder 1996; Maskan *et al.* 2000; Taniguchi and Kimura 2000).

However, in full-scale RO processes with highly permeable RO membranes, key operating parameters, such as permeate flux, salt concentration, crossflow velocity and driving pressure, can vary substantially along the long membrane channel like a plug-flow reactor. The performance of such RO processes is affected not only by membrane properties, but also by these locally changing operating parameters along the membrane channel. Treating such RO membrane processes as a homogeneous system in the calculations of permeate flux or recovery leads to inaccurate or erroneous results. In the last few years, Song and his research group have systematically investigated the performance of long filtration channels with highly permeable RO membranes (Song *et al*. 2002; Song *et al*. 2003; Zhou *et al*. 2006). They found that long crossflow RO membrane channels functioned more like plug-flow reactors than completely mixed reactors. The system could be only accurately described by taking into account the

localized permeate flux, crossflow velocity, salt concentration, and frictional pressure loss in the membrane channel. The performance of a full-scale RO membrane water treatment plant in Florida, USA was adequately simulated with a mathematical model based on the localized variables or parameters (Song *et al*. 2002). Recently, they further demonstrated that the vertical concentration polarization effect on the filtration performance was less critical than that of the salt accumulation along the membrane channel (longitudinal concentration polarization) (Zhou *et al*. 2006).

2.2 Membrane Fouling

2.2.1 Definition of Membrane Fouling

Despite numerous advantages over other conventional separation processes, widespread acceptance of RO is often limited by a critical problem manifested in the form of membrane fouling. Owing to its ability to reject most of the particles, colloids, solutes and ions, the RO process is susceptible to membrane fouling. Generally, membrane fouling refers to the attachment, accumulation, or adsorption of foulants onto membrane surfaces and/or within the membrane, resulting in a decline in product water flux and quality over time (Zhu and Elimelech 1995). In RO processes, pore plugging is seldom the main contributor to fouling because of the "non-porous" nature of RO membranes. The main fouling mechanism in RO processes is often associated with the formation of fouling layer above the membrane surface (Zhu and Elimelech 1997). Therefore, in this study, membrane fouling in RO processes is defined precisely as the increase in resistance across the membrane caused by the formation of a fouling layer on the membrane surface.

The rate of membrane fouling is affected by many factors. The most important factor is the feed water characteristics (Winfield 1979; Wilf and Klinko 1998), such as foulant types and concentration, ionic strength and pH. A higher foulant concentration naturally poses a greater fouling problem with the availability of larger pool of foulants for deposition. The foulant type and composition influence the porosity of the fouling layer which, in turn, determines the hydraulic resistance of the fouling layer. For example, a fouling layer consisting of organic matter and colloidal particles can have higher resistance than that made up of same colloidal particles only. The organic matter can fill up the voids between the colloidal particles, reducing the pathways the feed water can take to reach the membrane surface. Ionic strength and the pH of feed water affect the membrane-foulant and foulant-foulant interactions by altering the surface properties of membrane and foulants (Fane *et al*. 1983; Brinck *et al*. 2000). Generally, a high ionic strength and low pH enhance the accumulation of foulants on membrane surface.

The physical and physicochemical properties of the membrane channel can also affect the rate of membrane fouling. Feed water is usually passed through a narrow membrane channel, so that the crossflow velocity generates sufficient wall shear to remove the foulants from the membrane surface. Some membrane channels are constructed in a way such that the feed water is forced to travel through a series of bends within the channel to enhance the shearing effect and promote mixing (Mulder 1996). The development of unstable feed water flow can be achieved with the use of feed spacers commonly found in spiral-wound membrane modules. However, it is important to note that the use of narrow channels and the generation of turbulence can significantly reduce the downstream driving pressure. In addition, the presence of feed

spacers may trap or capture the suspended foulants, leading to a "clogging" problem. Hydrophobicity of RO membranes is also known to affect membrane fouling in RO processes (Bates 1998). It is believed that hydrophobic membranes attract organic foulants more easily than hydrophilic ones. This is why some hydrophobic RO membranes are pretreated to give them a hydrophilic surface.

Another important factor that affects membrane fouling is the driving pressure (Rabie *et al*. 2001; Davey *et al*. 2004). Foulants are brought to the membrane surface by the fluid flow as water permeates through the membrane. As permeate is primarily driven by the driving pressure, an increase in driving pressure increases the accumulation of foulant on membrane surface. Driving pressure also affects the porosity of the fouling layer. A more compact fouling layer reduces the rate at which water reaches the membrane surface, and increases the rate of fouling.

2.2.2 Types of Fouling in RO Processes

Membrane fouling is a complicated process and fouling behavior varies according to the types of feed water and operating conditions. In RO processes, the common types of fouling are colloidal (Yiantsios and Karabelas 1998), organic (Winters 1997; Gwon *et al.* 2003), biological (Flemming *et al*. 1997; Vrouwenvelder and Kooij 2001) and scaling (Potts *et al.* 1981). More often, fouling involves a combination of different mechanisms depending on the constituents in the feed water.

Colloidal particles are major foulants in all kinds of membrane processes. The size of these small suspended particles ranges from a few nanometers to a few micrometers. They are ubiquitous in natural waters, and examples of them include clays minerals,

colloidal silica and silicon (Zhu and Elimelech 1997). Under the drag force of permeate flux, these colloidal particles accumulate on the RO membrane surface to form a cake layer. The increase in thickness of this cake layer increases the membrane resistance, becoming what is known as colloidal fouling.

Organic fouling is one of the most prevalent problems in water treatment and reclamation plants (Hong and Elimelech 1997; Suratt *et al.* 2000). An example of organic materials is the natural organic matter (NOM), which is a complex heterogeneous mixture of different organic macromolecules from degradation and decomposition of living organisms. Humic substances in NOM can be categorized into humic acids, fulvic acids and humin, according to their solubility in acidic solutions. Organic fouling has a larger effect on membrane processes than colloidal fouling. In addition to surface adsorption (Childress and Elimelech 1996), organic materials can form a more compact fouling layer at high ionic strength, low pH and in the presence of multivalent ions (Hong and Elimelech 1997; Costa and de Pinho 2002).

Biological fouling or biofouling occurs when microorganisms entering the membrane module are transported onto the membrane surface, where they adsorb and form a thin fouling layer (Ridgway and Flemming 1996). Once attached, the microorganisms may grow and multiply at the expense of feed water nutrients, forming a biological film or biofilm that increases the membrane resistance.

Fouling by sparingly insoluble salts is commonly known as scaling and is a phenomenon that plagues the operation of desalination units (Sheikholeslami 2004). As the salt concentration in the feed increases downstream due to the loss of water

through permeation, dissolved inorganics such as Ca^{2+}, Mg^{2+}, CO_3^{2-}, SO_4^{2-}, silica and iron are most likely to precipitate as insoluble salts (or scales) on the membrane surface if the solubility limits are exceeded.

2.2.3 Pretreatment and Membrane Cleaning

Pretreatment refers to the process that provides feed water of a quantity and quality that allows the continuous operation of downstream equipment and protects this equipment from variability in the feed (Gare 2002). In full-scale RO processes, the major role of pretreatment is to slow down the rate of membrane fouling by reducing the fouling strength of the feed water, so that cleaning frequency and duration can be reduced. The reduction of fouling strength of the feed water can be achieved by the physical removal of foulants, or the chemical conditioning of feed water to discourage foulant accumulation on the membrane surface. Some examples of pretreatment are given below:

a. Removal of large particles using coarse strainers. For smaller particles, microfiltration is used (Vial and Doussau 2002);
b. Water disinfection with chlorine;
c. Clarification and hardness removal using lime;
d. Addition of scale inhibitor and;
e. Water sterilization using UV radiation.

To optimize performance of a full-scale RO system, the pretreated feed water must satisfy the requirements set by the plant operators. For example, to reduce the potential of organic fouling, designers can limit the Total Organic Carbon (TOC) to 3 ppm, Biological Oxygen Demand (BOD) to 6 ppm and Chemical Oxygen Demand (COD)

to 8 ppm (Bates 1998). The Silt Density Index (SDI) is widely used to determine the potential for colloidal/suspended fouling. Generally, the maximum allowable SDI of the feed water is about 5 or less (Bryne 1995).

Membrane cleaning is a direct method to alleviate membrane fouling by restoring the permeability of RO membranes. Membrane cleaning is an important part of full-scale RO operation, without which an early plant failure may occur or frequent replacement of membranes may be required. The membrane cleaning efficiency is affected by numerous factors, including the types of cleaning agents, types of foulant, chemical dosages, frequency of cleaning and contact time (AWWA 1998). The efficiency of membrane cleaning and its effects on the performance of full-scale RO process are usually evaluated from past experiences or through pilot studies (Sadhwani and Veza 2001; Graham *et al*. 1989; Ebrahim and El-Dessouky 1994). As a guide, cleaning is usually done when there is a 10% decrease in water production (Avlonitis *et al*. 2003) at constant operating conditions, or a 10% increase in the driving pressure to maintain the same production at constant temperature, or an increase of 15-20% in the pressure differential between feed and reject flows (Sadhwani and Veza 2001). In full-scale RO processes where spiral-wound membrane modules are the predominant membrane configuration, membrane cleaning is commonly done with chemicals (Madaeni *et al.* 2001). Chemical cleaning is generally divided into low and high pH cleanings, which are used to remove inorganic and organic foulants, respectively. Cleaning agents are categorized into strong/weak acids and bases, as shown in Table 2.3 (Hydranautics 2003).

In practice, both inorganic and organic fouling occur together and membrane cleaning usually starts off with acid cleaning to remove inorganic scale or soluble colloidal materials, before the membranes are subjected to high pH cleaning to remove any remaining insoluble inorganic colloidal material, organic material and/or biological organisms. Membrane cleaning reduces production time and increases operating costs. In addition, excessive cleaning may damage the membranes, resulting in more frequent membrane replacement.

Table 2.3. General categories of cleaning agents

Category	Chemicals	Adjusted pH
Weak acidic	Citric acid	4.0
Weak basic	Sodium tripolyphosphate (STPP) and sodium ethylene-diamine-tetraacetate (Na-EDTA)	10.0
Strong acidic	Hydrochloric acid (HCl)	2.5
Strong basic	STPP and sodium dodecylbenzene sulfonate (Na-DDBS)	10
	Sodium hydroxide (NaOH)	11.5

*From Hydranautics Technical Service Bulletin 107.10

2.2.4 Costs Associated with Fouling Control and Membrane Cleaning

Membrane fouling can be significantly reduced by appropriate pretreatment of the feed water to the RO process. The fouled membranes can be cleaned to restore their permeability. However, the costs associated with fouling control and membrane cleaning represent a significant proportion of the total operating cost. According to Dudley (Dudley *et al*. 2000), scale inhibition and cleaning chemicals account for about

6.9% of the total cost for a typical sea-water RO system. Another study by Shahalam (Shahalam *et al.* 2002) has calculated the pretreatment cost in RO systems in Middle East to range between 10% and 25% of the total cost. Madaeni *et al.* (2001) showed that the cost of membrane cleaning represents about 5% to 20% of the operating cost. If membrane fouling is not effectively controlled and the extent of fouling is so severe that membrane cleaning fails to reverse the decline in water production, as in the case of Yuma Desalting Plant in Arizona (Kaakinen and Moody 1985), the plant has to be shut down and membrane replacement has to be carried out.

2.3 Measurement of Feed Water Fouling Strength

The huge economic impact and possible plant failure due to membrane fouling highlight the importance of effective fouling control. An effective control of membrane fouling requires a good diagnosis of the fouling strength of the feed water. The commonly used indicators of feed water fouling strength in RO applications include Silt Density Index (SDI) and the Modified Fouling Index (MFI). The SDI is the most widely used fouling index to quantify the fouling potential of colloidal particles in feed water (Bryne 1995; Mulder 1996; Brauns *et al.* 2002). This simple test, with the apparatus shown in Fig. 2.4, involves filtering the feed water through a 0.45μm filter membrane at constant pressure in dead-end flow. As shown in Eq. (2.5), the index is calculated based on the time taken to filter a fixed volume of feed water through a clean membrane and the time required to filter the same volume of feed water after the membrane has been used for a defined length of time.

$$\mathrm{SDI} = \frac{100(1 - t_i / t_f)}{t} \tag{2.5}$$

where t_i and t_f are the time to collect the initial and final 500 ml of sample, respectively, and t is the total running time of test.

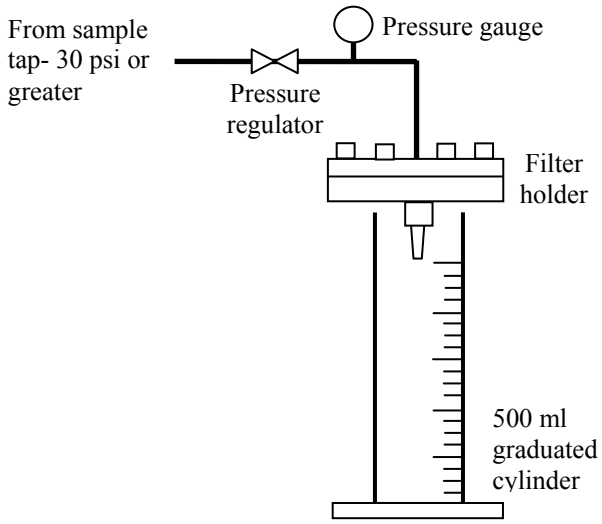

Figure 2.4. A schematic diagram of a SDI test unit

However, the accuracy of SDI is questionable in the light of reports that the index was not proportional to the colloidal concentration (Schippers and Verdouw 1980). In addition, the SDI was not theoretically developed based on the filtration mechanisms occurring during the test. Hence the SDI cannot be used in model to predict the rate of flux decline due to particulate fouling. Modified Fouling Index (MFI) was proposed in view of the deficiencies in SDI (Schippers and Verdouw 1980; Boerlage *et al.* 2003). The MFI is determined using the same equipment for SDI, but the filtrate volume is recorded every 30 seconds over a 15-min filtration period instead. Figure 2.5 shows the schematic curve of inverse flow against cumulative volume of a MFI test. Typically three regions of blocking filtration, cake filtration and cake failure/compaction can be observed on a MFI plot. MFI is calculated in the cake filtration region with the following expression (Schippers and Verdouw 1980).

$$\mathrm{MFI} = \frac{\eta_{20}}{\eta} \cdot \frac{\Delta p}{210} \cdot \tan\alpha \tag{2.6}$$

where η_{20} and η are the viscosity at 20oC and water temperature, respectively, Δp is the applied pressure in kPa and tan α is the slope of the straight part of the curve. Unlike the SDI that is empirically derived, MFI is based on the theory of cake filtration and can be used to model flux decline in membrane system assuming particulate fouling is dominated by cake filtration (Schippers *et al.* 1981). The MFI is also observed to be proportional to the colloidal concentration in the reported tests (Schippers and Verdouw 1980).

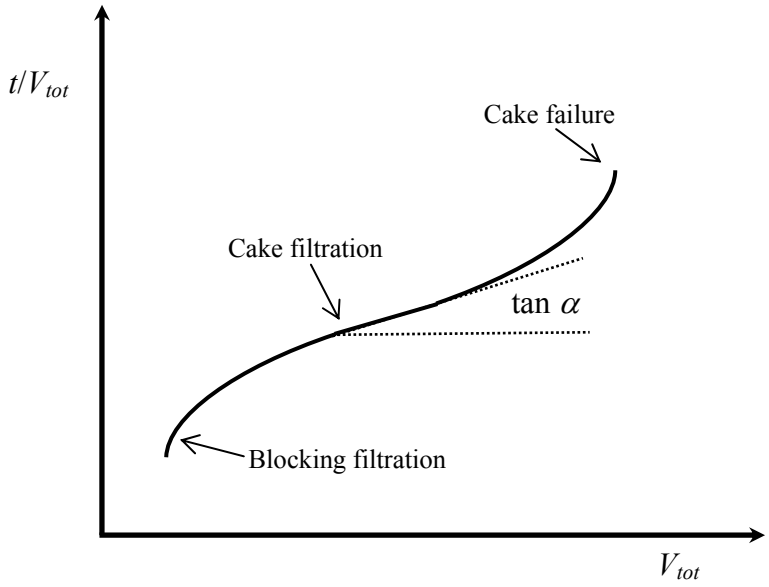

Figure 2.5. A schematic MFI plot to determine MFI

Although SDI and MFI are widely used in engineering practices, they often fail to reflect the true fouling strength of the feed water. Apparently, these fouling indices cannot measure the fouling strength of all foulants on RO membrane with their 0.45μm filter membrane. Calculations based on cake filtration model show that measured MFI values are too low to explain the observed flux decline in practice

(Schippers *et al.* 1981). It is likely that particles smaller than 0.45μm that are not retained by the test membranes are the cause for the observed flux decline rates. Thus recent studies devoted their effort to improve the MFI by modifying the filter membrane to retain as much particulates in the feed water as possible. To incorporate smaller colloidal particles into the MFI measurement, Boerlage proposed a polyacrylonitrile membrane with a molecular weight cut-off (MWCO) of 13 kDa as a reference membrane for MFI-UF (Boerlage *et al*. 2003). Tests at Ijssel Lake and River Rhine RO pilot plants had shown that the MFI-UF of the influent feedwater was approximately 700-2400 times higher than the corresponding MFI and SDI values, indicating the retention of smaller particles. More recently, Khirani proposed using nanofiltration (NF) membranes to include dissolved organics into MFI measurements on biologically treated secondary effluent (Khirani *et al*. 2006). In the experiments, NF membrane with MWCO of 1500 kDa was able to retain 73% of the NOM at constant transmembrane pressure. However, when another NF membrane with MWCO of 500 Da was used to measure MFI of a synthetic secondary treated sewage, the rejection of the organic matter was only 35-40%.

It is apparent that the aforementioned fouling indices cannot accurately reflect the actual fouling strength of the feed water, as the membranes used in the tests cannot retain all the possible foulants on a RO membrane. In addition, the fouling indices adopt the same apparatus used for dead-end filtration, which does not emulate the crossflow system in actual RO membrane elements. Operating flow mode can affect the fouling behavior of the foulants on the RO membrane surface. In dead-end filtration, foulants are forced onto the filter. In actual RO elements, a portion of the foulants will flow across the RO membrane and end up in the concentrate stream.

Therefore the fouling indices with dead-end filtration may overestimate the rate of fouling in actual RO membrane system.

The impact of membrane fouling underline the need for accurate characterization of membrane fouling in RO processes to effectively control and alleviate fouling. The dynamics of membrane fouling in long RO membrane channel has to be better understood in order to develop an effective fouling characterization method. In the following chapters, studies on the behavior of long membrane channels and feed water fouling strength are reported and form the basis for a better understanding of fouling development in long membrane channels. An effective fouling characterization method is developed based on the fouling characteristics in the long membrane channels.

Chapter 3

THE BEHAVIOR OF PERMEATE FLUX IN A LONG RO MEMBRANE CHANNEL

The performance of a RO process is generally governed by membrane properties, operating conditions and feed solution (Todtheide *et al*. 1997). Behaviors of full-scale RO processes have been customarily described with fundamental transport theories and models (Soltanieh and Gill 1981; Mason and Lonsdale 1990), which relate the permeate flux linearly with the driving pressure. But it was observed in some full-scale RO processes that the average permeate flux did not increase linearly with the driving pressure (Alvarez *et al*. 1997; Rautenbach *et al*. 2000). Some studies attributed this phenomenon to concentration polarization on the membrane surface (Manttari *et al*. 1997; Turan 2004). However, this argument became doubtful when Song and his coworkers developed a mathematical model (Song *et al*. 2002) that could adequately reproduce the non-linear relationship without considering concentration polarization. In his model, the long membrane channel was treated as a heterogeneous system, where operating parameters varied along the length of membrane channel. Localized operating parameters had to be calculated numerically along the membrane channel before meaningful parameters such as average permeate flux could be determined.

In this chapter, the governing equations for the permeate flux along a long crossflow RO membrane channel are introduced based on the fundamental principles of mass conservation and membrane transfer. The key feature of the governing equations is that the localized variables and parameters are used to describe the membrane systems.

An analytical model for the recovery of the long membrane channel is developed with the assumptions of constant driving pressure along the membrane channel and complete salt rejection. These assumptions are reasonable or at least acceptable approximations of today's membrane processes. The validity of the assumptions was verified by comparing the analytical solutions with the numerical solutions of the governing equations under identical operating conditions. The behavior of the permeate flux and the possible flux-controlling mechanisms in full-scale RO processes are discussed and delineated. It is revealed that the behavior of a long RO membrane channel can be well characterized by a lumped parameter. The theoretical findings of the permeate flux in a long membrane channel are compared with experimental results for a 4m long RO membrane channel in the laboratory.

3.1 Model Development

3.1.1 Governing Equations for Heterogeneous Membrane Channel

Spiral-wound module is the predominant RO configuration in full-scale RO processes. In this system, the feed stream flows along the membrane channel parallel to the central line of the module and the curvature of membrane module has an insignificant effect on system's performance (Van der Meer 1997). Therefore, an unwound flat sheet membrane with same channel height and spacers would adequately describe the operating characteristics of the corresponding spiral-wound RO module. The long membrane channel, which is made up of several spiral-wound modules connected in series, consists of a permeable membrane on one side and an impermeable wall on the other as shown in Fig. 3.1. Complete mixing in the transverse direction (along the width of channel) and absence of concentration polarization are reasonably assumed as

the height of the spacer-filled membrane channel is usually very small (about 0.7×10^{-3} m).

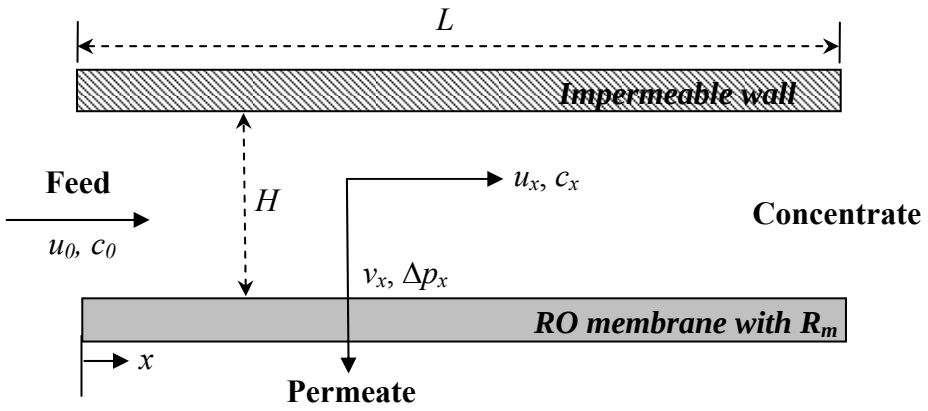

Figure 3.1. Schematic diagram of a long RO membrane channel

The permeate flux at any point along the membrane channel is governed by the basic membrane filtration equation,

$$v = \frac{\Delta p - \Delta \pi}{R_m} \tag{3.1}$$

where v is the localized permeate flux, Δp is the localized driving pressure, $\Delta \pi$ is the osmotic pressure and R_m is the membrane resistance. The osmotic pressure is a function of salt concentration and usually a linear correlation between osmotic pressure and salt concentration can be used as,

$$\Delta \pi = f(c) = f_{os} c \tag{3.2}$$

where c is the localized salt concentration, and f_{os} is the correlation (osmotic) coefficient.

The localized crossflow velocity in the channel can be determined by applying the principle of mass conservation to the water,

$$u = u_0 - \frac{1}{H}\int_0^x v d\xi \tag{3.3}$$

where u is the localized crossflow velocity, u_0 is the feed crossflow velocity, H is the height of the membrane channel, ξ is the dummy variable and x ($0 \le x \le L$, with L being the length of the channel) is the distance from the entrance.

Localized salt concentration can be determined by applying the mass conservation principle to salt:

$$c(x,t) = \frac{1}{u(x,t)H}\left[c_0 u_0 H - (1 - r_{rej})\int_0^x c(\xi,t)v(\xi,t)d\xi\right] \tag{3.4}$$

where c_0 is the feed salt concentration and r_{rej} is the salt rejection.

The driving pressure decreases along the channel due to friction caused by the membrane surfaces and spacers, and is described by

$$\Delta p(x,t) = \Delta p_0 - \frac{12\lambda\eta}{H^2}\int_0^x u(\xi,t)d\xi \tag{3.5}$$

where Δp_0 is the driving pressure, η is the water viscosity, and λ (≥ 1) is a friction coefficient that accounts for the decrease in driving pressure due to the spacers in membrane channel. λ is equal to 1 if the channel does not contain any spacer.

Eqs. (3.1)–(3.5) describe a heterogeneous membrane system where operating parameters vary along the membrane channel. The solution to key operating parameters can be easily determined using numerical method. The numerical solutions provide a more realistic description for a long membrane channel of highly permeable RO membranes than the calculations for homogeneous membrane system.

3.1.2 Analytical Model

An analytical model provides a more direct and convenient way to analyze filtration performance and to optimize system design of RO processes. By making two reasonable assumptions, a concise analytical model for the long membrane channel can be obtained rigorously from the numerical model described in previous section.

Assumption 1: Current RO membranes used in water treatment and reclamation have salt rejection above 98%. So it is reasonable to assume complete (100%) salt rejection In that case, mass conservation of solute is described by,

$$cu = c_0 u_0 \tag{3.6}$$

Assumption 2: The variation of the driving pressure along the membrane channel is much smaller than the change in other variables. Hence pressure loss along the channel is not considered and the variable Δp can be replaced by a constant Δp_0.

Combining Eqs. (3.1)–(3.3) and Eq. (3.6),

$$c\left[u_0 - \frac{1}{HR_m}\int_0^x (\Delta p_0 - f_{os}c)dx\right] = c_0 u_0 \tag{3.7}$$

Taking derivatives of both sides with respect to x,

$$\frac{dc}{dx}\left[u_0 - \frac{1}{HR_m}\int_0^x (\Delta p_0 - f_{os}c)dx\right] - \frac{1}{HR_m}(\Delta p_0 - f_{os}c)c = 0 \tag{3.8}$$

Combining Eqs. (3.7) and (3.8) to eliminate the integration term results in

$$\frac{dc}{dx} - \frac{\Delta p_0}{HR_m c_0 u_0}\left(1 - \frac{f_{os}c}{\Delta p_0}\right)c^2 = 0 \tag{3.9}$$

Eq. (3.9) can be written in dimensionless form as follows:

$$\frac{dC}{dX} - C^2(\Delta P - \Pi_0 C) = 0 \tag{3.10}$$

with the introduction of a parameter and four dimensionless variables shown below,

$$\Delta p^* = \frac{u_0 HR_m}{L} \tag{3.11}$$

$$C = \frac{c}{c_0} \tag{3.12}$$

$$X = \frac{x}{L} \ (0 \le \mathrm{X} \le 1) \tag{3.13}$$

$$\Pi_0 = \frac{f_{os}c_0}{\Delta p^*} \tag{3.14}$$

$$\Delta P = \frac{\Delta p_0}{\Delta p^*} \tag{3.15}$$

The collective parameter (u_0HR_m/L) introduced by Eq. (3.11) has a unit of pressure and, therefore, is denoted as Δp^*. It will be seen later that Δp^* is one of the most important characteristics of a membrane filtration system. The rest are dimensionless variables.

Separating the variables of Eq. (3.10) and integrating the resulting equation over the entire filtration length, i.e.,

$$\int_{1}^{C_e} \frac{dC}{C^2\left(\Delta P - \Pi_0 C\right)} = \int_{0}^{1} dX \tag{3.16}$$

we have

$$\frac{1}{\Delta P}\left(1-\frac{1}{C_e}\right)+\frac{\Pi_0}{\Delta P^2}\ln\frac{\left(\Delta P-\Pi_0\right)C_e}{\Delta P-\Pi_0 C_e}=1 \tag{3.17}$$

The performance of a membrane system is commonly indicated by the permeate recovery r, which is defined as

$$r = 1-\frac{Q_e}{Q_0}=1-\frac{c_0}{c_e}=1-\frac{1}{C_e} \tag{3.18}$$

where Q_0 and Q_e are the feed and exit (concentrate) flow rates respectively, and c_e and C_e are the concentrate concentration in dimension and dimensionless forms respectively. From Eqs. (3.17) and (3.18), the recovery of the long membrane channel can be finally determined as,

$$r=\frac{\left(\Delta P-\Pi_0\right)-\left(\Delta P-\Pi_0\right)e^{-\frac{\Delta P\left(\Delta P-r\right)}{\Pi_0}}}{\Delta P} \tag{3.19}$$

Substituting Eqs. (3.14) and (3.15) into Eq. (3.19), the recovery is represented by the real parameters of the membrane system,

$$r=\left(1-\frac{\pi_0}{\Delta p_0}\right)\left[1-e^{-\frac{\Delta p_0}{\pi_0}\left(\frac{\Delta p_0}{\Delta p^*}-r\right)}\right] \tag{3.20}$$

where π_0 is the osmotic pressure of the feed water. Eq. (3.20) is the analytical solution to the recovery of RO process. Because the recovery r appears in both sides of Eq. (3.20), a simple iterative procedure is needed to determine the value of recovery. By substituting an arbitrary initial recovery (r_0) into the right hand side of Eq. (3.20), the recovery value of the first iteration r_1 is determined. The recovery value of the second iteration r_2 can be calculated by substituting r_1 into the right hand side of Eq. (3.20). The process is repeated until a preset convergent criterion is satisfied. It is observed that the iteration does not converge for some operating conditions. Fortunately, in this case, a converged solution can still be obtained with a similar iteration procedure from the following equivalent form of Eq. (3.20):

$$r = \frac{\pi_0}{\Delta p_0} \ln\left[\left(1 - r - \frac{\pi_0}{\Delta p_0}\right) \Big/ \left(1 - \frac{\pi_0}{\Delta p_0}\right)\right] + \frac{\Delta p_0}{\Delta p^*} \tag{3.21}$$

3.1.3 Validity of the Assumptions

To investigate the validity of the assumptions that were used to derive the analytical model, recoveries from numerical solutions and the analytical model were simulated over a range of driving pressures under the operating conditions given in Table 3.1.

Fig. 3.2 and Fig. 3.3 show the variation of recoveries with the driving pressure for different feed salt concentrations and feed crossflow velocities, respectively, as calculated using both the numerical and analytical solutions. Non-linearity is observed in all data plots (both numerical solutions and analytical recoveries) over the entire driving pressure range. This phenomenon will be discussed in detail in the next section. The numerical solution curves indicated that recovery increases with an increasing rate over a narrow region of the driving pressures just above the osmotic pressure of the feed water, before it increases linearly with the driving pressure. This situation arises when the net driving pressure (driving pressure minus osmotic pressure) is comparable to the frictional pressure loss in the membrane channel. As a result, permeate flux would only be produced in the upstream region of the membrane channel. The recovery increases linearly with driving pressure when the net driving pressure is much larger than the frictional pressure loss along the channel such that the permeate flux is produced by the entire membrane channel. The small differences between the numerical solutions and analytical recoveries in Fig. 3.2 and Fig. 3.3 show that the assumptions are reasonable for real situations.

Table 3.1 Operating conditions used in numerical solutions and analytical model to simulate permeate recovery

Operating Parameters	Numerical	Analytical
Channel length (m)	6	6
Channel Height (m)	0.7×10^{-3}	0.7×10^{-3}
Feed Salt Concentration (mg/L)	1000, 3000, 5000	1000, 3000, 5000
Osmotic coefficient	69	69
Feed crossflow velocity (m/s)	0.05, 0.1, 0.15	0.05, 0.1, 0.15
Clean membrane Resistance (Pa·s/m)	8×10^{10}	8×10^{10}
Solute Rejection	0.99	-
Friction coefficient	10	-
Water Viscosity (Pa·s)	1×10^{-3}	-

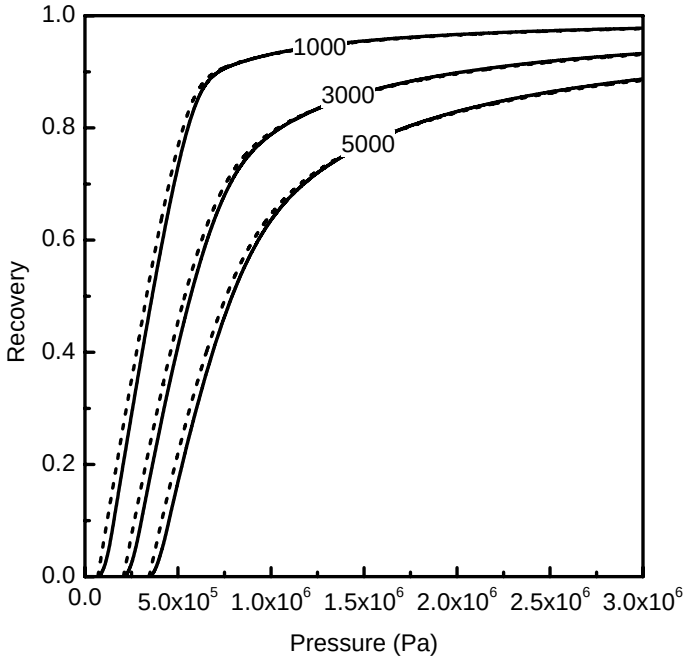

Figure 3.2. Comparison between numerical solutions (solid curve) and analytical (dashed curve) recoveries with driving pressures at different feed salt concentrations

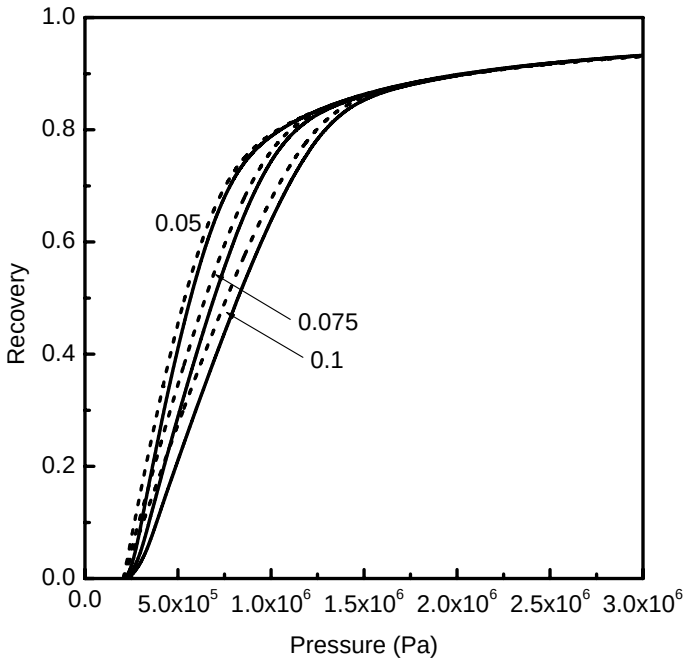

Figure 3.3. Comparison between numerical solutions (solid curve) and analytical (dashed curve) recoveries with driving pressures at different feed crossflow velocities

3.2 Non-Linear Behavior of Permeate Flux

Substantial variation of key operating parameters along the long highly permeable RO membrane channel means the membrane channel has to be treated as a heterogeneous system. There is a need to understand to what extent the variations affect the average permeate flux or recovery in the long RO membrane channel. The general solution shown in Eq. (3.20) gives the recovery of a long membrane channel under any operating conditions. Possible mechanisms governing permeate flux in different pressure regions are delineated from the general solution.

3.2.1 Mass Transfer Pressure Region

When $\Delta p_0 << \Delta p^*$, according to Taylor series expansions of exponential functions, Eq. (3.20) becomes,

$$r = \left(\frac{\Delta p_0}{\pi_0} - 1 \right) \left(\frac{\Delta p_0}{\Delta p^*} - r \right) \tag{3.22}$$

From Eq. (3.22), the recovery r can be determined as,

$$r = \frac{(\Delta p_0 - \pi_0)}{\Delta p^*} = \frac{L}{u_0 H R_m} (\Delta p_0 - \pi_0) \tag{3.23}$$

From Eq. (3.23), the average permeate flux of the membrane channel can be obtained as,

$$\bar{v} = \frac{u_0 H}{L} r = \frac{\Delta p_0 - \pi_0}{R_m} \tag{3.24}$$

Eqs. (3.23) and (3.24) shows that the recovery and average permeate flux in a long membrane channel are linearly related to the driving pressure Δp in a pressure region much smaller than the characteristic parameter Δp^*. In this case, the RO process is said to be ***mass transfer*** controlled. Interestingly, this expression is actually the well-known governing equation (Eq. (3.1)) for a homogeneous membrane channel (Soltanieh and Gill 1981; Mason and Lonsdale 1990). Recovery that is controlled by mass transfer is sensitive to changes in physical parameters such as channel dimensions and feed crossflow velocity. From Eq. (3.23), recovery can be proportionally increased with membrane channel length. This principle is adopted in many full-scale RO processes where several spiral-wound membrane modules are connected in series in a single stage to increase permeate recovery.

3.2.2 Thermodynamic Equilibrium Pressure Region

When $\Delta p >> \Delta p^*$, the whole exponential term becomes negligible and Eq. (3.20) simply becomes,

$$r = 1 - \frac{\pi_0}{\Delta p_0} \tag{3.25}$$

Eq. (3.25) shows that the recovery is solely dependent on the thermodynamic parameters of the RO processes, such as the feed salt concentration and the driving pressure, when the driving pressure is much higher than the characteristic parameter Δp^*. This permeate flux or recovery is said to be under ***thermodynamic equilibrium*** restriction.

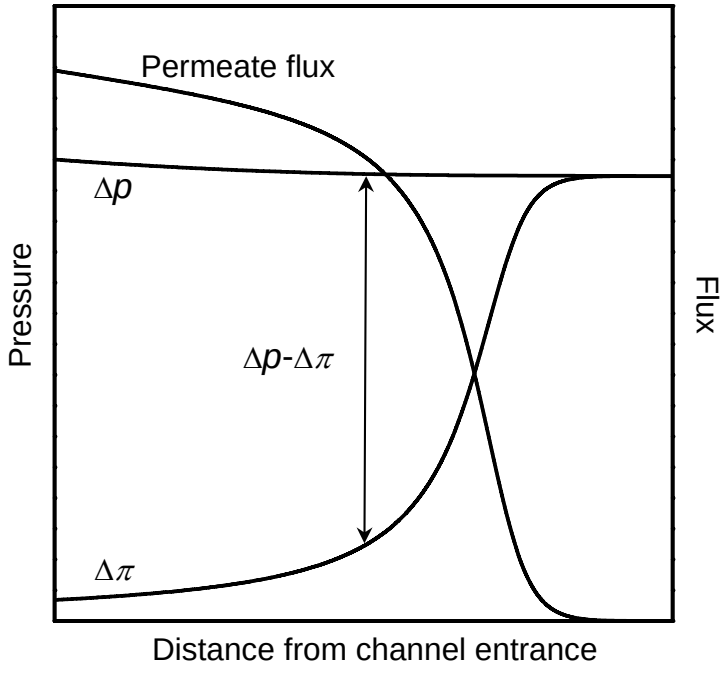

Figure 3.4. A schematic illustration of thermodynamic equilibrium restriction in a long RO membrane channel

The variation of key localized parameters in a membrane channel under thermodynamic equilibrium restriction is schematically illustrated in Fig 3.4. At the beginning of a long membrane channel, permeate flux is high because of the large net driving pressure, which is indicated in the figure by the distance between Δp and $\Delta \pi$. The osmotic pressure increases along the membrane channel as water passes through the membrane as permeate. The increase in the osmotic pressure reduces the net driving pressure and consequently reduces the permeate flux. At one point along the membrane channel, the osmotic pressure can become equal to the driving pressure, resulting in zero flux from that point to the end of membrane channel. The permeate recovery under thermodynamic equilibrium restriction is the maximum recovery that can be reclaimed from the feed water. Any attempt to increase the recovery through the adjustment of physical parameters, such as channel dimensions and feed flow rate, will not be successful.

The validity of Eqs. (3.23) and (3.25) is clearly shown in Fig. 3.5, in which permeate recoveries (broken lines) controlled respectively by mass transfer and thermodynamic equilibrium mechanisms are plotted with actual recovery (solid line) calculated with Eq. (3.20). It is observed that the actual recovery in the whole pressure range behaves non-linearly with driving pressure and is circumscribed by the mass transfer and thermodynamic equilibrium lines. The mass transfer restricted recoveries approach the actual recovery line towards the low end of the pressure range, while the thermodynamic equilibrium restricted recoveries give a good representation of the actual recoveries at high end of the pressure range. A transition zone exists at the region where the mass transfer and thermodynamic equilibrium lines intersect. Recoveries in this zone are influenced by both mass transfer and thermodynamic

equilibrium restrictions and provide a smooth transition between the two flux-controlling mechanisms.

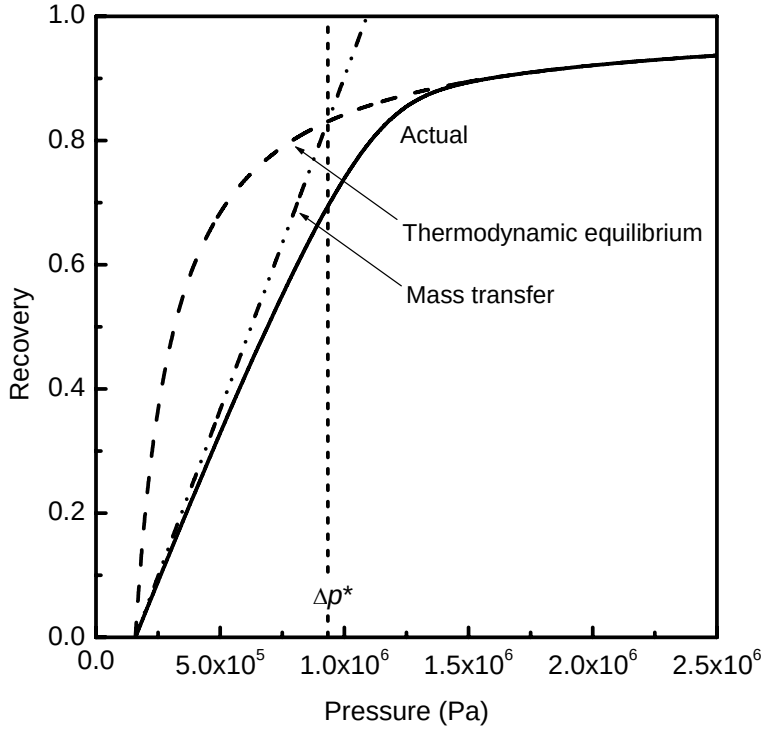

Figure 3.5. Non-linear dependence of actual recovery on driving pressure. The characteristic pressure Δp^* indicates the turning point of the recovery. L=6 m, H=0.7×10^{-3} m, u_0=0.1 m/s, c_0=2000 mg/L, f_{os}=79 Pa·L/mg, R_m=8.0×10^{10} Pa·s/m

3.2.3 Characteristic Pressure

Fig. 3.5 shows that the actual recovery curve can be divided into lower and upper pressure regions by the characteristic parameter Δp^*. In the lower pressure region, recovery is mainly controlled by water transfer through the membrane, while the recovery in the upper pressure region is predominantly restricted by thermodynamic parameters of the system. This characteristic parameter is termed as the ***characteristic pressure*** (since it has the same unit as pressure) and is an important characteristic of the RO membrane channel. It represents a critical turning point in the performance

curve of a long membrane channel. When the driving pressure is much lower than the characteristic pressure, the membrane channel could be approached as a homogeneous system and the recovery could be reasonably calculated with Eq. (3.23). However, when the driving pressure is comparable to or even higher than the characteristic pressure, the membrane channel has to be treated as a heterogeneous system and the more sophisticated Eq. (3.20) has to be used.

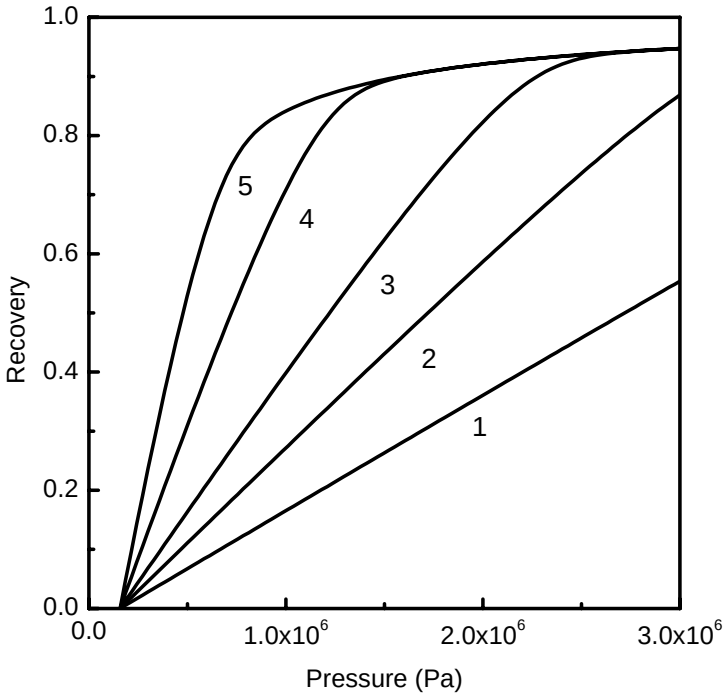

Figure 3.6. The theoretical recoveries of the membrane channel at different characteristic pressures: (1) 5×10^6 Pa; (2) 3×10^6 Pa; (3) 2×10^6 Pa; (4) 1.0×10^6 Pa; (5) 5×10^5 Pa. c_0=2000 mg/L, f_{os}=79 Pa·L/mg

Recoveries in RO membrane channels with different characteristic pressures were calculated with Eq. (3.20) (in case it did not converge, Eq. (3.21) was used instead) for a pressure range up to 3.0 MPa, and the results are presented in Fig. 3.6. When the characteristic pressure of a membrane channel is greater than the pressure range, the

membrane channel can be reasonably represented as a homogeneous system, as indicated by Line 1. However, when the characteristic pressure falls within the pressure range, the membrane channel becomes a heterogeneous system that is evidenced by the strong non-linearity of Lines 3-5. Line 2 with the characteristic pressure of 3.0 MPa represents a marginal case in which a slight curvature is starting to appear at the higher end of the pressure range.

Table 3.2 lists the typical characteristic pressures of some commercial RO membranes. For old RO membranes in the normal configuration (6 modules in series contained in a pressure vessel), the characteristic pressure is very much above the common driving pressures (similar to Line 1 in Fig. 3.6). This explains why the performance of early RO processes of long membrane channels could be adequately approximated by membrane transfer theory (i.e. treated as homogeneous systems).

Table 3.2. Typical characteristic pressures for a 6m membrane channel of various RO membranes[*]

RO Membranes	Membrane resistance (Pa·s/m)	Characteristic pressure (Pa)
Low-pressure membranes	8.00×10^{10}	9.33×10^{5}
Seawater membranes	3.00×10^{11}	3.50×10^{6}
Old membranes	2.00×10^{12}	2.33×10^{7}

[*]Channel height $H=7\times10^{-4}$ m, and feed crossflow velocity $u_0=0.1$ m/s.

3.3 Experimental Verification and Discussions

In this section, non-linear behavior of average permeate flux with driving pressure was verified using a sodium chloride solution in a 4m long RO channel in the laboratory. Permeate recovery was measured over a range of driving pressures at different feed crossflow velocities and salt concentrations. The effects of feed crossflow velocity and salt concentration on recovery at different driving pressures were examined.

3.3.1 Materials and Method

Membrane Modules - Four thin-film composite (TFC) polyamide spiral-wound reverse osmosis membrane modules from Hydranautics (ESPA-2540, Hydranautics, Oceanside, CA, USA) were used in the experiments. Each membrane module is about 1 m in length and has an external diameter of 63.5 mm (2.5 inch). The nominal surface area of each module is about 2.6 m^2 (28 ft^2) and the production rate is 2.8 m^3/day (750 gpd) under the standard testing conditions (1.05 MPa/150 psi pressure and 1,500 mg/L sodium chloride solution). According to the specifications given by the manufacturer, the membrane module has a minimum salt rejection of 98% and the recommended pH range for continuous operation is 3–10. The maximum operating pressure and temperature are 2.1 MPa (300 psi) and 45^oC, respectively.

Experimental Setup - The experimental RO setup used in this study is schematically shown in Fig. 3.7. Two 2-meter long pressure vessels (Advanced Structures Inc., Escondido, California, USA), each holding two RO modules were connected in series to form a 4 m long membrane channel. Feed water consisting of deionized water and sodium chloride was stored in a 400-L polyvinyl chloride (PVC) rectangular tank. The feed water was fed into the RO membrane system by a stainless steel plunger pump

(WM3615C, General Pump, Minnesota, USA) that was capable of generating a pressure of up to 10 MPa (1,500 psi) and a maximum flow rate of 14 L/min (3.6 gpm). Driving pressure was adjusted and controlled by a needle valve located after the membrane system. Inlet and outlet pressures were monitored by two digital pressure gauges (ECO-1, Wika, Klingenberg, Germany) installed just before and after the membrane channel. Permeate and concentrate flow rates were measured by two digital flow meters (F-2000, Blue-White Industries, Huntington Beach, CA, USA). Both permeate and concentrate were circulated back into the feed tank in which mixing was provided. The temperature of the feed water was controlled at 25°C by a locally fabricated chiller that was driven by an Electrolux compressor (A106, Electrolux Group, Stockholm, Sweden).

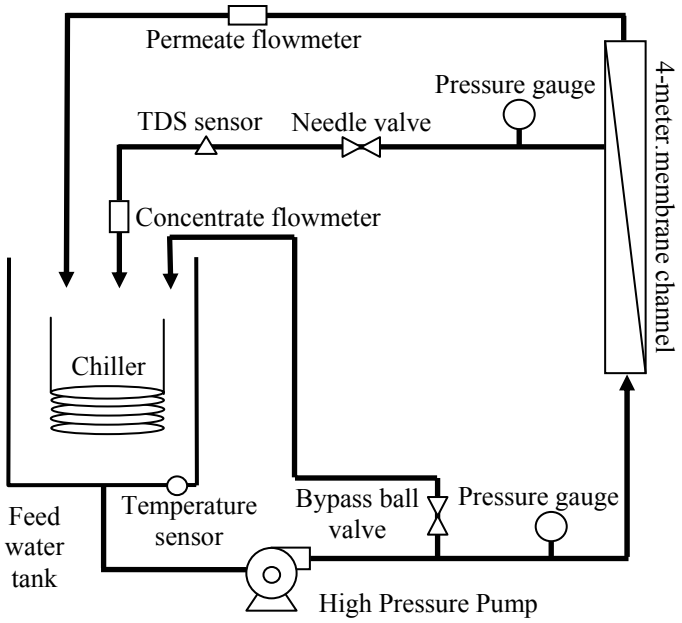

Figure 3.7. Schematic diagram of the experimental RO setup with a 4m membrane channel

Experimental procedure - The RO membrane system was first flushed with deionized water before the start of the experiment to remove preservatives inside the membrane modules. The system was run with deionized water at increasing and decreasing pressure steps to eliminate the effect of membrane compaction during the experiments. Temperature was maintained at 27±0.5°C and uncontrolled pH was 6.5±0.5. Permeate flow rate was recorded at different driving pressures and the clean membrane resistance was calculated and shown in Fig. 3.8. It was verified that membrane compaction was not significant in the pressure range tested. The average clean membrane resistance was calculated to be about 8.4×10^{10} Pa·s/m.

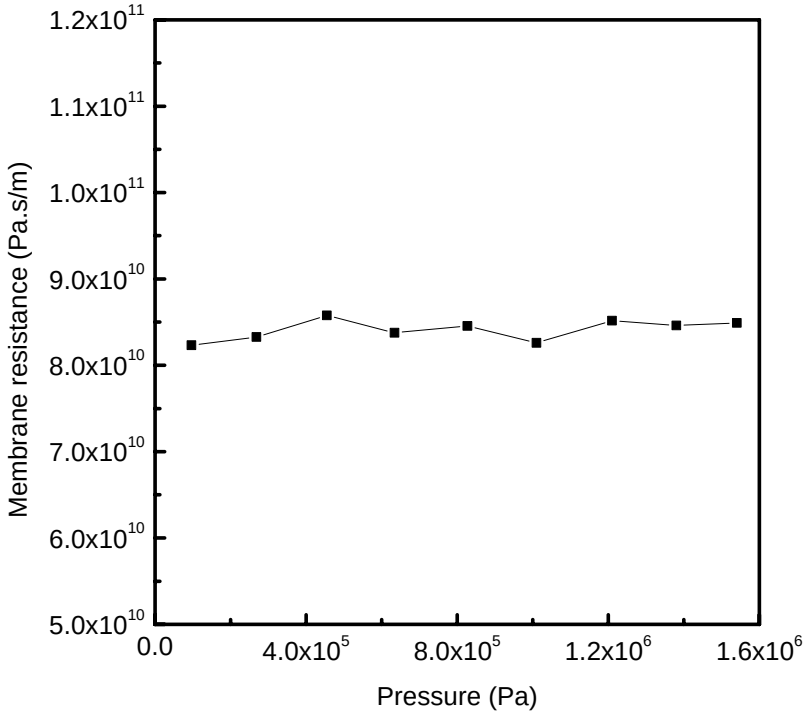

Figure 3.8. Clean membrane resistances of 4m RO channel at different driving pressures

When the preset driving pressure and feed flows were stabilized, concentrated sodium chloride stock solution was added into the feed tank to achieve the intended salt

concentration. The needle valve after the membrane system and the bypass ball valve were then adjusted to fine-tune the designed feed flow rate and driving pressure. Once the desired operating conditions had been established and stabilized, the permeate and concentrate flow rates were recorded. The two valves were then adjusted for another preset combination of feed flow rate and driving pressure until the permeate and concentrate flow rates for all designed combinations were measured. The experiments under all operating conditions were run in duplicate to ensure reproducibility of the results. When the experiments for a feed salt concentration had been completed, more concentrated NaCl solution was added into the feed tank to increase the salt concentration to the next designed value. The permeate and concentrate flow rates were measured again according to the same procedure outlined above. This process was repeated until all designed feed salt concentrations had been covered.

Three feed crossflow velocities (0.05, 0.075 and 0.1 m/s) and three feed salt concentrations (500, 1,000 and 3,000 mg/L of sodium chloride) were used for the experiments in this study. The maximum driving pressure was initially set at 1.72 MPa (250 psi) for all experiments. However, during the execution of the experiments, it was noticed that almost 100% of the feed became permeate at driving pressures markedly lower than 1.72 MPa (250 psi) for some combinations of low feed salt concentration and low feed crossflow velocity. For this reason, some experiments in this study were stopped at lower driving pressures.

3.3.2 Effect of Feed Crossflow Velocity on Recovery at Different Pressures

Permeate recoveries of the long membrane channel at three different feed crossflow velocities were plotted as scattered points in Fig. 3.9. The lines in Fig. 3.9 are the calculated recoveries with Eq. (3.20) using exact operating conditions in experiments. Generally, the equation could nicely reproduce the recovery behavior in the whole pressure range without any adjusting parameters. The turning points for recoveries at all three feed crossflow velocities are found to coincide with the calculated characteristic pressures shown in Table 3.3.

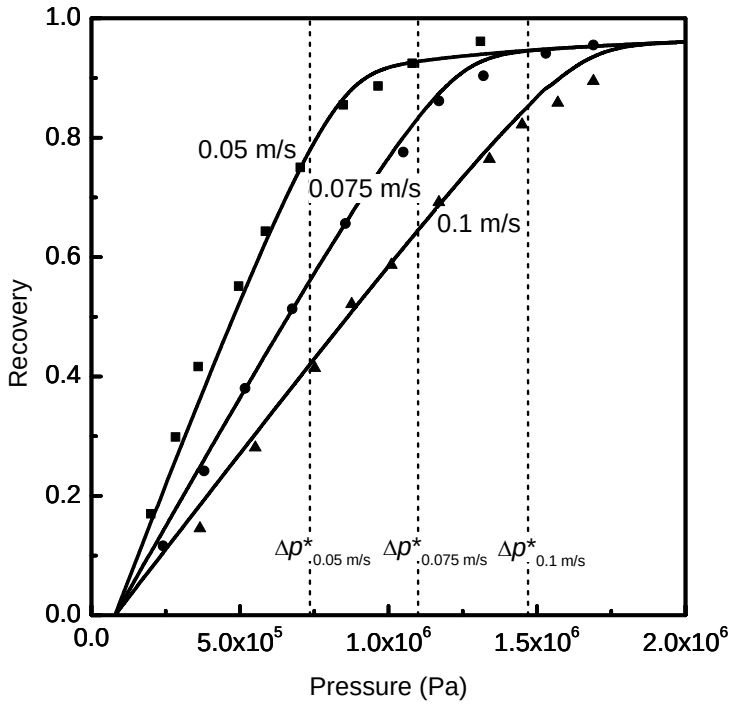

Figure 3.9. Non-linear behavior of experimental (symbols) and calculated (solid lines) recoveries for feed crossflow velocities of 0.050, 0.075 and 0.10 m/s. L=4 m, H=0.7×10^{-3} m, c_0=1000 mg/L, f_{os}=79 Pa·L/mg, R_m=8.40×10^{10} Pa·s/m

Table 3.3. Characteristic pressures of 4m long RO membrane channel at different feed crossflow velocities

Membrane module	ESPA-2540		
Channel height (mm)	0.7		
Channel length (m)	4		
Membrane resistance (Pa·s/m)	8.40×10^{10}		
Feed crossflow velocity (m/s)	0.05	0.075	0.1
Characteristic pressure (Pa)	7.35×10^{5}	1.10×10^{6}	1.47×10^{6}

As speculated, a strong non-linearity between the recovery and the driving pressure is observed in all the three feed crossflow velocities. Recoveries are observed to be linear at lower driving pressures where mass transfer restriction is dominant, with the gradient of the recovery defined by the feed crossflow velocity according to Eq. (3.23). At higher driving pressures, the change in recovery is not proportional to the change in driving pressure i.e., a large driving pressure increase is required to increase the recovery marginally. This is a special feature of thermodynamic equilibrium restriction as the recovery is the maximum recovery from the operating conditions. In addition, the recoveries for all three feed crossflow velocities approach the same limiting line when the driving pressure is significantly high. Under thermodynamic equilibrium restriction, the recovery is not affected by the change in the feed crossflow velocity. This phenomenon verifies the speculation that the membrane channel is not a homogeneous system because otherwise the recovery would be inversely related to the feed crossflow velocity.

In the discussion of the two flux-controlling mechanisms, it was speculated that the recovery independent of the physical membrane parameters may be controlled by

equilibrium between the osmotic pressure of the concentrate and the driving pressure. To verify this speculation, the osmotic pressures of the concentrate were calculated from measured salt concentrations. The results are shown with outlet pressures in Table 3.4 for the feed crossflow velocity of 0.075 m/s at increasing driving pressures. The osmotic pressure at the outlet of the membrane channel was found to be about the same as the outlet pressure at 1.67×10^6 Pa. This shows that the thermodynamic equilibrium restriction indeed existed in the RO process with a long membrane channel when the driving pressure was sufficiently high.

Table 3.4. The measured outlet pressures and calculated osmotic pressures of the concentrate at increasing driving pressures

Outlet Pressure (Pa)	Concentrate Salt Concentration (mg/L)	Osmotic Pressure* (Pa)
1.31×10^5	1121	8.86×10^4
2.76×10^5	1294	1.02×10^5
4.34×10^5	1548	1.22×10^5
6.21×10^5	1985	1.57×10^5
8.00×10^5	2980	2.35×10^5
1.00×10^6	4580	3.62×10^5
1.14×10^6	6220	4.91×10^5
1.30×10^6	8860	7.00×10^5
1.50×10^6	15040	1.19×10^6
1.67×10^6	20860	1.65×10^6

*Osmotic pressure was calculated with Eq. (3.2) with osmotic coefficient being 79 Pa/[mg/l] (Partanen and Minkkinen 1991)

3.3.3 Effect of Feed Salt Concentration on Recovery at Different Pressures

Permeate recoveries at three feed salt concentrations were measured for a wide range of driving pressure and are plotted in Fig. 3.10. Again, the agreement is excellent between the calculated permeate recoveries with Eq. (3.20) and the measured values without using fitting parameters. At low driving pressures, the recoveries for all feed salt concentrations are observed to be linear with driving pressure. The recovery lines shift towards the right hand side of the graph at higher feed salt concentrations as higher driving pressure is needed to overcome the increasing osmotic pressure. All recovery lines under the mass transfer regime have the same gradient since the physical parameters in Eq. (3.23) remain unchanged. A marginal increase in recovery is observed at higher driving pressures where thermodynamic equilibrium is the dominant flux-controlling mechanism. However, the magnitude of the thermodynamic equilibrium restricted recovery decreases with increasing feed salt concentration. This phenomenon is self-explanatory with Eq. (3.25).

Although feed salt concentration affected the magnitude of the permeate recovery, the three recovery curves have turning points at the same characteristic pressure Δp^*. This experimental observation verifies that the characteristic pressure is unaffected by the feed salt concentration, which is correctly reflected in Eq. (3.11). Because the characteristic pressure divides the pressure range into mass transfer and thermodynamic equilibrium pressure regions, the experimental results reveal that feed salt concentration does not affect the controlling mechanism of a heterogeneous membrane channel although it is one important parameter of any RO process.

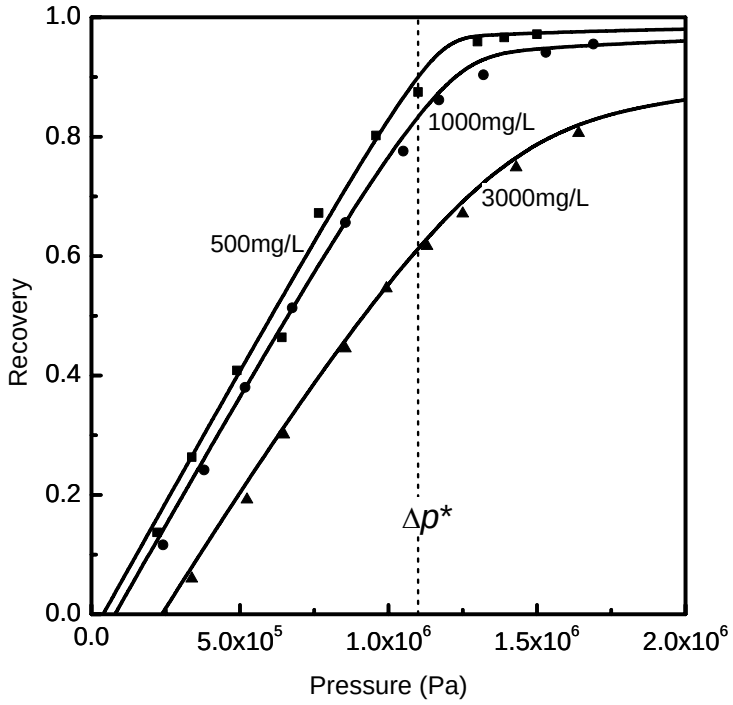

Figure 3.10. Experimental (symbols) and calculated (solid lines) recoveries of the membrane channel for feed salt concentrations of 500, 1000, and 3000 mg/L. L=4 m, H=0.7×10^{-3} m, u_0=0.075 m/s, f_{os}=79 Pa·L/mg, R_m=8.40×10^{10} Pa·s/m

3.4 Implications of Heterogeneous RO Membrane Channel

It was demonstrated in preceding sections that with the use of highly permeable RO membranes, the long RO membrane channel should be treated as a heterogeneous system, rather than a homogeneous system. The variation in key operating parameters along the membrane channel is supported with the findings by Wilf (Wilf 1997) and Nemeth (Nemeth 1998) who reported the phenomena of hydraulic imbalance in long RO membrane channels. Hence the use of conventional membrane transfer theories, which are only valid for homogeneous system, to describe or calculate permeate flux in heterogeneous system will produce erroneous results.

Thermodynamic equilibrium can be the dominant flux-controlling mechanism when the long RO membrane channel operates like a heterogeneous system. Operating in the thermodynamic equilibrium regime does not produce optimum performance in terms of permeate production as increasing the driving pressure cannot yield a proportionate increase in average permeate flux or recovery. Theoretically, the performance of a RO process is at its highest efficiency when it is operating at a driving pressure equal to the characteristic pressure. This represents the highest possible recovery before the increase in recovery slows down with driving pressure. The characteristic pressure could be very useful when designing a membrane system for optimum recovery. Since the characteristic pressure is a lumped parameter involving the membrane channel height and length, feed crossflow velocity and membrane resistance, various combinations of these parameters could be used to achieve the same characteristic pressure. For example, if a RO membrane with twice the permeability is used, the length of the membrane channel should be reduced by one-half to maintain the characteristic pressure.

Another area of concern associated with heterogeneous membrane system is the characterization of membrane fouling under thermodynamic equilibrium regime. In the derivation of recovery under the thermodynamic equilibrium restriction, it was found that recovery is not affected by a change in membrane resistance. Membrane fouling may not be accurately reflected by the average permeate flux or recovery when long RO membrane channels operate as heterogeneous systems. If this is true, an alternative fouling indicator is needed to give accurate fouling characterization.

3.5 Summary

When highly permeable RO membrane was used, the long RO membrane channel did not behave like a homogeneous system. The key operating parameters, such as permeate flux, crossflow velocity and salt concentration, were found to vary substantially along the membrane channel. By treating the long membrane channel like a heterogeneous system, an analytical solution for recovery in the long RO membrane channel was rigorously developed from the fundamental principles of mass conservation and mass transfer, assuming negligible pressure loss along the membrane channel and complete salt rejection. The analytical solution provides a direct and convenient way to analyze performance of a long membrane channel for any operating conditions. Simulations demonstrated that analytical recoveries fitted exactly with the numerical solutions at higher recovery.

The long RO membrane channel was represented by a lumped parameter termed the characteristic pressure. When the driving pressure was smaller than the characteristic pressure, recovery could be reasonably approximated with a homogeneous system i.e. the recovery was directly proportional to the net driving pressure and other physical parameters (mass transfer restriction). At driving pressures much higher than the characteristic pressure, the membrane channel had to be treated as a heterogeneous system and the recovery was restricted only by thermodynamic parameters (thermodynamic equilibrium restriction).

With the use of a highly permeable RO membrane, the permeate flux or recovery in a long membrane channel was no longer linear with driving pressure over the entire pressure range. Recovery increased at a slower rate rather than linearly with the

driving pressure in the thermodynamic equilibrium pressure region. This non-linear behavior was verified with a 4m long RO membrane channel in the laboratory under different feed crossflow velocities and salt concentrations. The analytical model reproduced the experimental recoveries for all cases without using any adjusting parameter.

Chapter 4

FEED WATER FOULING STRENGTH QUANTIFICATION

The extent of membrane fouling in a RO system is very much dependent on the concentration and physical and chemical properties of foulants in the feed water that can be represented by a single entity known as fouling strength. The SDI and MFI are the commonly used indicators of the fouling strength of RO feed water. The obvious drawback of both indices is that they do not take into account the contribution of smaller foulants, which are considered more potent foulants to RO membranes.

A desirable indicator of feed water fouling strength should be capable of indicating the collective fouling strength of all the foulants that contribute to fouling on RO membranes. In addition, the fouling strength indicator can be used in models to quantitatively predict fouling development in full-scale RO processes. Strictly speaking, fouling strength is an intrinsic property of the feed water that should not be dependent on the operating parameters. Hence an ideal fouling strength indicator should give a consistent value for the same feed water, even when the measurements are conducted under different sets of operating parameters, such as membrane resistance and driving pressure.

This chapter describes the development of a more effective measurement of feed water fouling strength using a RO membrane device. A new fouling strength indicator was derived from fundamental principles to quantify the fouling strength of the feed water.

The effectiveness of the proposed fouling strength indicator was investigated with synthetic feed water that consisted of silica colloids in sodium chloride solution. The apparatus and procedure to conduct the measurements and the method to calculate the proposed fouling strength indicator are described in detail. The properties of the proposed fouling strength indicator were systematically studied with fouling experiments at different colloidal concentrations, different driving pressures and with different RO membranes.

4.1 A More Effective Fouling Strength Indicator

Under the driving pressure, permeate flux moves perpendicularly to the membrane surface from the bulk solution and passes through the RO membrane. The foulants contained in the feed water are retained on the membrane surface. The foulant deposition rate onto the membrane surface induced by the permeate flow is

$$j_{\perp} = vc_{f0} \tag{4.1}$$

where $j_{\perp}$ is the foulant flux in the direction perpendicular to the membrane surface, v is the permeate flux at any time and c_{f0} is the foulant concentration. The total amount of foulant M deposited over time t is calculated based on

$$M = \int_0^t j_{\perp} dt = c_{f0} \int_0^t v dt \tag{4.2}$$

The hydraulic resistance of the fouling layer at any point of time is linearly related to the amount of accumulated foulants

$$R_f = r_s M = r_s c_{f0} \int_0^t v dt = k_f \int_0^t v dt \tag{4.3}$$

where k_f is termed as the *fouling potential* and is the product of the specific resistance of the fouling layer (r_s) and particle concentration (c_{f0}). Although fouling potential can be calculated based on r_s and c_{f0} for mono-disperse spherical colloids (as used in the experiments), it may be more practical, especially when the feed water contains more than one type of foulant, to measure fouling potential with a simple fouling experiment discussed later in this chapter. The total hydraulic resistance (R_m) across the membrane and fouling layer can be represented by

$$R_m = R_{m0} + R_f \tag{4.4}$$

where R_{m0} is the clean membrane resistance. Concentration polarization is neglected in Eq. (4.4) as the presence of feed spacer in the membrane cell and the small feed channel height is expected to reduce its significance on the filtration process. Substituting Eq. (4.3) into Eq. (4.4)

$$R_m = R_{m0} + k_f \int_0^t v dt \tag{4.5}$$

Rearranging

$$k_f = \frac{R_m - R_{m0}}{\int_0^t v dt} \tag{4.6}$$

From the above equation, the fouling potential is defined as the increment in membrane resistance when a unit volume of permeate is produced per unit membrane area. The values of R_m and R_{m0} can be easily calculated with

$$R_m = \frac{\Delta p - \Delta \pi}{v_t} \tag{4.7}$$

$$R_{m0} = \frac{\Delta p - \Delta \pi}{v_0} \tag{4.8}$$

where v_t and v_0 represent the measured permeate flux at any time t and t=0 respectively and $\Delta\pi$ is the osmotic pressure. Unlike in most ultrafiltration and microfiltration processes, the permeate flux in RO processes usually declines with time at an almost constant rate. This is because the resistance of the fouling layer is much smaller than the resistance of RO membranes and near constant permeate flux can be maintained during the fouling experiment. In this case, the integral term in Eq. (4.6) can be simplified as

$$\int_0^t v dt = \frac{t}{2}(v_0 + v_t) \tag{4.9}$$

Substituting Eq. (4.7)–(4.9) into Eq. (4.6),

$$k_f = \frac{2(\Delta p - \Delta \pi)}{t} \frac{(v_0 - v_t)}{v_0 v_t (v_0 + v_t)} \tag{4.10}$$

The fouling potential in Eq. (4.10) can be easily determined since all the terms on the right hand side of the expression can be either measured from a RO membrane device or pre-determined by the investigator.

4.2 RO Membrane Device and Procedure for Fouling Potential Measurements

The RO membrane device and measuring procedure for measuring the fouling potential of synthetic feed water that consists of commercial silica colloids in sodium chloride (NaCl, Merck, Darmstadt, Germany) solution are presented in this section.

According to the manufacturer, the commercial silica colloids (Snowtex ZL, Nissan Chemical Industries Ltd., Tokyo, Japan) had a diameter range of 70-100 nm. Samples of the synthetic feed water at different colloidal concentrations required in the fouling experiments were prepared and analyzed with a particle sizer (90Plus, Brookhaven Instruments Corporation, Holtsville, NY). The effective diameter range of the colloids was found to be 128–135 nm. Zeta potentials of the colloids in all synthetic feed water samples were measured with a zeta potential analyzer (ZetaPals, Brookhaven Instruments Corporation, Holtsville, NY) and were found to be negative i.e. coagulation of colloids was not expected in the fouling experiments.

4.2.1 RO Membrane Device

A schematic diagram of the RO membrane device for fouling potential measurements is shown in Fig. 4.1. Filtration was done with a Sepa CF membrane unit (Osmonics, Minnetonka, MN, USA), which had a maximum operating pressure of 6.89 MPa (1000 psi) and a maximum temperature of 177 ºC. A diaphragm pump (Hydra-cell M-03, Wanner Engineering Inc., Minneapolis, MN, USA) provided feed water circulation and driving force for filtration in the membrane cell. The stainless steel feed tank had a capacity of 40 liters and the temperature of the feed water was regulated at 27±0.5°C by the built-in chiller system. Mixing was provided in the tank when the bypassed feed water entered the tank through a specially constructed inlet. The desired driving pressure and the crossflow velocity were achieved by adjusting the bypass valve and the back-pressure regulator. Driving pressure was measured with a pressure gauge (Q828, Winters Instruments, NY, USA) located after the membrane cell. A flow sensor (Signet 2000, Signet, El Monte, CA, USA) was installed after the back-pressure regulator to measure the concentrate flow. Permeate was collected in a glass container

and weighed on a digital mass balance (PG4002-S, Mettler-Toledo, Greifensee, Switzerland).

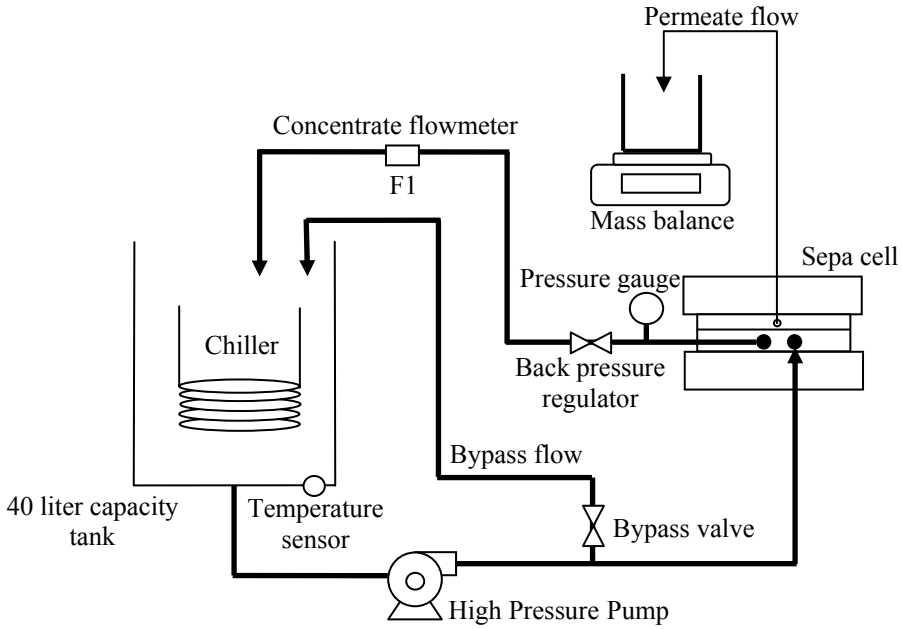

Figure 4.1. Schematic diagram of the crossflow RO membrane cell system

Precut flat sheet polyamide RO membranes (YMAGSP1905 and YMAKSP1905, Osmonics, Minnetonka, MN) with an effective contact area of 138 cm^2 provided the separation in the fouling experiments. Typical fluxes per unit pressure for AG and AK membranes were given by the manufacturers as 0.116 gfd/psi (R_{m0}=1.27×10^{11} Pa·s/m) and 0.226 gfd/psi (R_{m0}=6.47×10^{10} Pa·s/m) respectively. In order to determine the significance of membrane compaction during the fouling experiments, the resistances of both membranes were measured with deionized water (Ultra Clear, SG Water, Barsbüttel, Germany) at increasing driving pressures. From Fig. 4.2, it can be seen that the measured hydraulic resistances of both membranes are similar to the values given by the manufacturer and are not overly affected over the range of driving pressures tested.

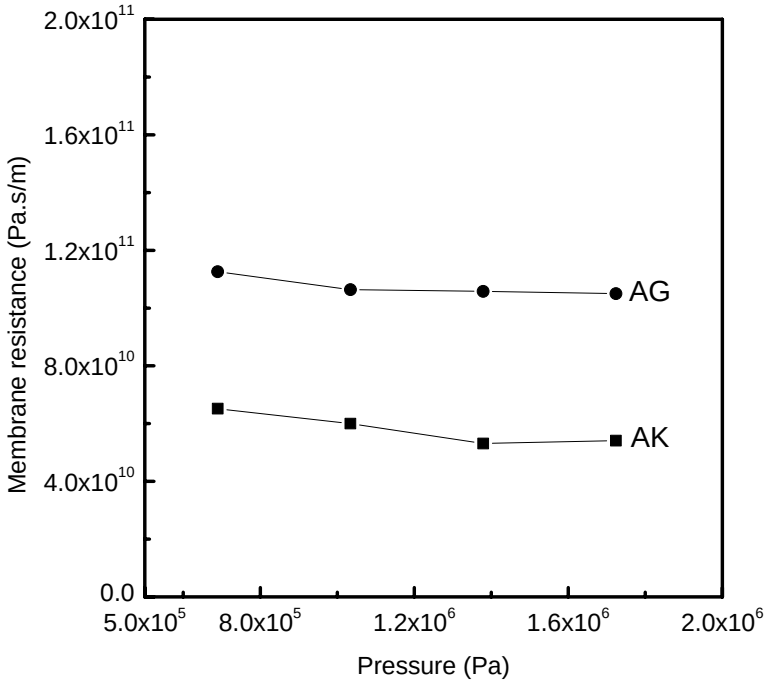

Figure 4.2 Clean membrane resistances of AK and AG membranes at different driving pressures

4.2.2 Measuring Procedure

New flat sheet RO membranes were soaked in deionized water for at least 24 hours at room temperature before being loaded into the membrane cell. Using only deionized water, each membrane was subjected to the required driving pressure at 0.15 m/s crossflow velocity for 24 hours. The first 2 liters of permeate was wasted as it might contain chemical preservatives. Thereafter, the permeate was collected in the glass container and was weighed and recorded every 15 min. The permeate flux was observed to be stable for 24 hours of operation, and the clean membrane resistance was calculated based on Eq. (4.8), with the osmotic pressure term equal to zero. Then sodium chloride stock solution was added into the feed tank to give the required electrolyte concentration of 1000 mg/L. The total dissolved solid (TDS) of feed water

and permeate was measured by conductivity meter (LF538, WTW, Weilheim, Germany) and salt rejection was calculated to ensure that the membrane was not damaged prior to the fouling experiment. Temperature was maintained at 27±0.5°C, and uncontrolled pH was 6.5±0.5. Silica colloids were then added into the feed tank to achieve the required colloidal concentration in the feed water. For the next 8 hours, the weight of permeate collected was recorded at 15 min interval and permeate fluxes were calculated. The colloidal concentrations in the feed water and permeate were measured with a UV spectrophotometer (UV-160A, Shimadzu Corp., Nakagyo-ku, Kyoto, Japan) at a wavelength of 294 nm every hour. While colloidal concentration in the feed water was observed to be stable, no colloids were detected in the permeate for the entire duration of all fouling experiments.

4.3 Properties of Feed Water Fouling Potential

An example of the decline in measured permeate flux with time in the fouling experiments is given in Fig. 4.3. From the measurements, the permeate fluxes at the beginning and the end of the experiment are identified and used with Eq. (4.10) to calculate the fouling potential. When there were fluctuations in the permeate fluxes, the data points could be fitted with a straight line, from which the initial and last permeate fluxes were determined. In this way, the experimental errors were reduced and more accurate fouling potentials could be obtained.

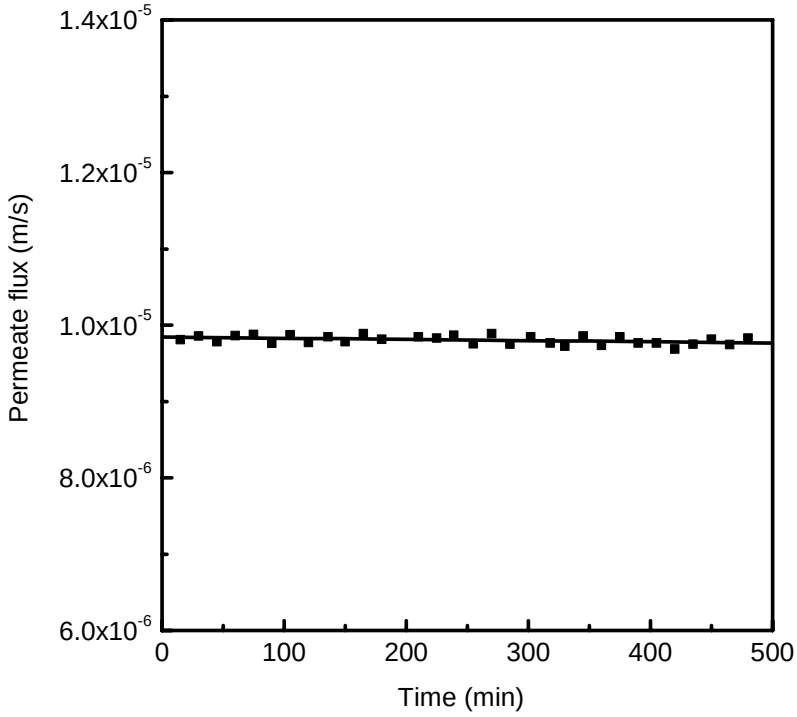

Figure 4.3. Decline of permeate flux with time in the fouling experiment. A smooth line was drawn to fit onto the measured permeate fluxes (symbols)

4.3.1 Effect of Colloidal Concentration

The effect of colloidal concentration on fouling potential was investigated in fouling experiments with AG membranes. Driving pressure, salt concentration and crossflow velocity were maintained at 1.5×10^6 Pa (217 psi), 1000 mg/L NaCl and 0.15 m/s respectively. The decline in the permeate flux with time at different colloidal concentrations is plotted in Fig. 4.4. For better clarity on the characteristics of the graphs, the graphs were fitted with linear lines and the initial permeate flux (y-intercept), rate of permeate flux decline (gradient) and fouling potential of each graph was calculated and shown in Table 4.1.

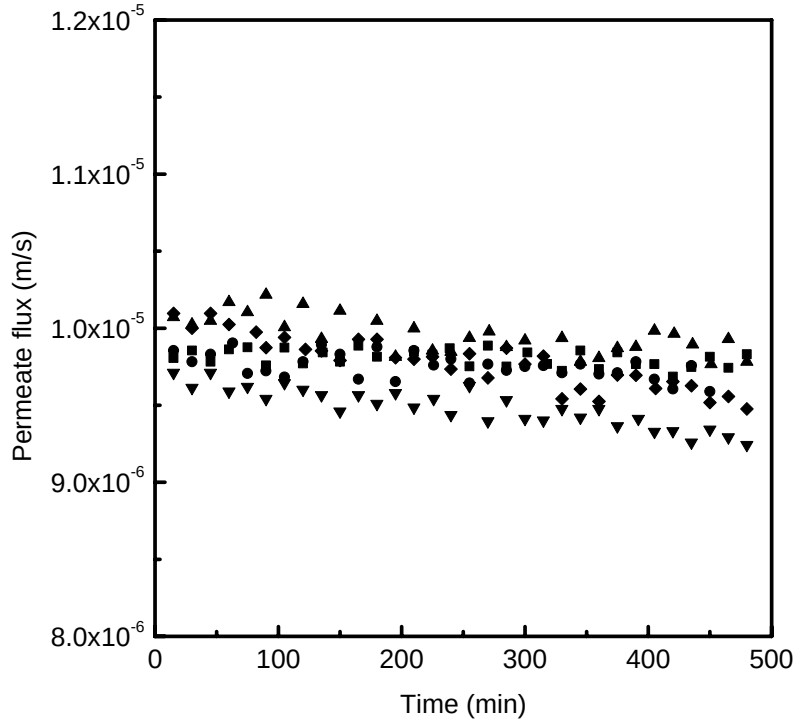

Figure 4.4. Decline of permeate flux with time at different colloidal concentrations of ■ 25 mg/L; ● 50 mg/L; ▲100 mg/L; ▼ 150 mg/L; ♦200 mg/L. Operating conditions: Δp=1.5×10^6 Pa; c_0=1000 mg/L NaCl; u_0=0.15 m/s

Table 4.1. Fouling potentials for different colloidal concentrations

Colloidal Concentration, c_{f0} (mg/L)	Rate of flux decline	Initial flux (m/s)	Fouling potential (Pa·s/m^2)
25	-1.55×10^{-10}	9.84×10^{-6}	3.97×10^9
50	-3.19×10^{-10}	9.83×10^{-6}	8.32×10^9
100	-5.99×10^{-10}	1.01×10^{-5}	1.47×10^{10}
150	-8.22×10^{-10}	9.69×10^{-6}	2.33×10^{10}
200	-1.11×10^{-9}	1.01×10^{-5}	2.87×10^{10}

From Table 4.1, the initial permeate fluxes (at t=0) for all colloidal concentrations are $9.9\pm0.2\times10^{-6}$ m/s. Fluctuation in the initial permeate fluxes is due to the difficulty in maintaining the exact driving pressure for all colloidal concentrations. The rate of flux decline is observed to increase with colloidal concentration. Close examination of the rate of permeate flux decline in Table 4.1 shows that the rate of flux decline is proportional to colloidal concentration. For example, the ratio of flux decline rate at colloidal concentration of 100 mg/L to that at 50 mg/L is about 2:1. This phenomenon could be reasonably explained by the increasing number of colloidal particles at higher colloidal concentration that were available for deposition on the membrane surface. The plot of fouling potential at different colloidal concentrations is shown in Fig. 4.5.

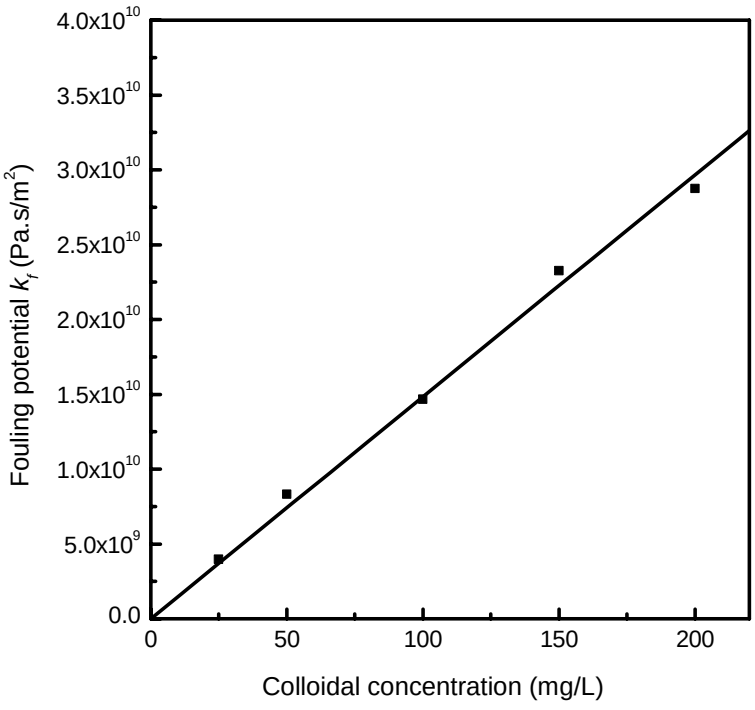

Figure 4.5. Linear relationship between fouling potential and colloidal concentration. Linear correlation coefficient r^2=0.995

The graph explicitly shows a strong linear relationship between the fouling potential and colloidal concentration, as verified in the linear correlation coefficient (r^2) of 0.995. Such linearity between the proposed fouling potential and the foulant concentration in the feed water is a desirable property of the fouling strength indicator.

4.3.2 Effect of Clean Membrane Resistance

Permeate fluxes for two types of RO membranes (AK and AG) were measured independently to determine the fouling potential of feed water with identical colloidal concentration. The driving pressure, crossflow velocity and colloidal concentration were kept at 1.38×10^6 Pa, 0.15 m/s and 50 mg/L respectively in both fouling experiments. The decline of permeate fluxes with time for AG and AK membranes is shown in Fig. 4.6. It is observed that the initial permeate flux of the AK membrane is about two times to that of the AG membrane. This is attributed to the lower membrane resistance of AK membrane as shown in Fig. 4.2. The higher particle deposition rate associated with higher permeate flux of AK membrane results in a higher flux decline rate for the AK membrane compared to the AG membrane. Fouling potentials for both membranes are shown in Table 4.2. The two percent difference in fouling potentials of these two membranes demonstrates that the fouling potential is virtually unaffected by the membrane type. The consistency in fouling potential for both membranes, despite a more rapid flux decline of AK membrane, is attributed to the $(R_m - R_{m0})$ and $\int_0^t v dt$ terms of Eq. (4.6) increasing by the same magnitude. In other words, the membrane permeability has no effect on the measurement of fouling potential even though it is the determinant of permeate flux.

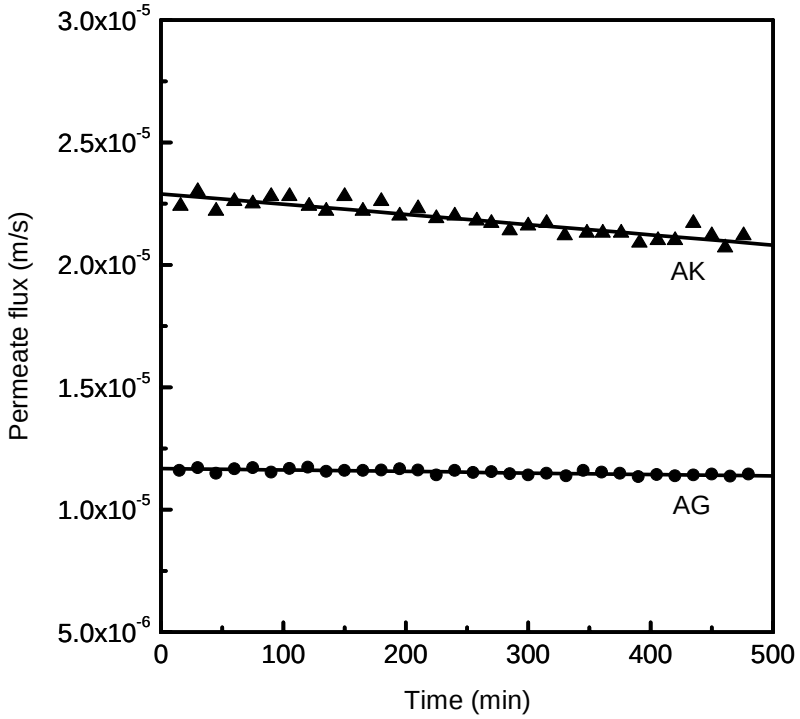

Figure 4.6. Decline of permeate flux with time at different membrane resistances. Operating conditions: Δp=1.38×10^6 Pa; c_0=1000 mg/L NaCl; u_0=0.15 m/s; c_{f0}=50 mg/L

Table 4.2. Fouling potentials with different RO membranes

Membrane type	Rate of flux decline	Initial flux (m/s)	Fouling potential (Pa·s/m^2)
AG	-5.977×10^{-10}	1.17×10^{-5}	8.51×10^9
AK	-4.133×10^{-09}	2.29×10^{-5}	8.66×10^9

4.3.3 Effect of Driving Pressure

As mentioned earlier in this chapter, the fouling potential is an intrinsic property of the feed water and should be ideally independent from the operating parameters. This theoretical definition is only valid if the fouling strength of the feed water remains unaffected by the change in operating conditions. However, if the properties of foulants in the feed water are affected by operating parameters, the fouling potential of the feed water will certainly change with the operating parameters. This is actually also an intrinsic property of the feed water. A fine example is the compaction of fouling layer at high driving pressure. A more compact fouling layer leads to a bigger increment in membrane resistance with the same amount of foulants, resulting in a higher fouling potential measured. The influence of driving pressure on fouling potential was investigated at different driving pressures with AG membranes. A colloidal concentration of 50 mg/L was used in all experiments.

Fig. 4.7 shows the decline of permeate flux with time at different driving pressures. It is observed that the permeate flux declines more rapidly at higher driving pressures, even though the colloidal concentration remains unchanged in the fouling experiments. The rapid flux decline could be attributed to the increase in particle deposition, which is caused by the increase in permeate flux that carries more silica colloids onto the membrane surface when the driving pressure is increased. The fouling potential at different driving pressures is presented in Table 4.3, and is plotted against driving pressure in Fig. 4.8. It shows that fouling potential is not affected by the change in driving pressure, i.e., the fouling potential remains at about 8.7×10^{9} Pa·s/m^2 in the pressure range tested. The reason for this phenomenon is similar to that given for different membrane resistances.

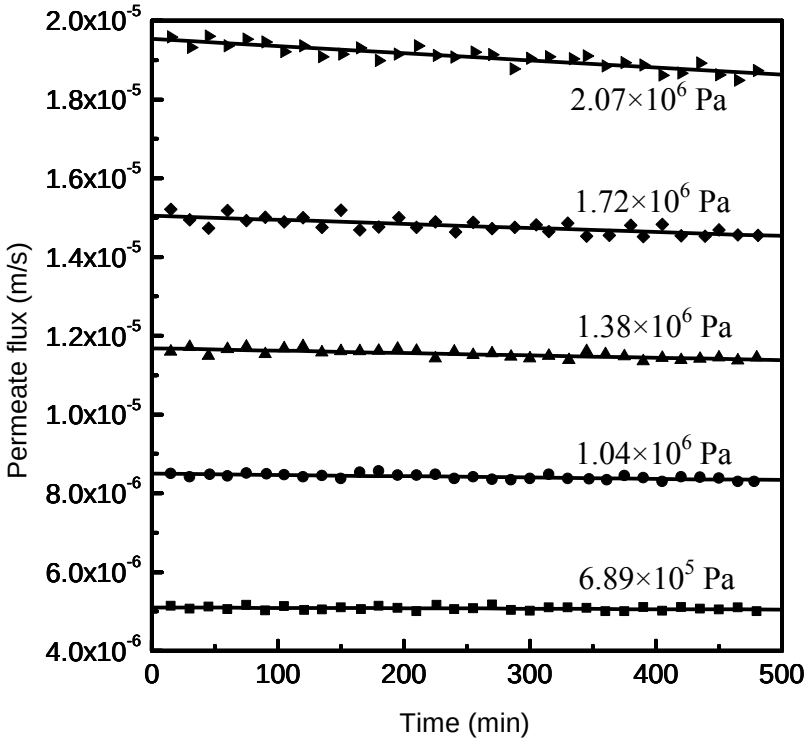

Figure 4.7. Decline of permeate flux with time at different driving pressures. Operating conditions: c_0=1000 mg/L NaCl; u_0=0.15 m/s; c_{f0}=50 mg/L

Table 4.3. Fouling potentials at different driving pressures

Pressure (Pa)	Rate of flux decline	Initial flux (m/s)	Fouling potential ($Pa \cdot s/m^2$)
6.90×10^5	-1.090×10^{-10}	5.10×10^{-6}	8.63×10^9
1.03×10^6	-3.247×10^{-10}	8.50×10^{-6}	8.76×10^9
1.38×10^6	-5.977×10^{-10}	1.17×10^{-5}	8.51×10^9
1.72×10^6	-1.028×10^{-9}	1.50×10^{-5}	8.77×10^9
2.07×10^6	-1.821×10^{-9}	1.95×10^{-5}	8.74×10^9

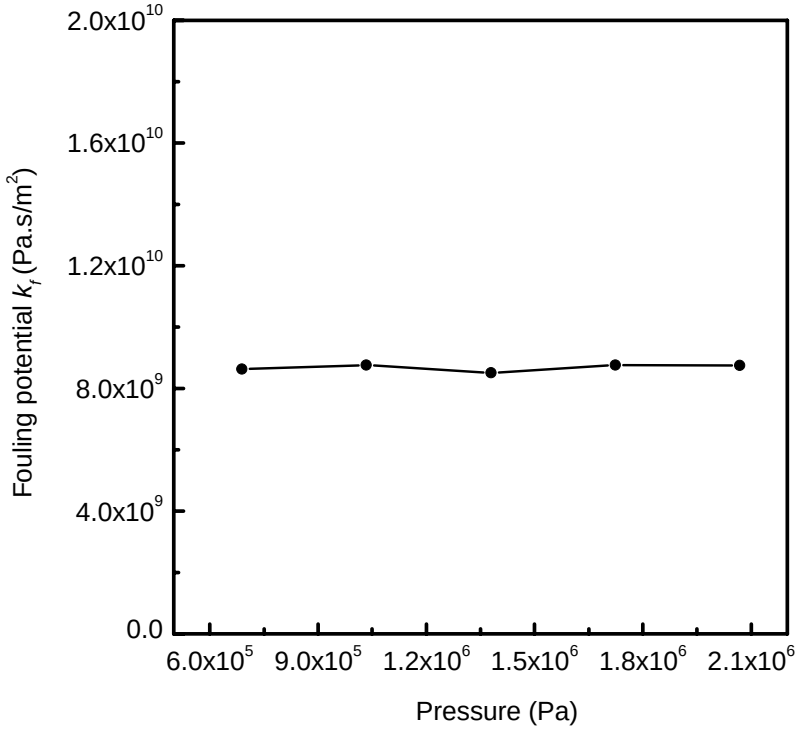

Figure 4.8. Invariant behavior of fouling potential to pressure change

Compaction of the fouling layer is not noticeable in the measured fouling potentials shown in Fig 4.8. The non-response of fouling potential to increasing driving pressure suggests that the duration of the fouling experiment could be shortened by increasing the driving pressure, so that the permeate flux can decline sufficiently to give meaningful results. However, precaution has to be taken to ensure that the fouling potential is measured without fouling layer compaction. Higher measured fouling potential due to fouling layer compaction would result in highly conservative fouling control design, which would increase the operating costs.

In this study, the independence of the fouling potential on driving pressure over the tested range of driving pressures was demonstrated with incompressible colloidal

particles in the synthetic feedwater. However when using real feedwater, significant compaction of the fouling layer can occur at higher driving pressures if the feedwater contains highly compressible foulants, such as organic materials. This could result in different measured fouling potentials with the same feedwater at different driving pressures. To better reflect the fouling strength of the foulants with fouling layer compaction, the fouling potential should be measured at the driving pressure similar to the real RO operation.

4.4 Summary

A more effective method to measure the fouling strength of feed water was developed with RO membranes. The use of RO membranes ensured that all possible foulants in the feed water were captured in the measurements. The fouling strength of feed water was quantified with an accurate fouling strength indicator, termed as fouling potential, which could be easily determined with a small RO membrane device. The derivation of fouling potential from fundamental principles allowed the fouling potential to be used in model to predict fouling development in full-scale RO processes.

The properties of the proposed fouling potential were investigated by conducting fouling experiments on a laboratory crossflow RO membrane cell with synthetic feed water that contained silica colloids. Results demonstrated that the fouling potential was linearly related to the colloidal concentration in the feed water. It was also shown that the fouling potential was not affected by the clean membrane resistance and the driving pressure in the pressure range tested. The insensitivity of the fouling potential to driving pressure in the fouling experiments suggests that the duration of measurement could be shortened by increasing the driving pressure. However,

precautions must be taken when measuring fouling potential at driving pressures higher than the actual value used in full-scale RO system to ensure the effect of fouling layer compaction is not factored into the measurements. When test is done with feedwater that contains highly compressible foulants, it is more accurate to measure the fouling potential at the same driving pressure in the actual full-scale RO operation.

Chapter 5

FOULING DEVELOPMENT AND QUANTIFICATION IN A LONG MEMBRANE CHANNEL

Despite the growing acceptance of RO processes for water and wastewater treatment in recent years, the economic viability of RO water treatment plants is still very much affected by membrane fouling and the effectiveness of fouling control (Bates 1998). Although many new pretreatment processes and membrane cleaning techniques have been developed over the years, membrane fouling has not been well controlled and still remains as the major threat to RO processes. One of the reasons for the ineffective efforts on fouling mitigation and control is the lack of an effective tool for fouling characterization. Hence it is critical to predict the development or extent of fouling in the RO processes and to have an accurate indicator or measurement to express the extent of fouling in RO processes.

It has been known for a long time that the permeate flux decline in a long RO membrane channel is quite different from that observed in a fouling test in a small laboratory membrane device. This fact makes it impossible to quantitatively predict permeate flux decline in the long membrane channel directly from the fouling strength determined with the laboratory membrane device without a well correlated mathematical model. In this chapter, a model that links the fouling behavior of a long RO membrane channel to the feed water fouling potential defined in the previous chapter is presented. Fouling development in a long membrane channel at different operating conditions is systematically investigated and discussed with numerical

simulations. Then the average permeate flux decline, widely used as an indicator for membrane fouling in full-scale RO processes, is examined. The ineffectiveness of the average permeate flux decline to represent membrane fouling in a long membrane channel is verified with a 4m RO membrane channel in the laboratory. Based on the results, a more effective method to measure membrane fouling in full-scale RO processes is proposed. Finally, the advantages of the newly proposed measurement method are demonstrated through numerical simulations.

5.1 Development of Membrane Fouling in Long Membrane Channel

5.1.1 Model Development

In Chapter 3.1.1, the governing equations for the permeate flux or recovery of a long RO membrane channel were developed based on the localized variables and parameters. These equations are also valid when membrane fouling is considered. However, in this case the variables and parameters become time-dependent as well because fouling is a continuous process with time. The governing equations therefore become

$$v(x,t)=\frac{\Delta p(x,t)-\Delta\pi(x,t)}{R_m(x,t)} \tag{5.1}$$

$$\Delta\pi(x,t)=f_{os}c(x,t) \tag{5.2}$$

$$c(x,t)=\frac{1}{u(x,t)H}\left[c_0u_0H-(1-r_{rej})\int_0^x c(\xi,t)v(\xi,t)d\xi\right] \tag{5.3}$$

$$u(x,t)=u_0-\frac{1}{H}\int_0^x v(\xi,t)d\xi \tag{5.4}$$

$$\Delta p(x,t) = \Delta p_0 - \frac{12\lambda\eta}{H^2}\int_0^x u(\xi,t)d\xi \tag{5.5}$$

One of the key difficulties in constructing a model of membrane fouling is to relate the fouling rate with the feed water quality. Quantifying feed water fouling strength with fundamental principles is difficult because of the complexity and the presence of various foulant types in actual feed water. The commonly used silt density index (SDI) and related indices do include all possible foulants in feed water and cannot be quantitatively related to the fouling development in the membrane channel. This problem can be overcome with the more effective fouling potential parameter introduced in Chapter 4. With the fouling potential, the total membrane resistance at any time can be obtained by rewriting Eq. (4.5) in form of localized variables:

$$R_m(x,t) = R_{m0} + k_f\int_0^t v(x,\xi)d\xi \tag{5.6}$$

where $R_m(x,t)$ is the localized total membrane resistance, R_{m0} is the clean membrane resistance and k_f is the fouling potential. The fouling potential provides the quantitative link between the fouling strength of feed water and fouling development in the RO process necessary for accurate prediction. Eqs. (5.1)–(5.6) can be solved numerically for the time dependent (local) permeate flux along the channel.

The average permeate flux, which is a performance parameter of the RO process, is determined as follows:

$$\bar{v}(t) = \frac{1}{L}\int_0^L v(\xi,t)d\xi \tag{5.7}$$

where $\bar{v}(t)$ is the average permeate flux.

5.1.2 Fouling Behavior in a Long Membrane Channel

Unless otherwise specified, the operating conditions for all simulations in this chapter are given in Table 5.1. The characteristic pressure at the start of the filtration is 6.67×10^5 Pa, which is lower than the driving pressure of 1.21×10^6 Pa. Therefore the RO process is initially operated in the thermodynamic equilibrium regime.

Table 5.1. Operating parameters used in the numerical simulations

Operating Parameters	Value
Channel length (m)	6
Channel Height (m)	0.5×10^{-3}
Driving pressure (Pa)	1.21×10^6
Feed Salt Concentration (mg/L)	1000
Osmotic coefficient	68.95
Feed crossflow velocity (m/s)	0.1
Clean membrane Resistance (Pa·s/m)	8×10^{10}
Solute Rejection	0.995
Operating period (days)	100
Fouling Potential (Pa·s/m^2)	1×10^9

Variation of membrane resistance along the membrane channel at different operating times is shown in Fig. 5.1. Membrane resistance is initially uniform along the membrane channel at 8×10^{10} Pa·s/m. When the filtration starts, membrane resistance is observed to increase at different rates along the membrane channel, with the highest rate at the channel entrance. Comparing Fig. 5.1 and Fig. 5.2, it can be seen that the increase of membrane resistance largely coincides with the distribution of the permeate flux along the membrane channel. This is reasonable because the rate of

foulant deposition increases with water flux. The permeate flux is almost negligible in the tail region of the channel during the time interval of 0 to 25 day. The zero-flux region or "unused" membrane channel corresponds to the region where membrane resistance remains unchanged from the clean membrane resistance.

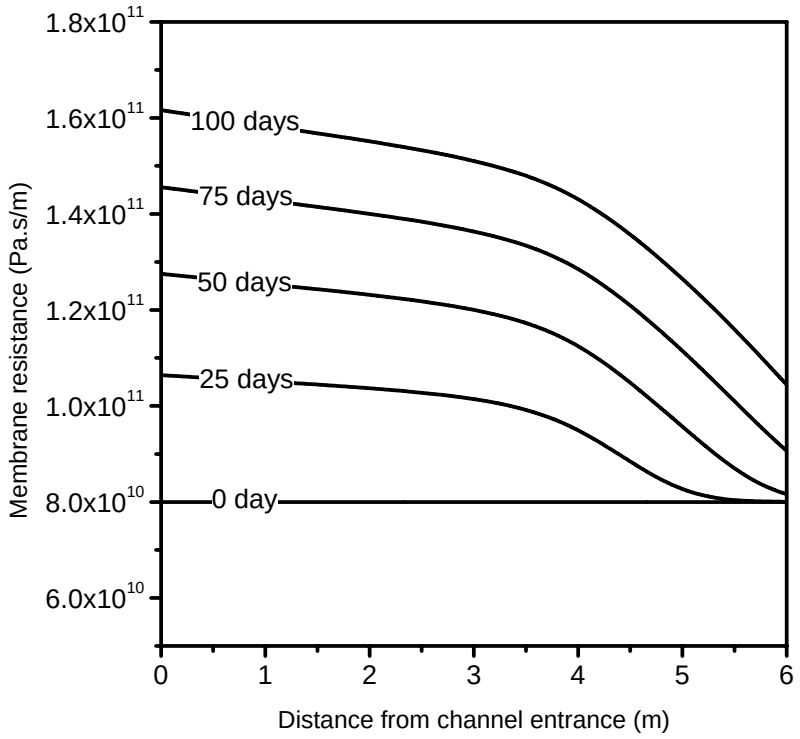

Figure 5.1. Membrane resistance profiles along the membrane channel at different operating times

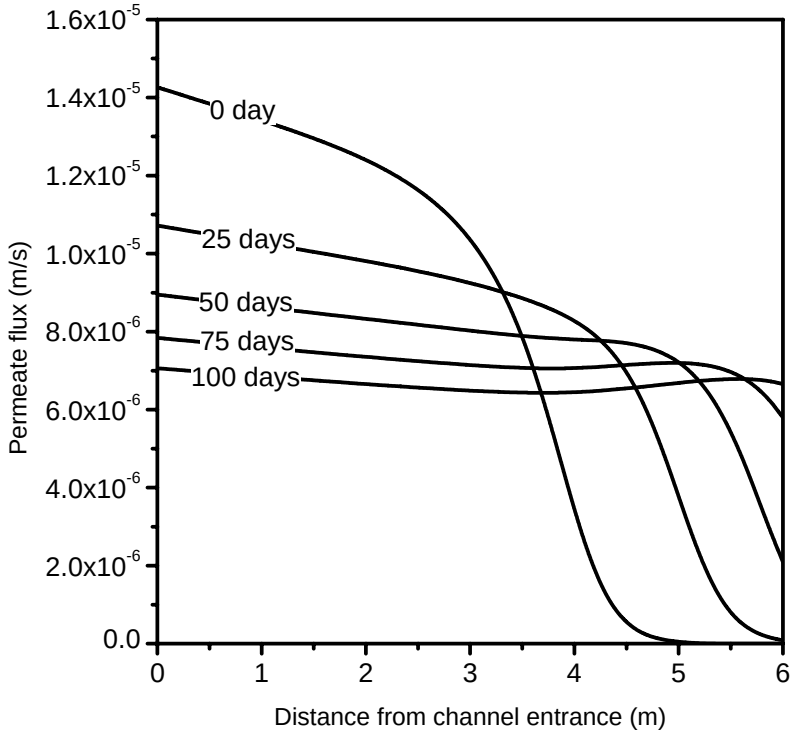

Figure 5.2. Permeate flux profiles along the membrane channel at different operating times

It is observed from Fig. 5.2 that the length of the "unused" membrane channel becomes smaller with membrane fouling. At the same time, the permeate flux at the channel entrance declines with time. After operating for 25 days, the entire membrane channel was utilized to produce permeate. A more evenly distributed permeate flux profile evolves as membrane fouling progresses. This phenomenon is attributed to the strong interplay between the local permeate flux and membrane resistance. At the beginning of filtration, permeate flux usually peaks at the channel entrance. The membrane resistance increases faster due to a higher rate of foulant deposition, which, in turn, causes a more rapid decline in permeate flux. In the region further downstream of the channel, the lower permeate flux induces a lower rate of foulant deposition and

consequently, lower rate of flux decline. Eventually, an evenly distributed flux profile forms along the membrane channel.

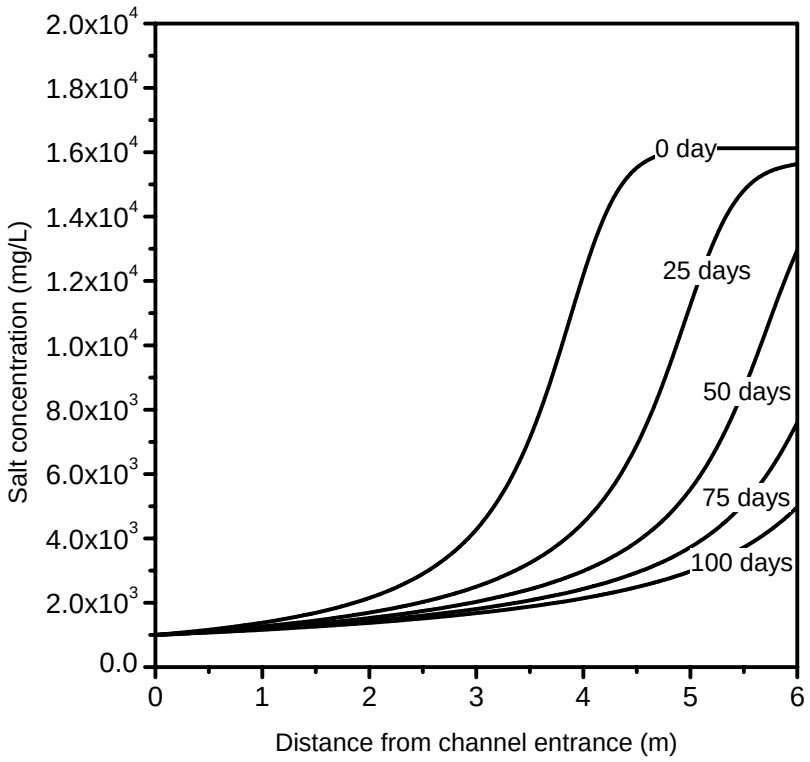

Figure 5.3. Variation of salt concentration along the membrane channel at different operating times

The rapid decline in permeate flux along the membrane channel at the start of filtration was attributed to the build-up of salt concentration along the channel due to the loss of permeate. Fig. 5.3 shows the profiles of salt concentration along the membrane channel at different times. At the start of the filtration, salt concentration is seen increasing rapidly along the membrane channel. The increased osmotic pressure associated with the salt concentration reduces the net driving pressure and permeate flux. The osmotic pressure becomes equal to the driving pressure at about 5m downstream from the channel entrance. Salt concentration remains unchanged in the

remaining part of the channel as there is no permeate flux due to zero net driving pressure. This membrane channel is said to be controlled by thermodynamic equilibrium. Fouling development results in reduced permeate flux that leads to lower salt concentration build-up in the membrane channel and the salt concentration profile shifts towards the channel exit with time. The salt concentration could not reach the equilibrium value within the membrane channel after 25 days of filtration.

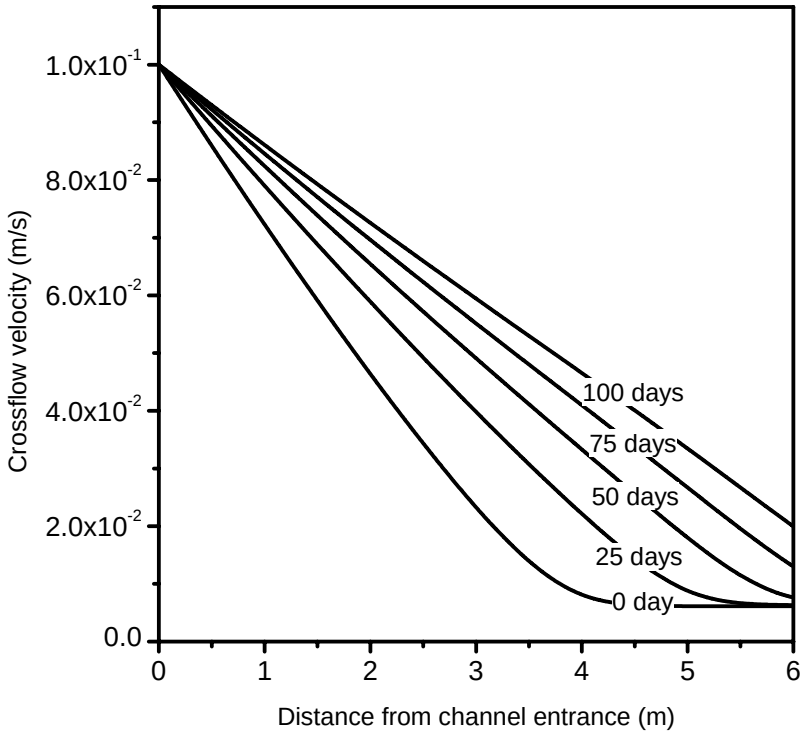

Figure 5.4. Decreasing crossflow velocity along the membrane channel at different operating times

The crossflow velocity profiles at different operating times are shown in Fig. 5.4. Generally, the crossflow velocity decreases along the channel as a result of permeate loss. Corresponding to the salt concentration profile at the start of filtration, the decreasing crossflow velocity becomes uniform along the channel at about 5m from the entrance because no permeate was produced in the remaining part of the channel.

Membrane fouling in the channel is reflected by the upward movement of the crossflow velocity profiles with time. The increase in crossflow velocity along the channel is caused by the reduced amount of water permeating through the membrane when membrane resistance increases with fouling.

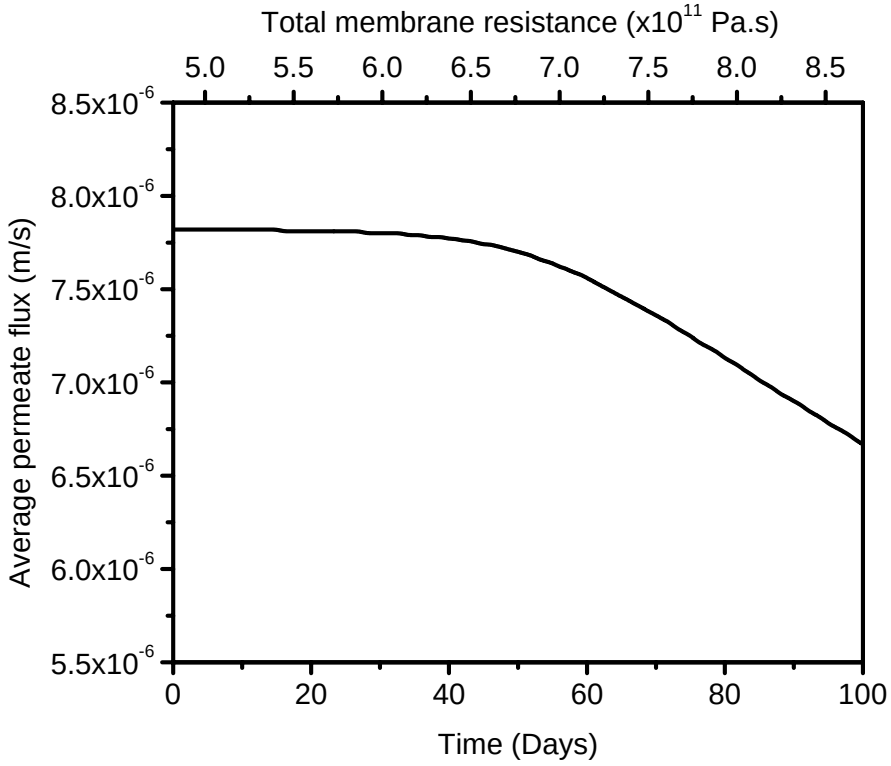

Figure 5.5. Decline of average permeate flux in a 6m long membrane channel at different times and total membrane resistances

The average permeate flux of the 6m membrane channel in the entire filtration period was calculated and is given in Fig. 5.5. The total membrane resistance (per unit width) of the channel at any time was also given in the figure. It is observed in this figure that the average permeate flux remains constant in the first 20 days of filtration before obvious flux decline occurs, despite fouling developing at the start of filtration. This observation is entirely different from those of the small laboratory RO membrane

devices, where the average permeate flux declined immediately at the start of the fouling experiments. The consistency in average permeate flux in the initial period of filtration could be explained based on the permeate flux profiles at t=0 and t=25 days in Fig. 5.2. It is noted that the areas under both curves, which represented permeate flow rate per unit width of channel, are closely identical. Fouling merely changes the permeate flux profile but the amount of permeate produced remains the same. The occurrence of constant average permeate flux coincides with the occasions when the tail region of the membrane channel is "unused" to produce permeate. This is a special feature of RO processes under thermodynamic equilibrium restriction. Fouling is manifested in a decline of the average permeate flux when the membrane channel is fully utilized to produce permeate after 20 days of filtration. The average permeate flux seems to readily decline only after the total membrane resistance has reached a threshold value. The invariant behavior of average permeate to membrane fouling in the initial period of filtration means that fouling development in a long membrane channel under thermodynamic equilibrium restriction cannot be interpreted by the basic membrane transfer theories.

Another unique feature of long membrane channels at thermodynamic equilibrium is that the increase in the driving pressure can only increase the average permeate flux marginally. The average permeate flux of a long membrane channel was simulated for driving pressures of 1.21×10^6 and 1.38×10^6 Pa with other operating parameters given in Table 5.1. As shown in Fig. 5.6, the increase in driving pressure by 15% could only yield about 2% increase in the average permeate flux. However, the increase in driving pressure increases the length of the "unused" channel to produce permeate and this

prolongs significantly the duration of constant average permeate flux in the initial period of filtration.

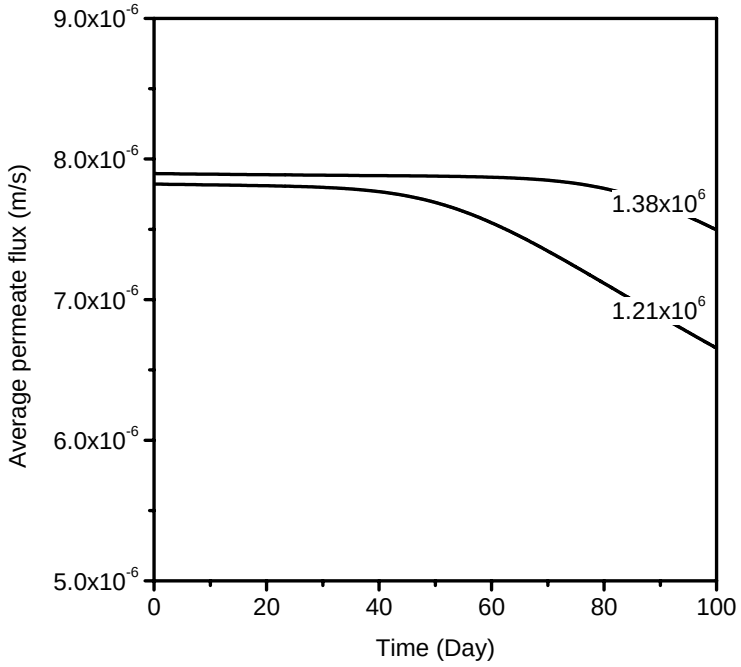

Figure 5.6. The effect of increasing driving pressure on average permeate flux with time

5.1.3 Effect of Fouling Potential on Fouling Behavior

The average permeate fluxes in a 6m long membrane channel were simulated over a period of 100 days for feed water of different fouling potentials with other operating parameters given in Table 5.1. The simulation results presented in Fig. 5.7 reveal the paramount importance of feed water fouling potential on fouling development in the membrane channel. The initial average permeate fluxes for feed waters of all fouling potentials are identical since the same clean membrane was used in the simulations. The period of constant average permeate flux becomes shorter as fouling potential increases. The threshold membrane resistance at which average permeate flux becomes sensitive to fouling is reached in a shorter time when more foulants at higher

fouling potential are deposited onto the membrane surface. It is also noted that the average permeate flux decline is more rapid for higher fouling potential. This phenomenon is similar to those observed in fouling tests using laboratory RO membrane cell systems.

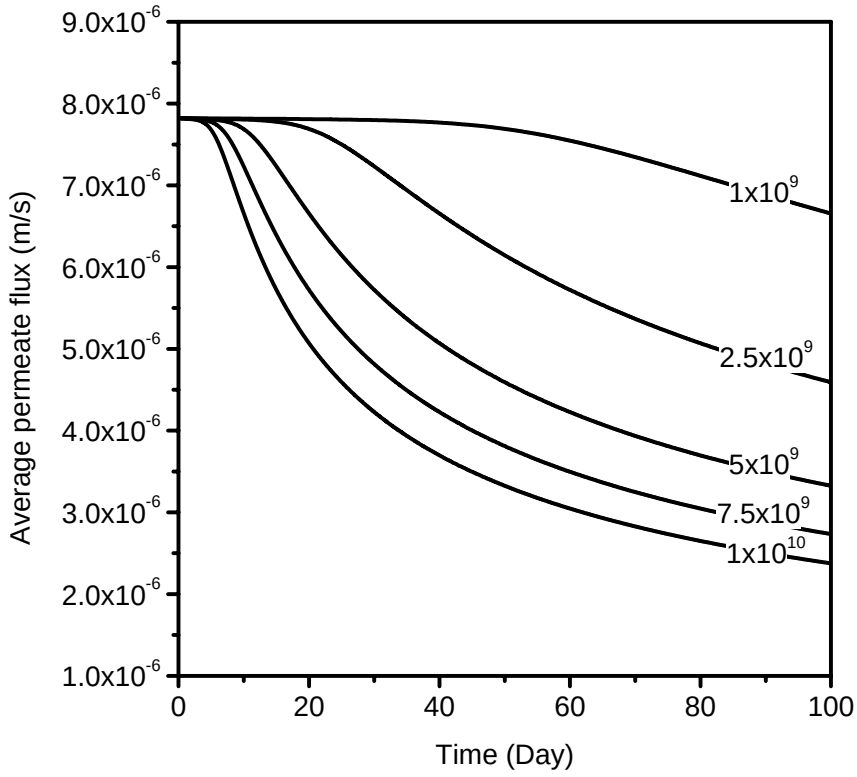

Figure 5.7. Fouling development in a 6m long membrane channel for different feed water fouling potentials

5.1.4 Effect of Channel Length on Fouling Behavior

A long membrane channel is commonly adopted in most full-scale RO systems to increase the permeate recovery. This is achieved by connecting several membrane elements in series in a pressure vessel. Under the operating conditions in Table 5.1, the average permeate flux in membrane channels of different lengths was simulated for feed water with a fouling potential of 10^9 Pa·s/m^2, and the results are shown in Fig. 5.8.

Channel length is found to play a key role on the behavior of average permeate flux with membrane fouling. A period of constant average permeate flux does not occur in 1m and 3m channel as the average permeate fluxes of both channels decline immediately from the start of the filtration. The profiles of these average permeate fluxes are similar to that obtained from the small laboratory RO systems. An initial period of constant flux is observed in 6m and 9m channels and the duration of the constant flux increases markedly with channel length.

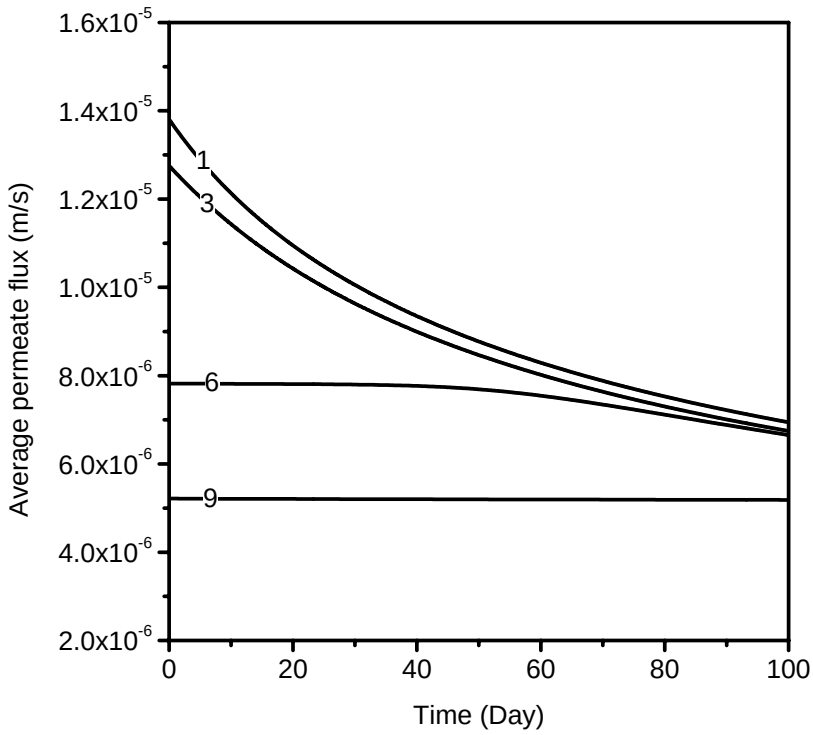

Figure 5.8. Effect of channel length on fouling development in a long membrane channel

It is also observed that longer membrane channels have lower initial average permeate fluxes, even though the operating parameters are identical. This finding indicates that the maximal recovery of the feed water has been reached and, therefore, it could not be

further increased by increasing channel length. Because the amount of permeate is fixed, a lower average permeate flux is obtained for a longer membrane channel. Interestingly, this behavior is not observed or reported in the older generation of RO membranes. These RO membranes have higher membrane resistances that cause the increase of permeate production with longer membrane channel. In a long membrane channel of highly permeable RO membranes, it is possible that the permeate rate is not influenced by the membrane area, but by the thermodynamic properties of the system.

5.1.5 Effect of Clean Membrane Resistance on Fouling Behavior

The advancement in membrane technology has led to the development of highly permeable membranes with high salt rejection. Current RO membranes are at least one order of magnitude more permeable than those in the 1980s. It is interesting to know how clean membrane resistance affects the fouling behavior in a long membrane channel. Fig. 5.9 shows the profiles of average permeate flux with time for two different clean membranes with operating conditions in Table 5.1. An initial period of constant average permeate flux is observed for the membrane channel with clean membrane resistance of 8×10^{10} Pa·s/m. In contrast, average permeate flux is observed to decline immediately from the start of filtration at clean membrane resistance of 1.5×10^{11} Pa·s/m with identical feedwater. The initial period of constant average permeate flux is absent in the RO channel with higher clean membrane resistance because the membrane channel works in the mass transfer controlled regime.

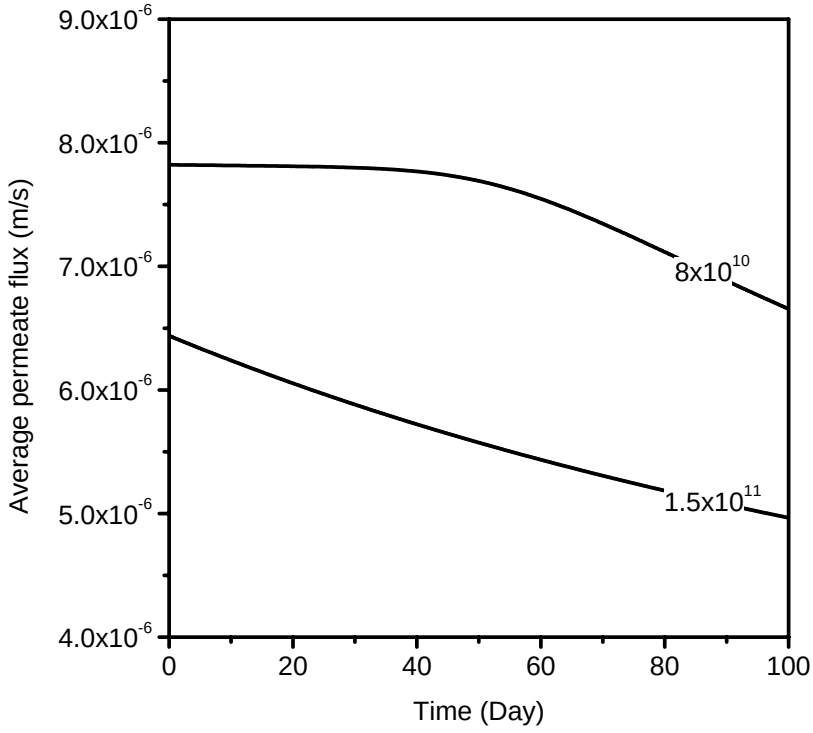

Figure 5.9. Fouling behavior for 6m long membrane channels with different clean membrane resistances

5.1.6 Effectiveness of Membrane Cleaning

When the performance of the RO membrane systems deteriorates to unacceptable levels, membrane cleaning is usually conducted to remove foulants from the membrane surface and reduce the membrane resistance. In this section, the effectiveness of membrane cleaning on the performance of a long membrane channel is simulated and investigated. The membrane resistance at the beginning of the n^{th} filtration run is determined by the following equation:

$$R_n = R_{n-1} + (1 - E_r)\Delta R_{n-1} \tag{5.8}$$

where R_{n-1} is the initial membrane resistance in the $n\text{-}1^{th}$ filtration run, and ΔR_{n-1} is the increment in membrane resistance during the $n\text{-}1^{th}$ filtration run. E_r is the characteristic removal percentage to indicate the efficiency of membrane cleaning with certain chemicals or procedures. When the initial membrane resistance is known, the change in average permeate flux as a result of fouling development in a long membrane channel and membrane cleaning can be simulated with Eqs. (5.1)-(5.8).

Fig. 5.10 shows the average permeate flux over the first 200 days of operating a long RO membrane channel. Operating parameters used in the simulation are shown in the figure caption. The filtration is initially controlled by thermodynamic equilibrium at the given driving pressure. Cleaning efficiency E_r was set at 85% on the assumption that membrane cleaning could not completely remove all the foulant on the membrane surface. Average permeate flux is observed to be constant in the first 20 days of filtration before it begins to decline thereafter. The first membrane cleaning was carried out at the 50^{th} day when average permeate flux declined by 10% of the start-up value. Since the simulation did not take into consideration the time taken to clean the membranes, restoration of average permeate flux was immediate and is shown as a vertical line. Average permeate flux could be fully restored by membrane cleaning even though the cleaning efficiency was only 85%. Membrane cleaning is able to bring the process back to the thermodynamic equilibrium restriction so that the average permeate flux could be completely restored. However, because of the incomplete removal of foulants, the time taken to the next membrane cleaning was shorter. This explains why the period of constant average permeate flux decreases with each cleaning. As more and more foulants remain after each cleaning, the average

permeate flux could not be fully restored after certain number of cleanings (the 3rd cleaning cycle in Fig. 5.10).

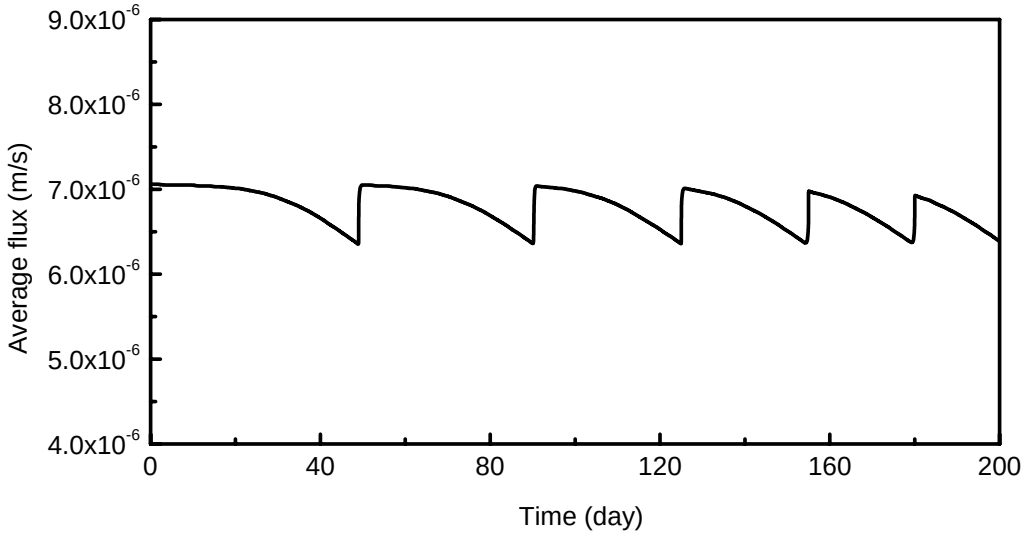

Figure 5.10 Behavior of average permeate flux with membrane cleaning in the first 200 days of filtration. Operating parameters are: L = 6 m, $H = 0.7\times10^{-3}$ m, $\Delta p = 1.5\times10^{6}$ Pa, u_0 = 0.1 m/s, c_0 = 3000 mg/L, f_{os} = 68.95 Pa·L/mg, λ = 10, $R_m = 8\times10^{10}$ Pa·s/m, $k_f = 3\times10^{9}$ Pa·s/m^2, allowable flux decline = 10% and cleaning efficiency = 85%. Δp^* was calculated to be 9.3×10^{5} Pa

The effectiveness of membrane cleaning could also be misrepresented by the observed cleaning frequency when the RO process was operating in thermodynamic equilibrium regime. An example is shown in Fig. 5.11a-b where simulations were done at different driving pressures. Although the cleaning efficiency and fouling rate are identical in both cases, a higher driving pressure seems to suggest better cleaning performance as the number of cleanings required at 1.7×10^{6} Pa is much less than that at 1.5×10^{6} Pa. The reason for lower cleaning frequency at higher driving pressure is attributed to the higher threshold membrane resistance required to shift the flux-controlling mechanism

to mass transfer restriction. Since the fouling rate was identical at both driving pressures, the time taken to observe any average permeate flux decline was longer at higher driving pressure. It should be noted, however, that the quantity of foulants in the membrane channel is not less at the higher driving pressure. With lower cleaning frequency, more foulants are expected to accumulate in the channel at higher driving pressure.

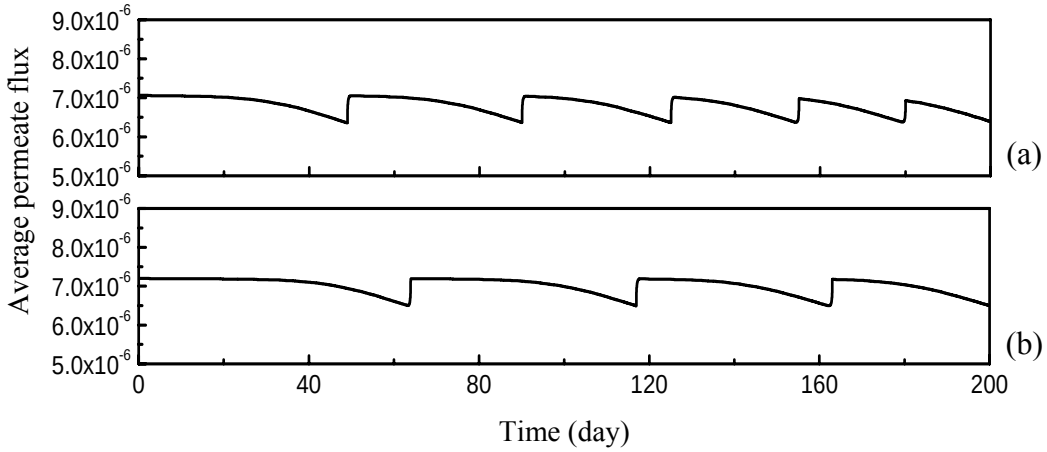

Figure 5.11 Effect of driving pressure on effectiveness of membrane cleaning in the first 200 days of filtration. (a) 1.5×10^6 Pa; (b) 1.7×10^6 Pa. Operating parameters are: L = 6 m, $H = 0.7\times10^{-3}$ m, $\Delta p = 1.5\times10^6$ Pa, u_0 = 0.1 m/s, c_0 = 3000 mg/L, f_{os} = 68.95 Pa·L/mg, λ = 10, $R_m = 8\times10^{10}$ Pa·s/m, $k_f = 3\times10^9$ Pa·s/m^2, allowable flux decline = 10% and cleaning efficiency = 85%

5.2 Inadequacy of Current Fouling Measurement Method

5.2.1 Current Fouling Measurement Method

Membrane fouling is customarily indicated or measured by flux decline with time in a RO process. In some research articles and books, membrane fouling is phenomenologically defined as "flux decline with time" (Mulder 1997; Saad 1999;

Rico and Arias 2001). It is commonly believed that under fixed operating conditions, any increase in total membrane resistance due to the accumulation of foulants on the membrane surface will result in a flux decline. Conversely, any occurrence of constant flux indicates the absence of membrane fouling. This method to measure membrane fouling is fundamentally based on the membrane transfer theories that water flux is inversely proportional to the total membrane resistance, which includes the clean membrane resistance and the additional resistance due to membrane fouling. This fouling measurement method has been used since the 1960s when the application of RO process in full-scale water treatment was still in its infancy. The method worked well with the older generations of membranes, which usually had very high clean membrane resistances. Average permeate flux was demonstrated to strictly follow a linear relationship with the net driving pressure and the reciprocal of the membrane resistance under all possible operating conditions. Any membrane fouling would be readily reflected by a decline in the average permeate flux.

5.2.2 Practical Observations

An initial period of constant average permeate flux up to several months was observed in full-scale RO processes before obvious flux decline occurred (Khedr 1998; Saad 1999; Rico and Arias 2001; Al-Wazzan *et al*. 2002). According to the current fouling measurement method, the constant average permeate flux indicates the absence of fouling. It is believed that membrane fouling could be effectively prevented if the average permeate flux is designed below a “critical” value. But this presumption becomes questionable when average permeate flux starts to decline after some time under the same operating conditions. The cleaning efficiency of a fouled membrane is usually measured by the extent of flux restoration. Foulants are deemed to be fully

removed if the average permeate flux is completely restored to its initial value. However, it was observed that this fully restored average permeate flux could not be maintained for as long as when new RO membranes were initially used (Saad 1999). The duration of fully restored flux became shorter in subsequent cleanings (Ebrahim and El-Dessouky 1994) until the initial average permeate flux could not be fully restored.

The above practical observations point out the ineffectiveness of the average permeate flux to reflect membrane fouling in the initial period of operation. The reason for such incompetency is that the RO membranes are most probably operated in the thermodynamic equilibrium regime. Simulations in the previous section demonstrated that membrane fouling in thermodynamic equilibrium restricted RO processes developed at the very beginning of filtration but was not readily reflected in the average permeate flux until the total membrane resistance had exceeded a threshold value such that mass transfer restriction becomes the dominating mechanism. The average permeate flux was also shown to be ineffective to reflect the increasing amount of foulants on the membrane surface after membrane cleaning when the membrane flux was controlled by thermodynamic equilibrium.

It is highly possible for RO processes to operate in the thermodynamic equilibrium regime under common operating conditions, given the drastic drop in the resistance of RO membranes over the years. Table 5.2 shows the clean membrane resistances of the new and the old generation of membranes calculated from the test data given by the membrane manufacturers. The drop in membrane resistance of the new highly permeable membranes reduces the characteristic pressure of the membrane channel

and places the system in thermodynamic equilibrium regime at common driving pressures.

Table 5.2. Clean membrane resistances of old and new generation RO membranes

Types of RO membrane	Resistance (Pa·s/m)
1980s membrane	
Homopolar Cellulose Acetate (CA)	2.07×10^{12}
Cellulose Triacetate (CTA)	1.83×10^{12}
Cellulose Acetate Propionate (CAP)	2.71×10^{12}
Cellulose Acetate Butyrate (CAB)	2.26×10^{12}
Currently used membrane	
Hydranautics SWC1 (CP)	4.11×10^{11}
Hydranautics LFC2 (CP)	1.13×10^{11}
Hydranautics ESPA (CP)	8.43×10^{10}
Osmonics SG4040F (TFC)	1.35×10^{11}
Osmonics SC8040F (TFC)	6.64×10^{11}

CP: Composite Polyamide; TFC: Thin-film composite

5.3 Experimental Verification and Discussions

The ineffectiveness of average permeate flux to reflect membrane fouling in the initial period of RO operation under the thermodynamic equilibrium regime was further verified with a 4m long RO membrane channel in the laboratory. The synthetic feed water contained silica colloids in sodium chloride solution. Fouling in the membrane system could be inferred from any decrease in colloidal concentration in the feed water, which was monitored with a UV spectrophotometer. Additional silica colloids were added into the feed tank to reinstate the designed colloidal concentration if there

was a drop in colloidal concentration in the feed water. Average permeate flux was measured with time at different colloidal concentrations and initial characteristic pressures by setting different feed crossflow velocities.

5.3.1 Materials and Method

Membrane Modules - The ESPA-2540 spiral-wound RO membrane modules (Hydranautics, Oceanside, CA, USA) were described in detail in Chapter 3.3.1.

Silica Colloids – Information on commercial silica colloids Snowtex ZL (Nissan Chemical Industries, Tokyo, Japan) was given in Chapter 4.2. Colloidal concentrations in the feed solution and permeate were measured with a UV spectrophotometer (UV-160A, Shimadzu Corp., Kyoto, Japan) at wavelength of 294 nm. In order to obtain the correlation between the absorbance (unit measured by the UV spectrophotometer) and the colloidal concentration, water samples containing known colloidal concentrations were prepared and measured with the UV spectrophotometer prior to the fouling experiments.

Experimental Setup - The experimental RO setup was described in detail and schematically shown in Chapter 3.3.1. An automatic logging system or datalogger was also installed to continuously monitor the vital operating parameters.

Experimental procedure - The RO membrane modules and feed tank were first cleaned with EDTA solution (high pH) and citric acid (low pH). Both cleaning solutions were drained without being circulated back into feed tank before the feed tank was filled with deionized water to flush the membrane modules. The feed tank

was refilled with deionized water and sodium chloride was added to provide the osmotic pressure. The salt solution was circulated throughout the RO system at the designed driving pressure and feed flow. Temperature was maintained at 27±0.5°C and uncontrolled pH was 6.5±0.5. The RO system was run for 12 hours to ensure stable operating conditions, after which silica colloids were added into the feed tank to give the designed colloidal concentration. Operating parameters were recorded every 10 mins by the automatic datalogger. Driving pressure was maintained by adjusting the back pressure needle valve. The colloidal concentration of the feed and permeate water was measured every hour with the UV spectrophotometer for 10 hours everyday. Additional silica colloids required to maintain the colloidal concentration were calculated after each measurement and added into feed tank.

Table 5.3. Operating parameters used in the fouling experiments

Parameters \ Experiment	A	B	C	D
Feed NaCl concentration (mg/L)	980	1000	994	1079
Driving pressure (Pa)	1.26×10^{6}	1.01×10^{6}	1.05×10^{6}	1.14×10^{6}
Feed crossflow velocity (m/s)	0.052	0.051	0.058	0.072
Feed colloidal concentration (mg/L)	30	10	300	300
Clean membrane resistance (Pa·s/m)	7.85×10^{10}	7.97×10^{10}	6.21×10^{10}	6.11×10^{10}
Characteristic pressure (Pa)	7.13×10^{5}	7.1×10^{5}	6.25×10^{5}	7.7×10^{5}

Table 5.3 shows the actual operating conditions used in the fouling experiments. The characteristic pressure for each experiment was calculated with Eq. (3.11) and is shown in the table. All fouling experiments were expected to operate in the thermodynamic equilibrium regime as the driving pressures were significantly above the respective characteristic pressures. Slight variations in non-testing operating parameters were reasonably permitted as repeating the experiments under exact conditions proved to be highly difficult and time consuming. This is because most of the operating parameters were interdependent i.e. adjusting one parameter might affect other parameters. For example, adjusting the feed crossflow velocity would change the driving pressure.

5.3.2 Effect of Colloidal Concentration on Fouling Behavior

Fig. 5.12 shows the fouling behavior of the membrane over an operating period of 10,000 min with feed water containing of 30 mg/L of silica colloids. The average permeate flux in the first 1500 min is observed to be steady before obvious flux decline occurs. During this period of constant average permeate flux, the colloidal concentration in the feed water was measured at regular intervals and silica colloids were added into the feed tank to maintain the colloidal concentration. The fitted cumulative mass of silica colloids added into the feed tank is shown as a solid curve in Fig 5.12. The continuous addition of silica colloids into the feed tank is a clear indication that fouling is taking place in the experiment. However, the accumulation of colloids on membrane surface is not reflected as a decline in the average permeate flux. This is clearly a feature of RO processes operating in the thermodynamic equilibrium regime.

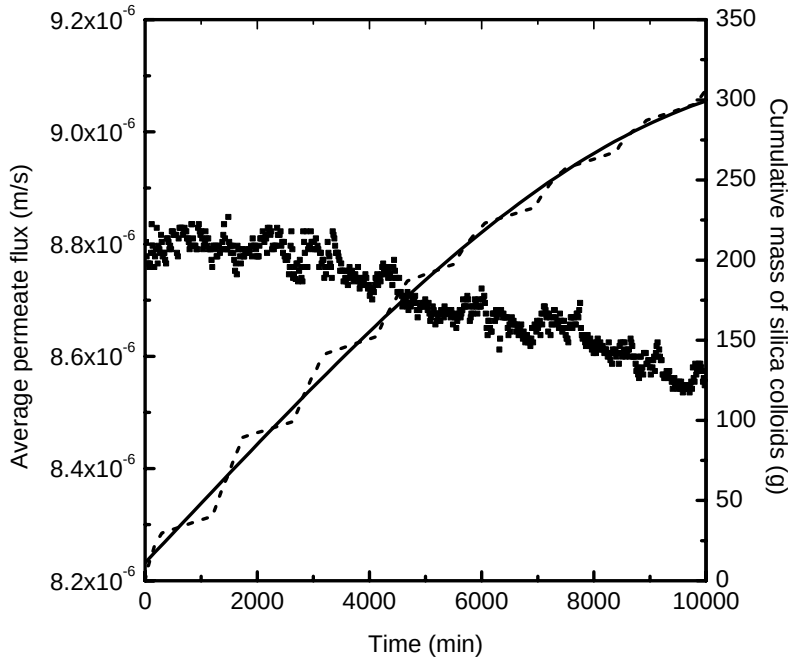

Figure 5.12. Decline of average permeate flux with time at colloidal concentration of 30 mg/L. Scatter points are measured average permeate fluxes; Dash curve is cumulative mass of silica colloids added to maintain colloidal concentration; Solid curve is Gaussian fit of dash curve with r^2=0.995

Under similar operating conditions, the colloidal concentration in the feed water was reduced to 10 mg/L in another experiment to investigate the effect of colloidal concentration on fouling development. It is revealed in Fig. 5.13 that the lower colloidal concentration increases the period of constant average permeate flux to about 4500 min. The longer duration of constant average permeate flux at lower colloidal concentration is attributed to a lower fouling rate, as fewer colloids deposited on the membrane surface. Hence more time is required for the total membrane resistance to reach the threshold value where the average permeate flux becomes sensitive to increasing membrane resistance (mass transfer regime). Theoretically, the total membrane resistance required to observe the decline in average permeate flux should

be about the same, if the operating conditions, other than colloidal concentration, are identical. However it is shown in Table 5.4 that the experiment with 30 mg/L of colloidal concentration requires slightly higher amount of silica colloids to observe the flux decline. This could be attributed to the higher driving pressure in the experiment, which requires a higher total membrane resistance to reach the mass transfer regime.

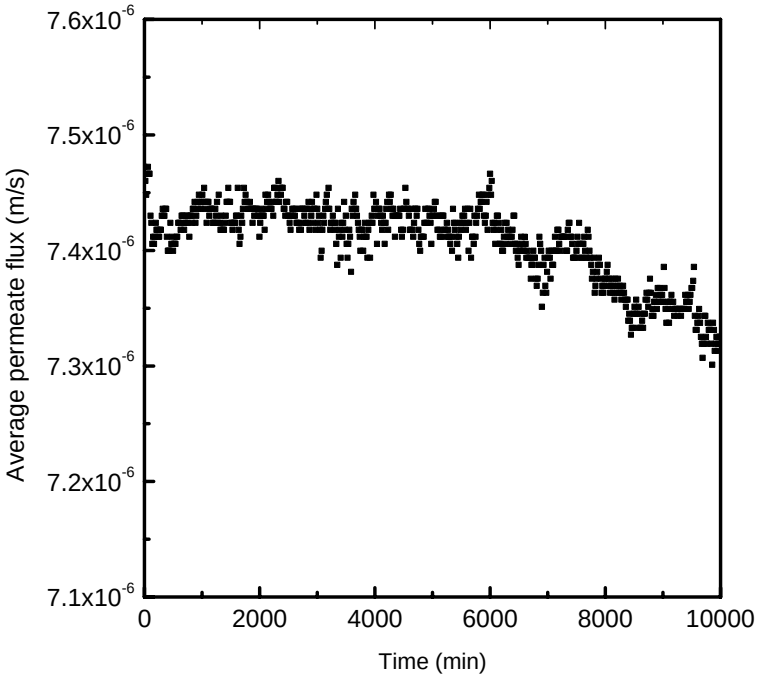

Figure 5.13. Fouling development in the 4m RO membrane channel using feed water with 10 mg/L of colloidal concentration

Table 5.4. Cumulative mass of silica colloids added at flux decline for different colloidal concentrations

Fouling Experiment	Colloidal Concentration (mg/L)	Cumulative mass of silica colloids added (g)
A	30	68
B	10	58

5.3.3 Effect of Characteristic Pressure on Fouling Development in Long RO Membrane Channel

The fouling behavior in a long membrane channel was investigated at different characteristic pressures by setting the feed crossflow velocities at 0.058 and 0.072 m/s. Figs 5.14 and 5.15 show the fouling behavior in the 4m RO membrane channel at characteristic pressures of 6.25×10^5 Pa and 7.7×10^5 Pa respectively. To reduce the experimental time, the colloidal concentration in both experiments was increased to 300 mg/L.

It is observed that constant average permeate flux is sustained over a period of about 150 min at a characteristic pressure of 6.25×10^5 Pa. When the characteristic pressure is increased to 7.7×10^5 Pa by adjusting the feed crossflow velocity to 0.072 m/s, a constant average permeate flux is only observed for about 100 min. Although both experiments were operating in the thermodynamic equilibrium regime (Table 5.3), the experiment with characteristic pressure nearer to the driving pressure required less total membrane resistance to reach the mass transfer regime. In this case, it would take a shorter time to observe average permeate flux decline with feed water of the same colloidal concentration. This finding is further verified in Table 5.5 where the cumulative mass of silica colloids that had been added at the beginning of the average permeate flux decline was found to be lower for higher characteristic pressure.

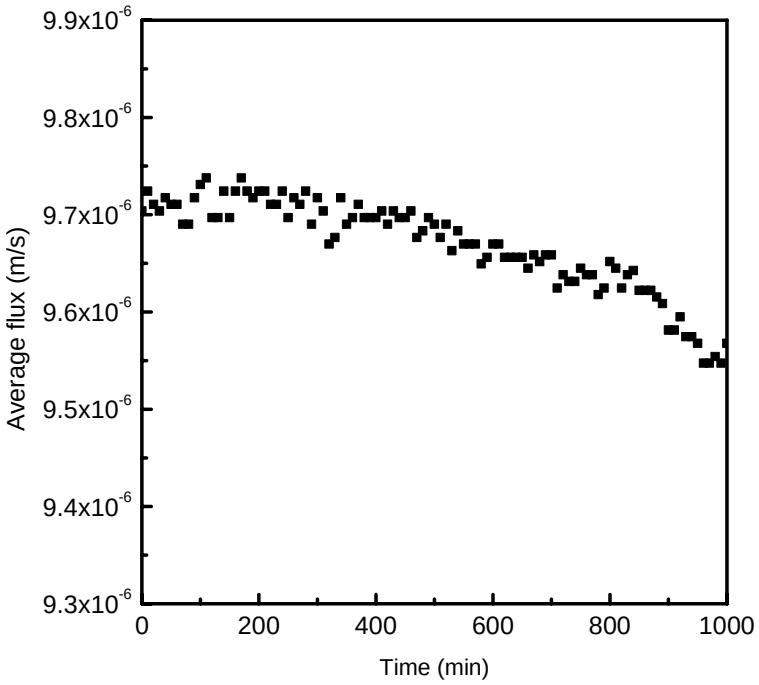

Figure 5.14. Variation of average permeate flux with time at characteristic pressure of 6.25×10^5 Pa

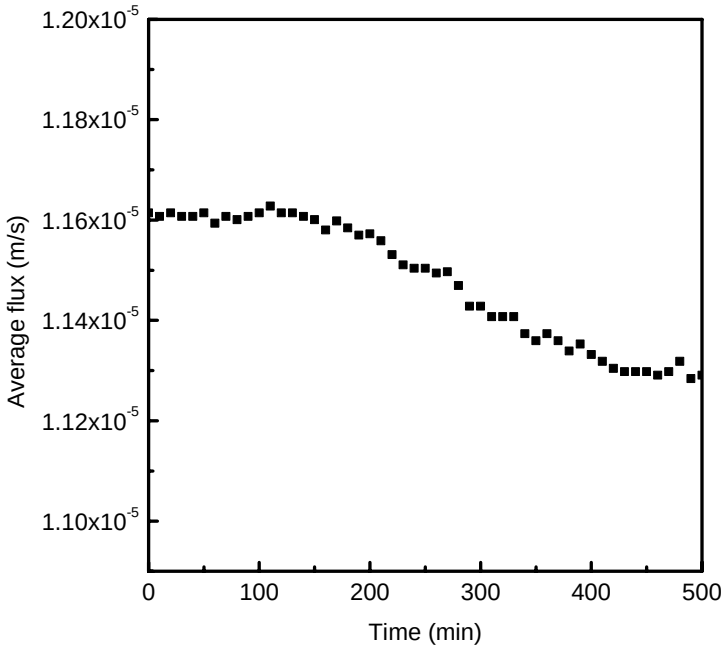

Figure 5.15. Fouling behavior observed with characteristic pressure of 7.7×10^5 Pa

Table 5.5. Cumulative mass of silica colloids added at flux decline for different characteristic pressures

Fouling Experiment	Characteristic pressure (Pa)	Cumulative mass of silica colloids added (g)
C	6.25×10^5	106
D	7.7×10^5	77

The occurrence of the thermodynamic equilibrium restriction in the RO processes signified the urgent need for more research efforts on fouling development and its quantification in a long membrane channel. Simulations and experimental observations demonstrated that average permeate flux in RO processes restricted by thermodynamic equilibrium was not affected by membrane fouling. The development of a more effective fouling measurement method to quantify membrane fouling in the thermodynamic equilibrium regime is imperative.

5.4 A More Effective Fouling Measurement Technique

A pertinent membrane fouling measurement technique should be able to detect the increase of membrane resistance because it is the most fundamental feature of membrane fouling. The fouling measurement technique should also be reasonably easy to implement. Based on these considerations, a lumped parameter termed as the filtration coefficient F, is introduced to reflect the overall membrane resistance as

$$F = \frac{1}{L}\int_0^L \frac{1}{R_m}\,dx \tag{5.8}$$

It can be seen from Eq. (5.8) that an increase in membrane resistance at any point of the membrane channel will cause a corresponding decrease in the filtration coefficient. When there is membrane fouling in the membrane channel, the value of the filtration coefficient of the membrane channel will decrease with time. Therefore, the filtration coefficient is an intrinsic indicator of fouling in a long membrane channel that is independent of average permeate flux. Only in cases when the flux is controlled by mass transfer, the average permeate flux can be related to the filtration coefficient by the following equation

$$\bar{v} = F\left(\Delta p - \Delta \pi\right) \tag{5.9}$$

Although the filtration coefficient is essentially a different way to represent the membrane resistance, its advantages over the direct use of the membrane resistance are obvious in a long membrane channel. First, the filtration coefficient is a collective parameter that describes the whole system with a single value while the membrane resistance is a distributive parameter that varies along the membrane channel. Secondly, it is practically impossible to measure or determine the membrane resistance distribution in the membrane channel, but the filtration coefficient of a membrane channel can be easily determined with a simple filtration test, which is conducted at any driving pressure below the characteristic pressure of clean membrane channel. The filtration coefficient can be readily calculated from the measured average permeate flux and the net driving pressure with Eq. (5.9).

The filtration coefficient is equivalent to the average permeate flux for fouling characterization in the mass transfer regime because in this regime any increment in membrane resistance is immediately reflected in the average permeate flux. The

filtration coefficient remains an effective fouling indicator in the thermodynamic equilibrium regime as well because it is directly related to the increase in membrane resistance. Membrane resistance increases as long as there is membrane fouling. The remaining problem is that the filtration coefficient cannot be determined in the thermodynamic equilibrium regime. The problem can be easily overcome by temporarily reducing the driving pressure to the mass transfer regime for the measurement of the filtration coefficient. This method, however, can give an accurate measurement of the filtration coefficient if the fouling layer is not affected by the change in the driving pressure. It may only give a qualitative indication of fouling development when the fouling layer is highly compressible. In the case of brackish water desalination highly permeable RO membranes, the proposed method to determine the filtration coefficient should be accurate because of the low driving pressure.

By comparing the filtration coefficient at any time with the initial filtration coefficient, membrane fouling can be quantitatively expressed by a fouling index I_f defined as

$$I_f = \frac{F_i - F_t}{F_i} \tag{5.10}$$

where F_i and F_t are the values of filtration coefficient at times 0 and t, respectively. The value of zero ($I_f = 0$) indicates absence of membrane fouling, while the value of one ($I_f = 1$) indicates the most serious fouling such that the membrane becomes impermeable. The fouling index can also be effectively used to assess the efficiency of membrane cleaning. By comparing the fouling indexes before and after membrane cleaning, the effectiveness of membrane cleaning can be realistically evaluated. If the

fouling index is reduced to zero, the membrane cleaning method is said to be capable of removing the foulants 100 percent from the fouled RO membrane.

The use of the filtration coefficient to describe fouling in the full-scale RO process is illustrated in Fig. 5.16. The driving pressure for the RO process is indicated in the figure by Δp_1. The straight lines, indicated with filtration coefficients F_0 to F_3, are the average permeate fluxes at different times under mass transfer restriction. The filtration coefficients are also the slopes of the straight lines. The average permeate flux restricted by thermodynamic equilibrium is plotted with dotted line. The line F_0 with the largest slope describes the average permeate fluxes of the clean RO membrane at the start of operation. At the start of the operation under pressure Δp_1, the average permeate flux of the membrane channel is indicated by Point A at the intersection of thermodynamic equilibrium curve and the driving pressure Δp_1. Thermodynamic equilibrium restriction is the limiting mechanism because it has a smaller average permeate flux than that with the mass transfer restriction at driving pressure Δp_1. The filtration coefficient decreases gradually with time as fouling develops in the membrane system. When the mass transfer flux line passes F_2, the average permeate flux restricted by mass transfer gives a lower value and the flux-controlling mechanism shifts from thermodynamic equilibrium to mass transfer restriction. The observed average permeate flux is now indicated by Point B, where flux line F_3 intersects with the driving pressure.

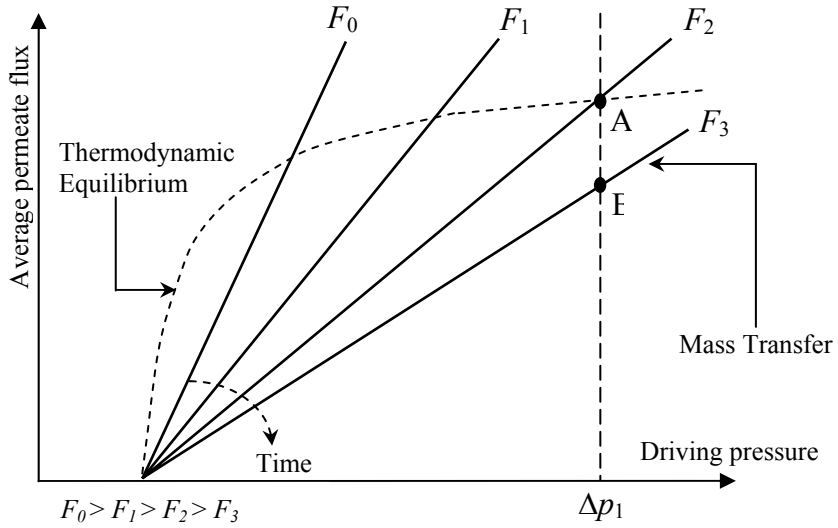

Figure 5.16. A schematic presentation of fouling development in a long membrane channel with the use of filtration coefficients

The effectiveness of the new fouling measurement method can also be demonstrated with the simulations presented in Table 5.6. At a driving pressure of 1.65×10^6 Pa, the performance of the RO system is evaluated at the end of the 2nd year. If the average permeate flux decline is used to indicate fouling, the constant average permeate flux over the two years would indicate an absence of fouling in the RO process. However, the fouling index has a value of 0.31, which is calculated using Eq. (5.10) by lowering the driving pressure to 0.35×10^6 Pa. The fouling index makes more sense because 20% annual increase in membrane resistance was assumed in the initial problem. In another scenario, membrane cleaning is carried out at the end of the 4th year and the total membrane resistance could be reduced to the level at the end of the 1st year ($I_f = 0.17$). Although the foulants are not 100 percent removed (I_f is not equal to zero), the initial average permeate flux can be fully restored.

Table 5.6. The effect of fouling development on average permeate flux for RO process (Observed average permeate fluxes under mass transfer restriction are given in bold)

Driving Pressure (10^6 Pa)	Thermodynamic equilibrium restricted average permeate flux (10^{-6} m/s)	Mass transfer restricted average permeate flux (10^{-6} m/s)				
		0 year	1	2	3	4
		Membrane resistance (10^{11} Pa·s/m) with assumed annual increment of 20%				
		2.19	2.63	3.16	3.79	4.55
0.21	0	**0**	**0**	**0**	**0**	**0**
0.35	1.67	**0.63**	**0.52**	**0.44**	**0.36**	**0.30**
0.69	2.92	**2.20**	**1.84**	**1.53**	**1.27**	**1.06**
0.83	3.13	**2.83**	**2.36**	**1.96**	**1.64**	**1.36**
1.1	3.39	4.09	3.41	**2.84**	**2.37**	**1.97**
1.38	3.54	5.35	4.46	3.71	**3.09**	**2.58**
1.65	3.65	6.61	5.51	4.58	3.82	**3.18**
1.93	3.72	7.87	6.55	5.45	4.55	3.79
2.21	3.78	9.13	7.60	6.33	5.28	4.39
2.48	3.82	10.39	8.65	7.20	6.00	5.00
2.76	3.85	11.65	9.70	8.07	6.73	5.61
3.03	3.88	12.91	10.75	8.95	7.46	6.21
3.31	3.91	14.17	11.80	9.82	8.19	6.82
3.59	3.93	15.43	12.85	10.69	8.91	7.43
Filtration coefficient F at Δp=0.35×10^6 Pa (m/Pa·s)		4.57×10^{-12}	3.8×10^{-12}	3.16×10^{-12}	2.64×10^{-12}	2.2×10^{-12}
Fouling Index		-	0.17	0.31	0.42	0.52

*feed salt concentration is 3000 mg/L

5.5 Summary

Membrane fouling is customarily indicated or measured by the average permeate flux decline with time in a RO process. This relationship is based on the membrane transfer theories which state that water flux is inversely proportional to the membrane

resistance. Hence the observation of constant average permeate flux with long RO membrane channel implies the filtration was free from membrane fouling. However, the average permeate flux began to decline after some time, even though the same operating conditions were maintained. In addition, the average permeate flux after membrane cleaning could not be fully restored for as long as when new RO membranes were initially used. The duration of fully restored flux became shorter in subsequent cleanings until the initial average permeate flux could not be fully restored.

Simulations demonstrated that thermodynamic equilibrium restriction could become the controlling mechanism for the average permeate flux in a long RO membrane channel under common operating conditions. Average permeate flux under the thermodynamic equilibrium regime was insensitive to the change in membrane resistance. This explains why the average permeate flux remained constant in the initial period of filtration, despite the increase in membrane resistance due to membrane fouling. It was only after the membrane resistance had reached a threshold value that mass transfer restriction became the dominating mechanism and any increase in membrane resistance was reflected in a decline of average permeate flux. It was also shown in the simulations that higher driving pressure and longer channel length could prolong the period of constant average permeate flux by increasing the threshold membrane resistance value.

The insensitivity of average permeate flux as an indicator of fouling under the thermodynamic equilibrium regime was verified with fouling experiments using a laboratory RO setup with a 4m long membrane channel. Experimental results demonstrated a period of constant average permeate flux under constant driving

pressure before the average permeate flux declined. Membrane fouling took place right from the start of the experiments, since additional silica colloids had to be added into the feed tank to maintain the colloidal concentration. Some operating parameters were varied in the fouling experiments and their effects on the average permeate flux were reasonably explained and discussed.

A more effective fouling measurement technique involving the use of a filtration coefficient and a fouling index was proposed. These indicators or measurements of membrane fouling in full-scale RO processes are more relevant than the average permeate flux decline because they are intrinsically related to the membrane resistance. The new method was equivalent to the conventional method of average permeate flux decline under mass transfer regime. Membrane fouling in the thermodynamic equilibrium restricted regime could also be readily reflected with the new method by temporarily reducing the driving pressure to the mass transfer restricted regime. The filtration coefficient and fouling index could also be used to assess the effectiveness of membrane cleaning.

Chapter 6

DEVELOPMENT OF DIFFERENTIAL PRESSURE IN A SPIRAL-WOUND MEMBRANE CHANNEL

The spiral-wound RO module, one of the most popular membrane configurations in water and wastewater treatments for its high packing density and other superior features, is characterized by a narrow feed channel filled with network structured spacers. These feed spacers are essential parts of the membrane module that provide mechanical support for the void space between membrane sheets. At the same time, feed spacers are highly susceptible to deposition and attachment of foulants containing in the feed stream (AWWA committee, 1998; Mulder, 1996). As schematically shown in Fig. 6.1, foulants in the feed flow are captured by spacers or preferentially accumulate near spacers, which reduces the cross-sectional area of the feed channel and leads to an increase in hydraulic impedance of the channel.

Channel narrowing or blockage by foulants captured by the spacers may not necessarily cause significant decline in permeate flux (Coker and Sehn, 2000; Duranceau, 2000). Due to the high pressure difference (usually >100 psi or 6.9×10^5 Pa) across the RO membranes, a dense fouling layer on the membrane surface with substantial hydraulic resistance is needed to noticeably affect the permeate flux. The foulants captured or accumulated on or around the spacers usually have a porous structure that would not completely cover the membrane surface to form a dense fouling layer. However, this type of fouling can cause substantial differential pressure in a long narrow channel. In fact, the differential pressure between the feed and exit

ends of the feed channel is often used as an indicator of membrane fouling (Coker and Sehn, 2000; Gabelich et al., 2003; Lopez-Ramirez et al., 2002; Redondo and Casanas, 2001). Driving pressure has to be increased with an increase of the differential pressure to maintain a constant feed flow rate to the RO membrane system. Membrane cleaning in practical RO processes is commonly triggered by a certain differential pressure in the pressure vessels.

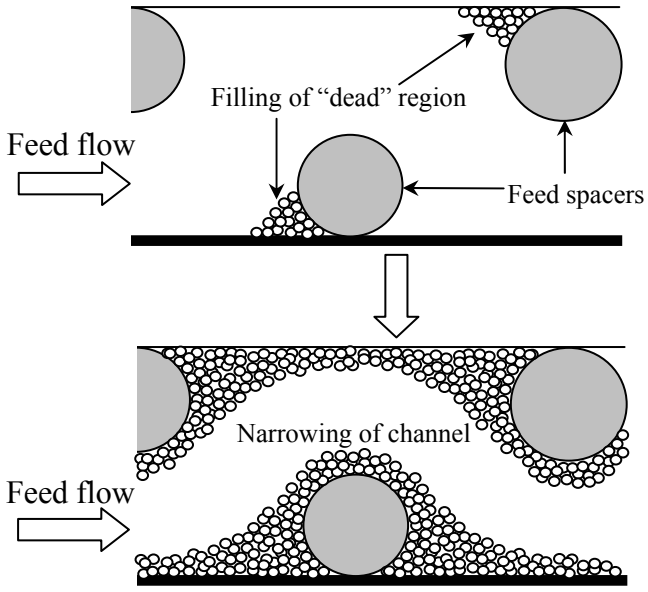

Figure 6.1. Illustration of channel blockage due to capture of foulants by the feed spacers

In this chapter, a mechanistic model is developed for the development of differential pressure in the feed channel with time. The differential pressure in the feed channel was simulated under various operating conditions and the effects of various factors on differential pressure are discussed with the simulations. Finally, simulations of the differential pressures are compared with the in-plant observations of a RO water reclamation plant.

6.1 Model Development

The feed channel of a spiral-wound module can be represented by an unwound flat channel with the same spacers, as the curvature of the module does not have significant influence on the system's performance (Van der Meer and Van Dijk, 1997). For easy interpretation, the complex structure of the spacer-filled channel is represented with an "equivalent channel". The equivalent channel is defined as an imaginary spacer free channel whose "hydraulic height" is so determined that its specific frictional pressure drop is equal to that in the real channel. Therefore the effects of the spacers and captured foulants on differential pressure are treated as the consequence of channel narrowing due to foulant deposition as shown in Fig. 6.2.

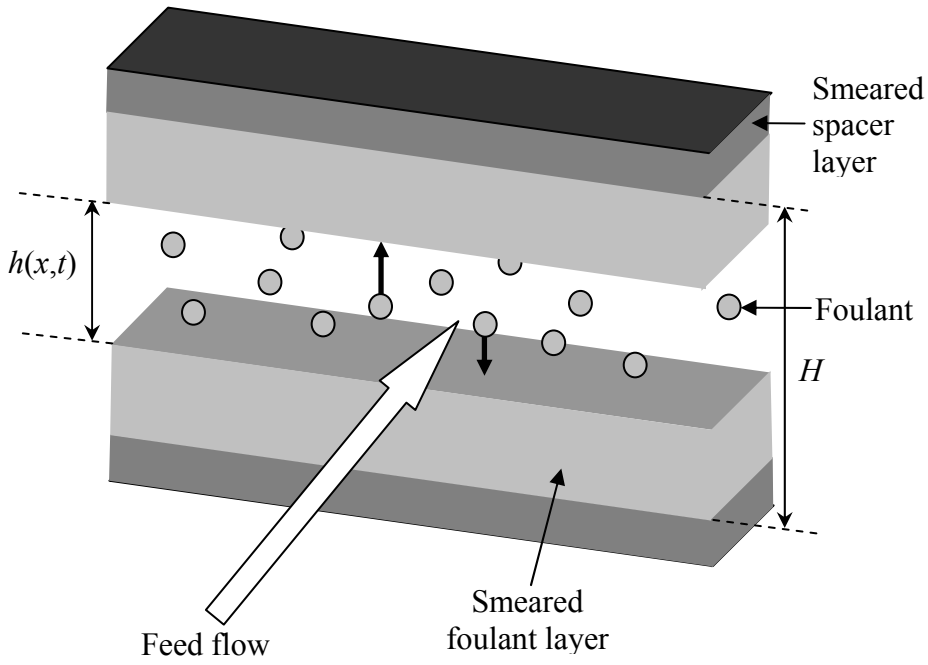

Figure 6.2. Schematic description of an equivalent spacer-free feed channel. Uniform dark grey layer indicates the smeared feed spacer and smeared foulant layer is shown in light grey

While the smeared layer for the spacers is a constant, the thickness of the smeared fouling layer increases as more foulants are captured. By tracking the change in fouling layer thickness, the differential pressure in the feed channel can be effectively related to the amount of foulants captured or accumulated in the feed channel.

The differential pressure in a channel can be calculated with the Darcy-Weisbach equation (Fried and Idelchik, 1989)

$$\Delta p_d = \frac{\lambda \rho_w}{2} \int_0^x \frac{u^2}{D_h} dx \tag{6.1}$$

where Δp_d is the differential pressure, λ is the friction coefficient, ρ_w is the density of the feed water, and D_h is the hydraulic diameter. For a rectangular channel whose width is much greater than its height, the hydraulic diameter is defined as

$$D_h = 2h \tag{6.2}$$

where h is the channel height. Therefore, the differential pressure in any location x of the feed channel at time t can be determined by

$$\Delta p_d = \Delta p_0 - \Delta p(x,t) = \frac{\lambda \rho_w}{4} \int_0^x \frac{u(\xi,t)^2}{h(\xi,t)} d\xi \tag{6.3}$$

where Δp_0 and $\Delta p(x,t)$ are feed and localized driving pressure respectively, and ξ is the dummy variable. In order to calculate the differential pressure in the feed channel with Eq. (6.3), the channel height and crossflow velocity in the channel are required.

The capture of foulants in the spacer-filled feed channel is a complex phenomenon and the structure of the captured foulants in the channel can be extremely complex. It is

practically impossible at this stage to model channel height accurately. Instead, a simple concept or scenario is proposed for tracking the change in channel height in this study. The central assumption is that the capture rate of the foulants at any section in the channel is proportional to the total foulant flux passing the section. Then the total foulant flux along the channel is governed by

$$\frac{dI}{dx} = -kI \tag{6.4}$$

where I is the total downstream foulant flux per unit width of the channel and k is the capture coefficient. The capture coefficient, which is assumed to increase with the narrowing of the feed channel, can be determined by

$$k = k_0 + \alpha\left(1 - \frac{h(x,t)}{H}\right) \quad \text{where } \alpha > 0 \tag{6.5}$$

where k_0 is the capture coefficient of clean channel, H is the clean membrane height and α is the correcting factor for the capture coefficient as a result of channel narrowing.

Accumulation of the captured foulants reduces the channel height at any location and is related to the total foulant flux with the following equation

$$\frac{dh}{dt} = -\frac{1}{\rho}\frac{dI}{dx} = -\frac{k}{\rho}I \tag{6.6}$$

where ρ is the density of the fouling layer. The change of channel height with time at any point of the channel can be determined numerically with Eqs. (6.4)-(6.6).

Following the derivation for the fixed channel height by Song *et al*. (2002), the water conservation relationship in the feed channel with variable channel height can be written as,

$$u(x,t)=\frac{1}{h(x,t)}\left[u_0 H-\int_0^x v(\xi,t)d\xi\right] \tag{6.7}$$

where u is the crossflow velocity, u_0 is the feed crossflow velocity, and v is the permeate velocity. In the modeling study, the crossflow velocity can be treated as evenly distributed along the channel height (Zhou *et al*., 2006). The permeate velocity is determined by the basic membrane transport equation

$$v(x,t)=\frac{\Delta p(x,t)-f_{os}c(x,t)}{R_m} \tag{6.8}$$

and

$$c(x,t)=\frac{1}{u(x,t)h(x,t)}\left[c_0 u_0 H-(1-r_{rej})\int_0^x c(\xi,t)v(\xi,t)d\xi\right] \tag{6.9}$$

where $c(x,t)$ and $\Delta p(x,t)$ are the salt concentration and driving pressure respectively, f_{os} is the osmotic pressure coefficient, R_m is the membrane resistance, and r_{rej} is the nominal salt rejection. Concentration polarization is reasonably assumed negligible with the presence of feed spacers and small channel height (Zhou *et al*., 2006). The driving pressure $\Delta p(x,t)$ (= $\Delta p_0 - \Delta p_d(x,t)$) can be easily determined when the differential pressure in the feed channel is known.

The development of differential pressure as a result of channel narrowing can be calculated numerically with Eqs. (6.3)-(6.9). For this purpose, the membrane channel is divided into n steps of equal interval Δx and the time domain is discretized with

equal interval Δt. The capture coefficient, sectional foulant flux, and permeate velocity of any length segment j at the current time step i are determined with,

$$k_{i,j} = k_0 + \alpha\left(1 - \frac{h_{i,j}}{H}\right) \tag{6.10}$$

$$I_{i,j} = I_{i,j-1} - k_{i,j-1} I_{i,j-1} \Delta x \tag{6.11}$$

$$v_{i,j} = \frac{\Delta p_{i,j} - f_{os} c_{i,j}}{R_m} \tag{6.12}$$

Then salt concentration, channel height, crossflow velocity, and driving pressure for the next time step $i+1$ are given by,

$$c_{i+1,j} = \frac{c_{i+1,j-1} u_{i,j-1} h_{i,j-1} - (1-r) v_{i,j-1} c_{i+1,j-1} \Delta x}{u_{i,j} h_{i,j}} \tag{6.13}$$

$$h_{i+1,j} = h_{i,j} - \frac{k_{i,j} I_{i,j}}{\rho} \Delta t \tag{6.14}$$

$$u_{i+1,j} = \frac{u_{i,j-1} h_{i,j-1} - v_{i,j-1} \Delta x}{h_{i,j}} \tag{6.15}$$

$$\Delta p_{i+1,j} = \Delta p_{i+1,j-1} - \frac{\lambda \rho_w u_{i+1,j-1}^2 \Delta x}{4 h_{i+1,j-1}} \tag{6.16}$$

It should be mentioned that the values of all the parameters at the feed end of the channel (j=0) are known. With the numerical solutions, the differential pressure of the feed channel at any time can be easily determined with

$$\Delta p_{i,d} = \Delta p_{i,0} - \Delta p_{i,n} \tag{6.17}$$

6.2 Simulations and Discussions

In this section, differential pressures in a 6m RO channel are simulated and discussed under various operating conditions listed in Table 6.1.

Table 6.1. Operating parameters used in numerical simulations for channel blockage

Operating parameter	Value
Channel length (m)	6
Clean channel height (m)	$0.3\times10^{-3} - 0.7\times10^{-3}$
Membrane resistance (Pa·s/m)	1.0×10^{11}
Driving pressure (Pa)	6.21×10^{5}
Feed salt concentration (mg/L)	1000
Feed foulant concentration (mg/L)	5.0
Initial feed flow velocity (m/s)	0.1
Salt rejection	0.995
Osmotic coefficient (Pa·L/mg)	68.95
Friction coefficient	10
k_0 (m^{-1})	0.01 – 0.05
α (m^{-1})	1.0
Foulant layer density (kg/m^3)	1100
Simulation period (day)	60

The spatial step Δx = 0.02m (The feed channel was divided into 300 equal segments) and the time step Δt = 1day were used in all numerical simulations. The feed flow rate to the membrane channel was maintained constant during the operation. Unless otherwise specified, the operating parameters in Table 6.1 were used in all the simulations.

6.2.1 Effects of Clean Channel Capture Coefficient

The clean channel capture coefficient is an indicator of the fouling characteristics of the feed water and the structure of the feed channel. The increase in differential pressure across the feed channel was simulated for different clean channel capture coefficients and the results are shown in Fig. 6.3. Generally, the differential pressure increases faster for a larger clean channel capture coefficient, which indicates a greater fraction of foulants is captured by the spacers in the feed channel. The simulations demonstrated that substantial differential pressure could be caused by channel narrowing due to foulant capture. For example, at k_0=0.05 m^{-1}, the differential pressure after 60 days of operation increases from about 1.65×10^5 Pa to near 5.00×10^5 Pa. It can also be seen that the increase in differential pressure accelerates with operating time.

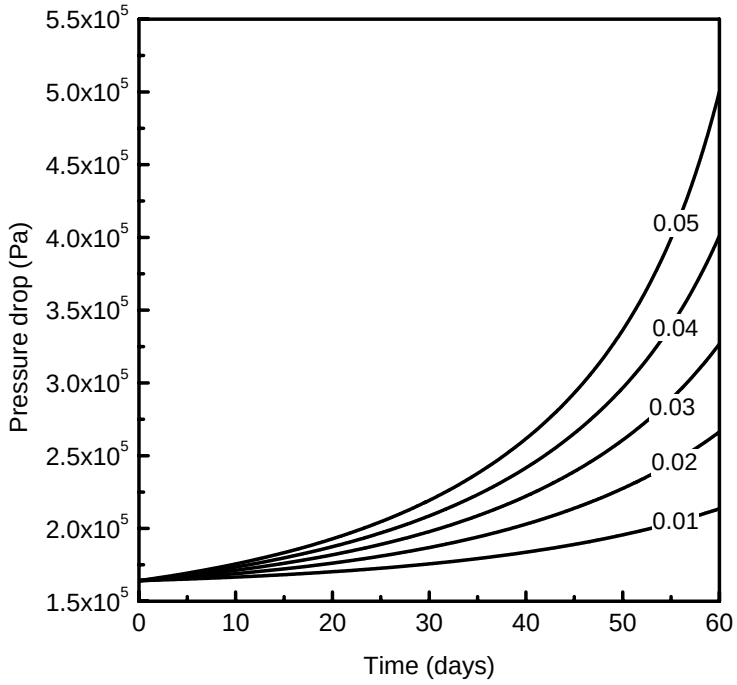

Figure 6.3. Differential pressures with time at different clean channel capture coefficients. Parameters used: H=0.5×10^{-3} m; α=1.0

Fig. 6.4 shows the channel height and crossflow velocity along the feed channel after 60 days of operation with different clean channel capture coefficients. At higher clean channel capture coefficient, more foulants accumulate within the feed channel, especially in the upstream region of the feed channel. As a result, the feed channel becomes narrower and crossflow velocity becomes higher in the feed channel. According to Eq. (6.3), the differential pressure across the feed channel is proportional to the square of crossflow velocity and inversely to channel height. Therefore, the pressure drop is expected to increase significantly with increasing clean channel capture coefficient.

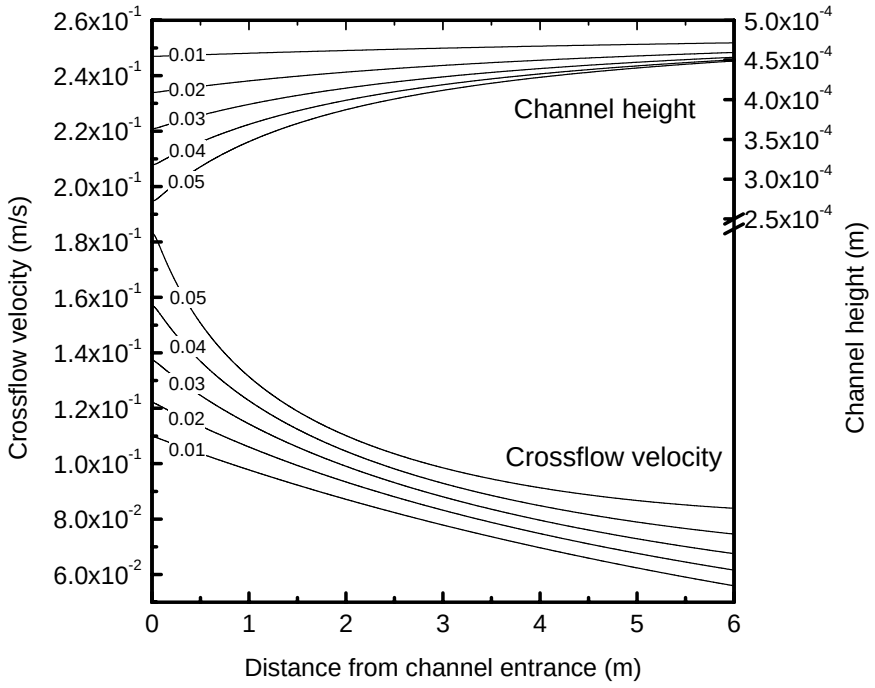

Figure 6.4. Variation of crossflow velocity and channel height along the feed channel for different clean channel capture coefficients at t=60 days. Parameters used: H=0.5×10^{-3} m; α=1.0

The effect of the clean channel capture coefficient on the foulant concentration in the concentrate stream was simulated with the model. Table 6.2 shows the simulated foulant concentrations in the concentrate stream of the membrane channel for different clean channel capture coefficients at different operating times. It can be seen that the foulant concentration in the concentrate stream is strongly affected by the value of the clean channel capture coefficient. The foulant concentration in the concentrate stream is higher for smaller clean channel capture coefficients as lesser amounts of foulants are captured in the feed channel. It is also observed that the foulant concentration in the concentrate stream decreases with time. This decrease was expected because the increased differential pressure reduced the driving pressure and the permeate flux in the downstream region of the channel, which meant more water was left in the concentrate stream.

Table 6.2. Foulant concentration in the concentrate for different clean channel capture coefficients at different days*

k_0 (m^{-1})	Foulant concentration (mg/L)		
	20 days	40 days	60 days
0.01	8.85	7.64	5.81
0.02	7.80	6.00	3.82
0.03	6.92	4.84	2.68
0.04	6.17	3.98	1.94
0.05	5.52	3.32	1.42

*Parameters used: H=0.5×10^{-3} m; Δp_0=6.21×10^5 Pa; c_{f0}=5 mg/L; α=1.0

It should be pointed that when a constant feed flow rate was assumed, the feed channel could not continue to narrow down. The feed channel height would inevitably reach

steady state at a certain value, in which the increased crossflow velocity (shear force) would make foulant deposition impossible. This mechanism was not incorporated into Eq. (6.5). With better knowledge of foulant capture dynamics in the channel, Eq. (6.5) could be modified or replaced by a more sophisticated expression for a better description of the foulant capture by the spacers.

6.2.2 Effects of Clean Channel Height

The development of differential pressure with time in the feed channel was simulated for different clean channel heights and the results are shown in Fig. 6.5. It is observed that differential pressure is strongly dependent on the channel height. It can also be seen that differential pressure becomes more sensitive to the change in channel height when the height is small.

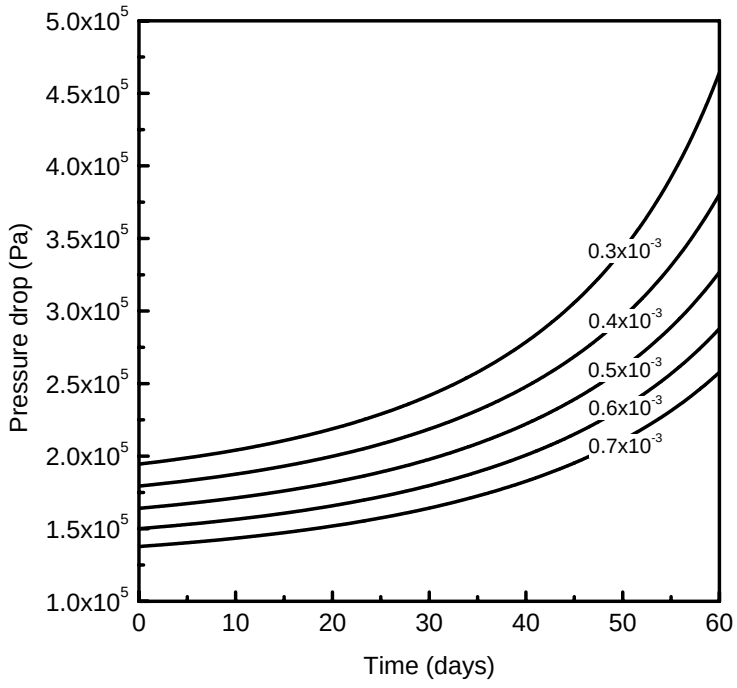

Figure 6.5. Differential pressures with time across the feed channel at different clean channel heights: Parameters used: k_0=0.03 m^{-1}; α=1.0

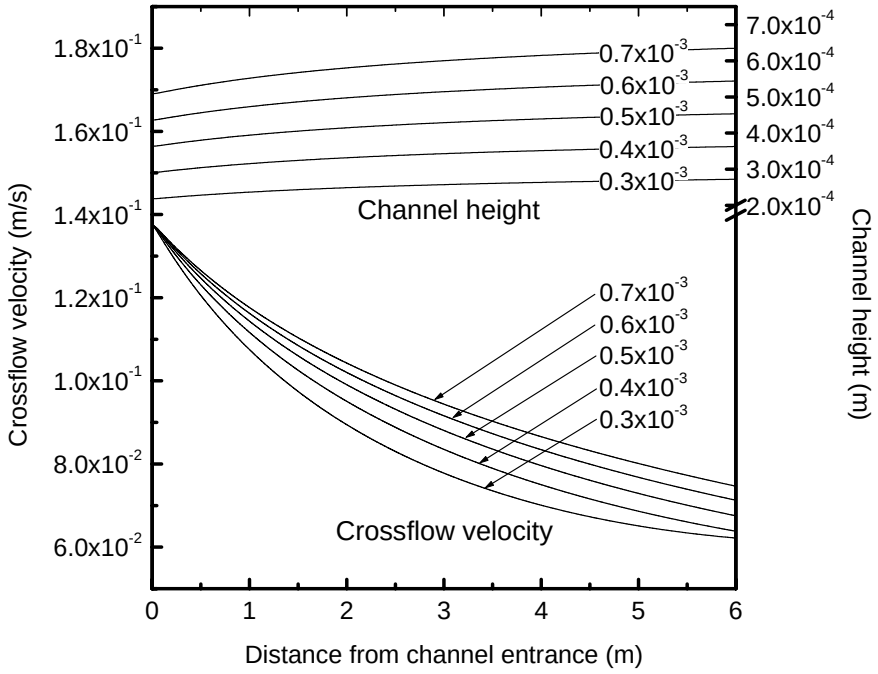

Figure 6.6. Variation of crossflow velocity and channel height along the feed channel for different clean channel heights at t=60 days. Parameters used: k_0=0.03 m^{-1}; α=1.0

The crossflow velocities and channel heights along the feed channel at t=60 days for different clean channel heights were simulated and are plotted in Fig. 6.6. Changes in channel height were apparently more substantial for greater clean channel height. This was attributed to larger amount of foulants (channel height-dependent only, since feed foulant concentration, feed crossflow velocity and clean channel capture coefficient were fixed for all clean channel heights) entering the feed channel that led to more foulant being accumulated in the feed channel. It is noted that the crossflow velocity for smaller clean channel height varies more significantly along the feed channel. The crossflow velocity decreased at a faster rate in the initial part of the channel for smaller clean channel height. This phenomenon was due to higher recovery experienced at

smaller clean channel heights. At higher recovery, more water was lost as permeate and crossflow velocity decreased more drastically along the feed channel.

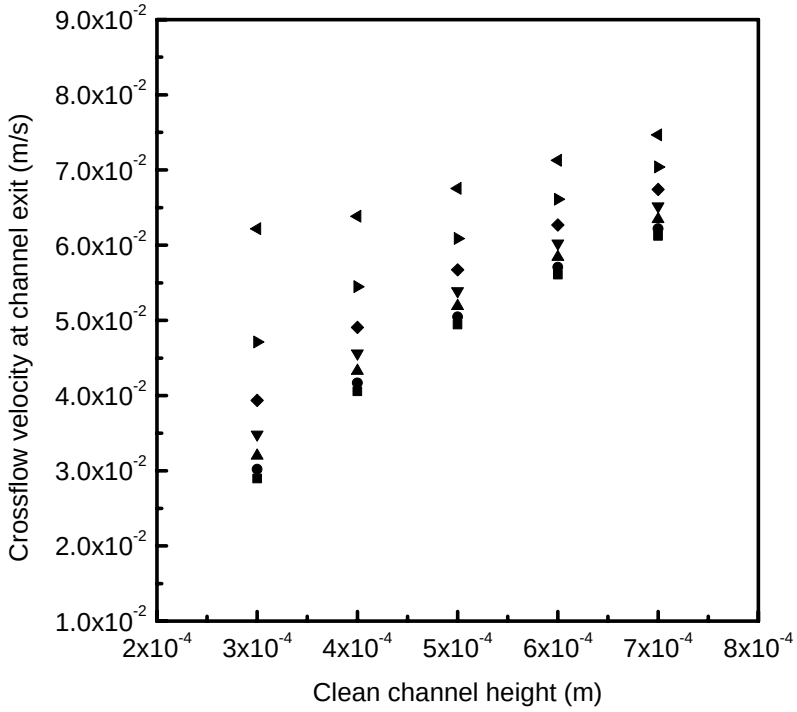

Figure 6.7. Variation of crossflow velocity at channel exit for different clean channel heights (m) at different times. Symbols used: ■ 0 days; ● 10 days; ▲ 20 days; ▼30 days; ♦ 40 days; ► 50 days; ◄ 60 days. Parameters used: k_0=0.03 m^{-1}; α=1.0

The effects of clean channel height on crossflow velocity at the channel exit for different operating times are shown in Fig. 6.7. As mentioned previously, the lower exit crossflow velocity at smaller clean channel height was attributed to higher recovery under similar operating conditions. However, the exit crossflow velocity at smaller channel height was observed to increase at a faster rate with operating time than at bigger clean channel height. As indicated earlier, differential pressure was more sensitive to the change in channel height with smaller channel height. Greater

differential pressure would develop in the narrower channel and driving pressure would become smaller downstream in the channel. Consequently more water would remain in the feed channel, leading to a larger increment in the concentrate flow velocity at the exit.

6.2.3 Variation of Driving Pressure Along Feed Channel

Driving pressure was simulated along the feed channel in the period of 60 days and the results are given in Fig. 6.8.

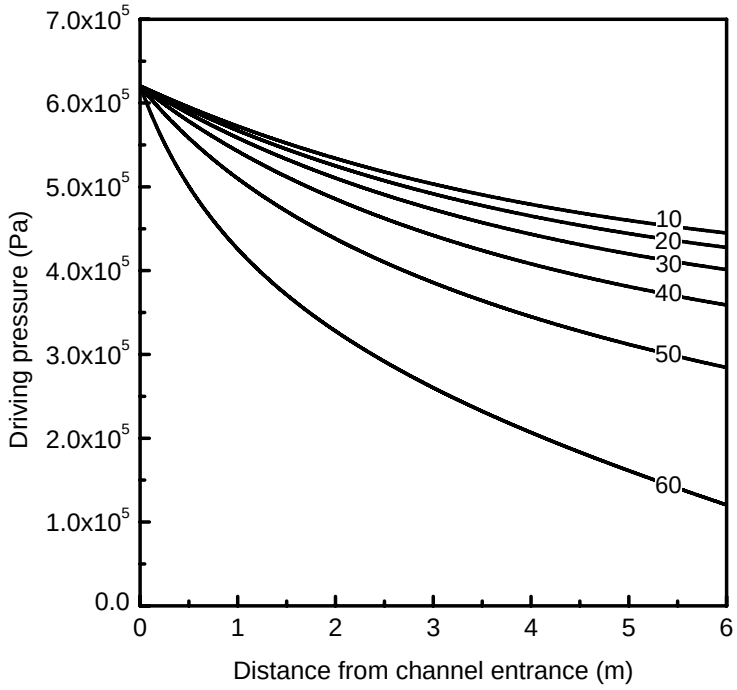

Figure 6.8. Decline of driving pressure along the feed channel at different operating times. Parameters used: H=0.5×10^{-3} m; k_0=0.05 m^{-1}; α=1.0

All driving pressure profiles showed a higher decline rate in the front region of the feed channel. The decline of driving pressure began to slow down as the feed water flowed through the channel. This phenomenon was attributed to the decrease in

crossflow velocity along the feed channel when water in the feed was lost as permeate. Variation of driving pressure along the feed channel became more significant for longer operating time. The driving pressure at the concentrate end of the feed channel was only about 20% of the driving pressure at the entrance after 60 days of operation. The simulations showed the significant impact of differential pressure on the driving pressure in the feed channel.

6.3 Simulations of Differential Pressures in a RO Water Reclamation Plant

Differential pressures of a two-stage RO water reclamation plant were monitored and compared with simulated values. The water reclamation plant, which produced potable water from effluent of a nearby wastewater treatment plant, operated in constant flux mode where the flow rate of product water was constantly maintained. In the observation period, the driving pressure and feed flow velocity were generally consistent with the initial values. However, substantial differential pressures were observed in both stages and the increase in the differential pressure accelerated with time. The membrane modules had to be frequently flushed to remove the captured foulants when the differential pressure exceeded the allowable limit. The differential pressure in Stage 2 was found to be more severe than Stage 1, probably due to the higher foulant concentration and greater capture coefficient.

Differential pressures in both stages (May 9-July 12 2004 for Stage 1 and June 8-24, 2004 for Stage 2) of the membrane process were separately simulated using the model developed in this study. The actual operating parameters and measured water quality parameters of the membrane process as given in Table 6.3 were used in the

simulations. The heights of the equivalent feed channel were determined to be about 0.67 mm 0.64 mm in Stage 1 and Stage 2 respectively. The difference in the heights of the equivalent channels in the two stages indicated different amounts of foulants remained in the channels after cleaning. Driving pressures and feed crossflow velocities in both stages were assumed constant in the simulations. Comparisons of actual and simulated differential pressures in both stages are shown in Fig. 6.9 and Fig. 6.10.

Table 6.3. Process parameters of the RO water reclamation plant

Process parameter	**Stage 1** (9/5/04–12/7/04)	**Stage 2** (8/6/04–24/6/04)
Channel length (m)	7.0	
Channel height (m)	0.67×10^{-3}	0.64×10^{-3}
Osmotic coefficient (Pa·L/mg)	68.95	
Membrane resistance (Pa·s/m)	6.1×10^{11}	6.0×10^{11}
Salt rejection	0.995	
Friction coefficient	10	
Foulant layer density (kg/m^3)	1100	
Foulant concentration (mg/L)	5.0	8.55
Feed salt concentration (mg/L)	700	1400
Feed flow rate per unit width (m^2/d)	6.3	6.8
Driving pressure (Pa)	7.57×10^5	6.53×10^5
Permeate pressure (Pa)	2.65×10^5	3.28×10^4
k_0 (m^{-1})	0.002	0.027
α	2.0	2.0

The observed and simulated differential pressures in the feed channel of Stage 1 are presented in Fig. 6.9. The simulated results were found to correlate well with the

observed differential pressures when k_0=0.002 m^{-1} and α=2.0 were used in the simulations. The simulations reproduce the behavior of the observed differential pressures, which increased moderately at the beginning before increasing rapidly with time. Similarly, the observed and simulated differential pressures in Stage 2 of the RO process are presented in Fig. 6.10. The feed foulant concentration (8.55 mg/L) for Stage 2 was determined from the concentrate flow out of Stage 1. The clean channel capture coefficient in Stage 2 to simulate the differential pressure was 0.027, which was much higher than that in Stage 1. One explanation for the much larger clean channel capture coefficient was the change in the feed water quality in these two stages. The elevated salt and foulant concentrations in Stage 2 appeared to enhance the capture of the foulants by the spacers.

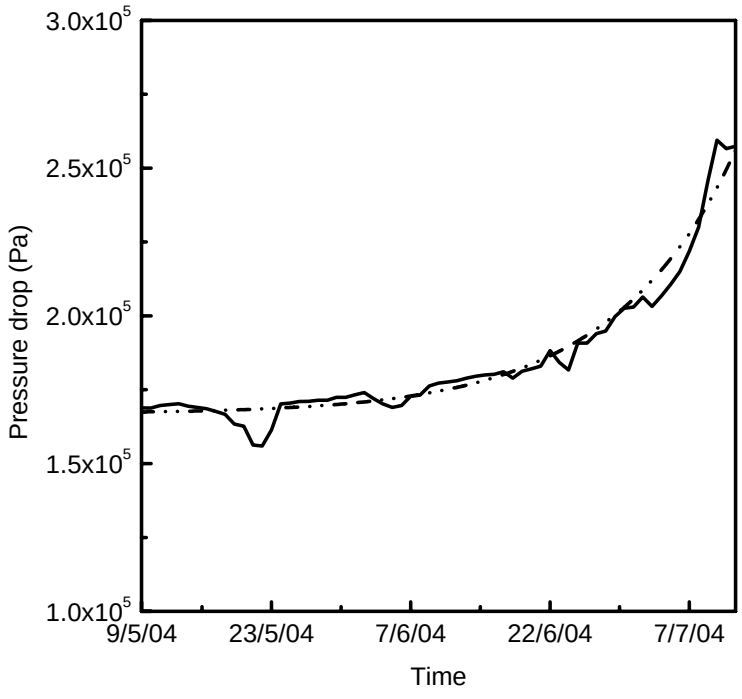

Figure 6.9. Actual (solid line) and simulated (dash line) differential pressures with time in Stage 1 of the full-scale RO water reclamation plant

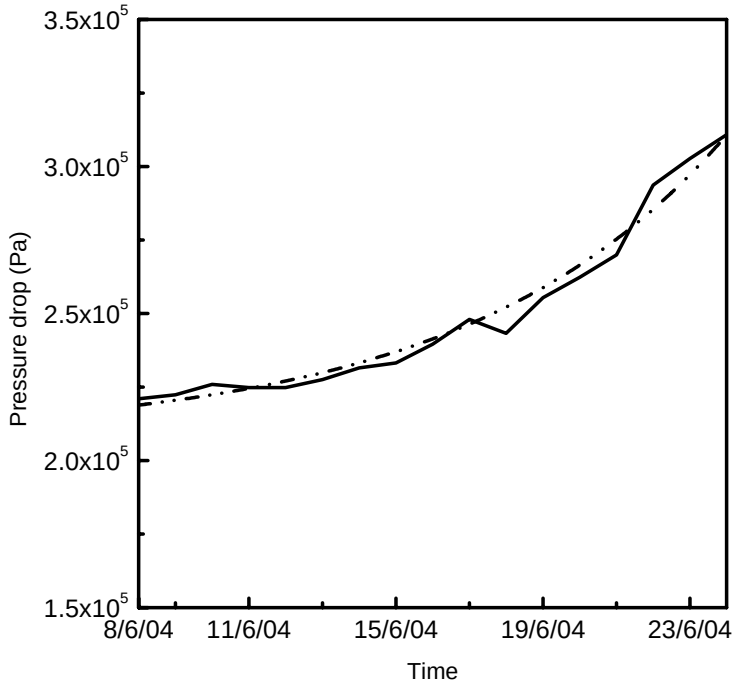

Figure 6.10 Actual (solid line) and simulated (dash line) differential pressures with time in Stage 2 of the full-scale RO water reclamation plant

6.4 Summary

Substantial differential pressure in the RO membrane feed channel can be caused by foulant capture onto spacers. A mathematical model was developed in this study to describe this rather important fouling process in the spiral-wound RO modules. The effects of capture coefficient and channel height on differential pressure development were investigated and discussed. Simulated results demonstrated that higher capture coefficient and smaller clean channel height could cause significant differential pressure through the feed channel with time. Differential pressures of the spiral-wound membrane modules in a two-stage full-scale RO water reclamation plant were simulated with the model. Results showed that the differential pressures in both stages of a RO water reclamation plant could be adequately described by the model.

Chapter 7

CONCLUSIONS AND RECOMMENDATIONS

The main focus of the work presented in this thesis is to study the dynamics of membrane fouling in a long RO membrane channel and propose a more effective fouling characterization method that can accurately quantify fouling in full-scale RO processes. This chapter summarizes the results of the research and recommends possible future work that can extend this research study.

7.1 Main Findings

1. A long channel with highly permeable RO membrane should be treated like a heterogeneous system because the key operating parameters, such as crossflow velocity, salt concentration, and permeate flux, vary substantially along the long membrane channel at common operating conditions. A high water permeation rate in the front region of the membrane channel can rapidly increase the salt concentration along the channel and the corresponding increase in osmotic pressure reduces the net driving pressure and consequently the permeate flux. Conventional membrane transfer theories, which are only valid with homogeneous system, cannot reasonably explain the permeate behavior in such a long membrane channel.

   A long RO membrane channel can be well characterized by a parameter termed the characteristic pressure. When the driving pressure is much lower than the characteristic pressure, the channel can be approached as a homogeneous system

and the average permeate flux is directly proportional to the net driving pressure (mass transfer restriction). At driving pressures sufficiently larger than the characteristic pressure, the increasing osmotic pressure at one point in the membrane channel can become equal to the driving pressure, resulting in a dead region of zero-flux from that point to the exit of the channel (thermodynamic equilibrium restriction). In this case, the performance of the long membrane channel is only dependent on thermodynamic parameters and the average permeate flux or recovery no longer increases linearly with the driving pressure. Furthermore, it can be shown theoretically and demonstrated experimentally that permeate flux or recovery is not sensitive to a change in membrane resistance when the membrane system is working under thermodynamic equilibrium.

2. Feed water fouling strength can be accurately measured with the newly proposed fouling potential. The major advantage of the fouling potential over existing fouling indices is that all possible foulants to the RO membranes are captured and accounted for in the measurement. The fouling potential can be easily determined with a small laboratory RO membrane device under conditions similar to the designed working conditions for any RO processes. The fouling potential was shown to be linearly related to the foulant concentration and independent of membrane resistance and driving pressure. The proposed fouling potential can be readily incorporated into a performance model of a long membrane channel to predict fouling development in the membrane channel.

3. In a long filtration channel of highly permeable RO membranes, although the distribution of the local permeate flux changes instantaneously with membrane

fouling, the average permeate flux or the overall recovery of the membrane channel may remain constant for a period of time after the start of filtration. The occurrence of constant average permeate flux is due to the existence of the "unused" membrane area in the channel, which provides additional or back-up membrane area to maintain the permeate flow rate when foulant deposition reduces the upstream permeate fluxes. The average permeate flux or recovery starts to decline when the "unused" membrane area in the channel becomes non-existent.

4. Membrane fouling in a long RO membrane channel can be more effectively measured with the proposed filtration coefficient and fouling index. These indicators are more relevant than the average permeate flux decline because they are intrinsically related to the membrane resistance. Even when the RO process is operating in thermodynamic equilibrium regime (no obvious average permeate flux decline is observed), the filtration coefficient remains an effective fouling indicator. The filtration coefficient in the thermodynamic equilibrium regime can be determined by temporarily reducing the driving pressure to the mass transfer regime. Both the filtration coefficient and the fouling index can also be used to assess the effectiveness of membrane cleaning.

5. The differential pressure in the RO membrane feed channel due to foulant capture by feed spacers can be simulated mathematically by treating foulant capture as a process of narrowing channel height and increasing crossflow velocity. It is also found that the differential pressure of a feed channel increases faster with higher capture coefficient and smaller clean channel height. The mathematical model is capable of simulating the differential pressures across the spiral-wound membrane

modules with time in each stage of a two-stage full-scale RO water reclamation plant.

7.2 Recommendations for Future Studies

There are several interesting directions that can be extended from the research study presented in this thesis. The following are the recommendations for future work.

1. Incorporate other fouling mechanisms into the mathematical model

   In this study, modeling of the performance of a long RO membrane channel was based on simple deposition of foulants on the membrane surface. However, membrane fouling in actual RO processes is a complex affair that usually involves more than a single fouling mechanism. In this study, "channel blockage" due to foulant capture by the feed spacers is discussed and an attempt is made to model such fouling mechanism based on simple concepts. Some other common fouling mechanisms include organic adsorption and biological growth. These fouling mechanisms are much more complicated than surface deposition, and hence require greater effort to understand and incorporate into the mathematical model. If the common fouling mechanisms can be adequately addressed in the mathematical model, the performance of a long RO membrane channel can be more accurately simulated. This will greatly reduce the time and costs required in running pilot tests.

2. Development of software for optimal design of full-scale RO processes

   It would be useful if knowledge on fouling characterization can be developed into a practical software application that allows plant designers and operators, or users

with basic knowledge of RO separation to design and predict the performance of full-scale RO processes based on several operating scenarios.

3. Implementation of pilot studies

   Much effort in this study is based on experimental testing, where experiments are conducted under controlled conditions in the laboratory. Pilot studies involving the use of actual feed water and operating conditions have to be implemented to determine the effectiveness of the proposed fouling characterization method.

7.3 Conclusion

This thesis has described the dynamics of membrane fouling in a long RO membrane channel and proposed an effective fouling characterization method that includes accurate quantification of feed water fouling strength and effective measurement of fouling in full-scale RO processes. The main contributions of the work are in the investigation of fouling characteristics in a long membrane channel and the development of a fouling characterization method that is effective under any operating conditions. The experimental results demonstrated the inadequacy of using average permeate flux to indicate fouling and the benefits of the proposed fouling characterization method.

REFERENCES

Almulla, A., M. Eid, P. Cote, and J. Coburn. Developments in high recovery brackish water desalination plants as part of the solution to water quantity problems, *Desalination*, 153, 237-243. 2002.

Alvarez, V., S. Alvarez, F.A. Riera, and R. Alvarez. Permeate flux prediction in apple juice concentration by reverse osmosis, *J. Membr. Sci.*, 127, 25-34. 1997.

Al-Wazzan, Y., M. Safar, S. Ebrahim, N. Burney, and A. Mesri. Desalting of subsurface water using spiral-wound reverse osmosis (RO) system: technical and economic assessment, *Desalination*, 143, 21-28. 2002.

American Water Works Association (AWWA) Manual. *Reverse osmosis and nanofiltration*. Colorado: AWWA. 1999.

AWWA membrane technology research committee. Committee report: Membrane processes, *J. AWWA*, 90(6), 91-105. 1998.

Aptel, P., and C.A. Buckley. Categories of Membrane Operations. In *Water Treatment Membrane Processes*, ed. by Mallevialle *et al*. New York: McGraw Hill. 1996.

Avlonitis, S.A., K. Kouroumbas, and N. Vlachakis. Energy consumption and membrane replacement cost for seawater RO desalination plants, *Desalination*, 157, 151-158. 2003.

Baker, R.C. *Membrane Technology and Applications*. 1st ed. New York: McGraw Hill, 2000.

Bates, W.T. Reducing the Fouling Rate of Surface and Waste Water RO Systems. In *International Water Conference*, October 1998, Pittsburgh, PA, USA.

Bergman, R.A., P.E. Bergman, H.W. Harlow, and P.E. Laverty. Resolution of RO flux decline problems at Eaglewood Florida, *Desalination*, 54, 55-74. 1985.

Boerlage, S.F.E., M. Kennedy, M.R. Dickson, D.E.Y. El-Hodali and J.C. Schippers. The modified fouling index using ultrafiltration membranes (MFI-UF): characterisation, filtration mechanisms and proposed reference membrane, *J. Membr. Sci.*, 197, 1-21. 2002.

Boerlage, S.F.E., M. Kennedy, M.P. Aniye and J.C. Schippers. Applications of the MFI-UF to measure and predict particulate fouling in RO systems, *J. Membr. Sci.*, 220, 97–116. 2003.

Brauns, E., E.V. Hoof, B. Molenberghs, C. Dotremont, W. Doyen and R. Leysen. A new method of measuring and presenting the membrane fouling potential, *Desalination*, 150, 31–43. 2002.

Bremere, I., M. Kennedy, A. Stikker and J. Schippers. How water scarcity will effect the growth in the desalination market in the coming 25 years, *Desalination*, 138, 7-15. 2001.

Brinck, J., S. Jönsson, B. Jönsson and J. Lindau. Influence of pH on the adsorptive fouling of ultrafiltration membranes by fatty acid, *J. Membr. Sci.*, 164, 187-194. 2000.

Bryne, W. *Reverse Osmosis – A Practical Guide For Industrial Users*. Littleton: Tall Oaks Publishing Inc. 1995.

Childress, A.E., and M. Elimelech. Effect of solution chemistry on the surface charge of polymeric reverse osmosis and nanofiltration membranes, *J. Membr. Sci.*, 119, 253-268. 1996.

Coker, S., and P. Sehn. Four years field experience with fouling resistant reverse osmosis membranes, *Desalination*, 132, 211-215. 2000.

Costa, A.R., and M.N. de Pinho. The role of membrane morphology on ultrafiltration for natural organic matter removal, *Desalination*, 145, 299-304. 2002.

Davey M., K. Landman, J. M. Perera, G. W. Stevens, N. D. Lawrence, M. Iyer. Measurement and prediction of the ultrafiltration of whey protein, *AIChE Journal*, 50, 7, 1431-1437. 2004.

Desai, A.M. Performance of Hydranautics reverse osmosis units at Yuma desalting test facility, *Desalination*, 23, 367-381. 1977.

Dudley, L., F. Vigo Pisano, and M. Fazel. Optimizing membrane performance — practical experiences. *Membr. Technol.*, 2000(121), 5–8. 2000.

Duranceau, S.J. Membrane replacement in desalting facilities, *Desalination*, 132, 243-248. 2000.

Durham, B., M.M. Bourbigot, and T. Pankratz. Membranes as pretreatment to desalination in wastewater reuse. *Membr. Technol.*, 2002(3), 8–12. 2002.

Ebrahim, S., and H. El-Dessouky. Evaluation of commercial cleaning agents for seawater reverse osmosis membranes. *Desalination*, 99, 169-188. 1994.

Elarde, J.R., and R.A. Bergman. The Cost of Membrane Filtration for Municipal Water Supplies. In *Membrane Practices for Water Treatment*, ed. by Duranceau. Denver, CO: American Water Works Association. 2001.

Element Specification Sheet. LFC1. California: Hydranautics. 2005.

Fane, A. G., C. J. D. Fell, and A. Suki. The effect of ph and ionic environment on the ultrafiltration of protein solutions with retentive membranes, *J. Membr. Sci.*, 16, 195-210. 1983.

Flemming, H.C., G. Schaule, T. Griebe, J. Schmitt, and A. Tamachkiarowa. Biofouling – the Achilles heel of membrane processes, *Desalination*, 113, 215-225. 1997.

Fried, E., and I.E. Idelchik. *Flow Resistance – A Design Guide for Engineers*. New York: Hemisphere Publishing Corporation. 1989.

Gabelich, C.J., T.I. Yun, B.M. Coffey, and I.H. Suffet. Pilot-scale testing of reverse osmosis using conventional treatment and microfiltration, *Desalination*, 154, 207-223. 2003.

Gare, S. RO systems: the importance of pre-treatment, *Filtration and Separation*, 39, 22-27. 2002.

Glater, J. The early history of reverse osmosis membrane development, *Desalination*, 117, 297-309. 1998.

Graham, S.I., R.I. Reitz, and C.E. Hickman, Improving reverse osmosis performance through periodic cleaning, *Desalination*, 74, 113-124. 1989.

Gwon, E., M. Yu, H. Oh, and Y. Ylee. Fouling characteristics of NF and RO operated for removal of dissolved matter from groundwater, *Water Res.*, 37, 2989-2997. 2003.

Hajeeh, M., and D. Chaudhuri. Reliability and availability assessment of reverse osmosis, *Desalination*, 130, 185-192. 2000.

Hong, S., and M. Elimelech. Chemical and physical aspects of natural organic matter (NOM) fouling of nanofiltration membranes, *J. Membr. Sci.*, 132, 159-181. 1997.

Hydranautics. Foulants and Cleaning Procedures for composite polyamide RO Membrane Elements (ESPA, ESNA, CPA, LFC, and SWC), *Hydranautics TSB*, 107.10, 1-14. 2003.

Industrial News. Tender awarded for Singapore's first desalination plant, *Filtr. Separat.*, 40(2), 8. 2003.

Kaakinen, J.W., and C.D. Moody. Characteristics of Reverse Osmosis Membrane Fouling at the Yuma Desalting Test Facility. In *Reverse Osmosis and Ultrafiltration*, ed. by S. Sourirajan and T. Matsuura. Washington D.C.: American Chemical Society. 1985.

Khedr, M.G. A Case Study of RO Plant Failure Due to Membrane Fouling, Analysis and Diagnosis, *Desalination*, 120, 107-113. 1998.

Khirani, S., Roger Ben Aim, and M.H. Manero. Improving the measurement of the Modified Fouling Index using nanofiltration membranes (NF-MFI), *Desalination*, 191, 1-7. 2006.

Koyuncu, I., M. Yazgan, D. Topacik, and H.Z. Sarikaya. Evaluation of the low pressure RO and NF membranes for an alternative treatment of Buyukcekmece Lake. *Water Sci. Technol.*: *Water Supply*, 1(1), 107–115. 2001.

Kurihara, M., H. Yamamura, T. Nakanishi, and S. Jinno. Operation and reliability of very high-recovery seawater desalination technologies by brine conversion two-stage RO desalination system. *Desalination*, 138, 191-199. 2001.

Larson, R.E., R.J. Petersen, and P.K. Eriksson. Test results on FT-30 eight-inch-diameter seawater and brackish water reverse osmosis elements, *Desalination*, 46, 81-90. 1983.

Lonsdale, H. K., U. Merten, and R. L. Riley. Transport Properties of Cellulose Acetate Osmotic Membranes, *J. Appl. Polym. Sci.*, 9, 1341-1362. 1965.

Lopez-Ramirez, J.A., D.S. Marquez, and J.M.Q. Alonso. Comparison studies of feedwater pre-treatment in a reverse osmosis pilot-plant, *Desalination*, 144, 347-352. 2002.

Madaeni, S.S., T. Mohamamdi, M.K. Moghadam. Chemical Cleaning of Reverse Osmosis Membranes, *Desalination*, 134, 77-82. 2001.

Mallevialle, J., P.E. Odendaal, and M.R. Wiesner. The Emergence of Membranes in Water and Wastewater Treatment. In *Water Treatment Membrane Processes*, ed. by Mallevialle *et al*. New York: McGraw Hill. 1996.

Manttari, M., J. Nuortila-Jokinen, and M. Nystrom, Influence of filtration conditions on the performance of NF membranes in the filtration of paper mill total effluent, *J. Membr. Sci.*, 137, 187-199. 1997.

Marinas, B.J., and R.E. Selleck. Reverse osmosis treatment of multicomponent electrolyte solutions, *J. Membrane Sci.*, 72**,** 211-229. 1992.

Martin-Lagardette, J.L. Competing Seawater Desalination Technologies Help to Meet Demand for Fresh water, *Membr. Technol.*, 124, 11-12. 2000.

Maskan, S.F., D.E. Wiley, L.P.M. Johnston, and D.J. Clements. Optimal design of reverse osmosis module networks, *AIChE Journal,* 46, 946-954. 2000.

Mason, E.A. and H.K. Lonsdale. Statistical-Mechanical theory of membrane transport, *J. Membr. Sci.*, 51, 1-81. 1990.

Matsuura, T. Progress in membrane science and technology for seawater desalination – a review, *Desalination*, 134, 47-54. 2001.

Mulder, M. *Basic Principles of Membrane Technology*. 2rd ed. London: Kluwer Academic Publishers. 1996.

Mulhern, N. Death, Taxes….and RO Membrane Fouling, *Water Technol.*, 11, 66-99. 1995.

Nemeth, J.E. Innovative system designs to optimize performance of ultra-low pressure reverse osmosis membranes. *Desalination*, 118, 63−71. 1998.

News. Singapore builds sea-water purifying plant, *Membr. Technol.*, 2004(3), 2. 2004.

Nicolaisen, B. Developments in membrane technology for water treatment, *Desalination*, 153, 355-360. 2002.

Pantell, S.E. *Seawater Desalination in California*. California Coastal Commission, California. 1993.

Partanen J. I., and P. O. Minkkinen, Activity and osmotic coefficients of dilute sodium chloride solutions at 273 K, *J. Chem. Eng. Data*, 36, 432-435. 1991.

Pietsch, A., W. Hilgendorff, O. Thom, and R. Eggers, Basic investigation of integrating a membrane unit into high-pressure decaffeination processing, *Sep. Sci Technol.*, 14, 107-115, 1998.

Potts, D. E., R. C. Ahlert, and S. S. Wang. A critical review of fouling of reverse osmosis, *Desalination*, 36, 235-264. 1981.

Qin, J.J., M.H. Oo, M.N. Wai, H. Lee, S.P. Hong, J.E. Kim, Y. Xing, and M. Zhang. Pilot study for reclamation of secondary treated sewage effluent, *Desalination*, 171, 299-305. 2004.

Rabie, H.R., P. Cote, and Adams N. A method for assessing membrane fouling in pilot- and full-scale systems, *Desalination*, 141, 237-243. 2001.

Rautenbach, R., T. Linn, and L. Eilers. Treatment of severely contaminated waste water by a combination of RO, high-pressure RO and NF — potential and limits of the process, *J. Membr. Sci*., 174, 231-241. 2000.

Redondo, J.A., and A. Casanas. Designing seawater RO for clean and fouling RO feed. Desalination experiences with the FilmTec SW30HR-380 and SW30HR-320 elements – Technical – economic review, *Desalination*, 134, 83-92. 2001.

Rico, D. P., and M.F.C Arias. A Reverse Osmosis Potable Water Plant at Alicante University: First Year of Operation, *Desalination*, 137**,** 91-102. 2001.

Ridgway, H.F., and H.C. Flemming. Membrane Biofouling. In *Water Treatment Membrane Processes*, ed. by Mallevialle *et al*. New York: McGraw Hill. 1996.

Riley, R.L. Reverse Osmosis. In *Membrane Separation Systems – Recent Developments and Future Directions*, ed. by R. W. Baker *et al.* New Jersey: Noyes Data Corporation. 1991.

Saad, M.A. *Optimize Water Cost by Early Prediction of Membrane System Fouling Trends*. In IDA World Congress on Desalination and Water Reuse, August 1999, San Diego, CA, USA.

Sablanl, S.S., M.F.A. Goosen, R. Al-Belushi, and M. Wilf. Concentration polarization in ultrafiltration and reverse osmosis: a critical review, *Desalination*, 141, 269-289. 2001.

Sablanl, S.S., M.F.A. Goosen, R. Al-Belushi, and V. Gerardosb. Influence of spacer thickness on permeate flux in spiral-wound seawater reverse osmosis systems, *Desalination*, 146, 225-230. 2002.

Sadhwani, J.J, and J.M. Veza. Cleaning tests for seawater reverse osmosis membranes, *Desalination*, 139, 177-182. 2001.

Samson, P., and B. Charrier. International Freshwater Conflict: Issues and Prevention Strategies, Green Cross International. 1997.

Schippers, J.C., and J. Verdouw. The modified fouling index, a method of determining the fouling characteristics of water, *Desalination*, 32, 137-148. 1980.

Schippers, J.C., J.H. Hanemaayer, C.A. Smolders, and A. Kostense. Predicting flux decline of reverse osmosis membranes, *Desalination*, 38, 339-348. 1981.

Schwinge, J., P.R. Neal, D.E. Wiley, D.F. Fletcher, and A.G. Fane. Spiral wound modules and spacers - Review and analysis, *J. Membr. Sci*, 242, 129-153. 2004.

Shahalam, A.M., A. Al-Harthy, and A. Al-Zawhry. Feed water pretreatment in RO systems: unit processes in the Middle East, Desalination, 150, 235-245. 2002.

Sheikholeslami, R. Assessment of the scaling potential for sparingly soluble salts in RO and NF units, *Desalination*, 167, 247-256. 2004.

Slater C. S., and C.A. Brooks. Development of a simulation model predicting performance of reverse osmosis batch systems. *Sep. Sci Technol.*, 27, 1361-1388. 1992.

Soltanieh, M., and W. N. Gill, Review of Reverse Osmosis Membranes and Transport Models, *Chem. Eng. Commun*., 12, 279-363. 1981.

Song, L.F., and M. Elimelech. Theory of concentration polarization in cross-flow filtration, *J. Chem. Soc. Faraday Trans.*, 91(19), 3389-3398. 1995.

Song, L., S. Hong, J.Y. Hu, S.L. Ong, and W.J. Ng, Simulations of full-scale reverse osmosis membrane process, *J. Environ. Eng.*, 128, 960-966. 2002.

Song, L., J.Y. Hu, S.L. Ong, W.J. Ng, M. Elimelech, and M. Wilf, Performance limitation of the full-scale reverse osmosis process, *J. Membr. Sci.*, 214, 239-244. 2003.

Sourirajan, S., Lectures on Membrane Separations, Indian Membrane Society, Baroda. 1991.

Strathmann, H. Membrane separation processes, *J. Membr. Sci.*, 9, 121-189. 1981.

Suratt, W.B., D.R. Andrews, V.J. Pujals, and S.A. Richards. Design considerations for major membrane treatment facility for groundwater, *Desalination*, 131, 37-46. 2000.

Taniguchi, M., and S. Kimura, Estimation of transport parameters of RO membranes for seawater desalination, *AIChE Journal*, 46, 1967-1973. 2000.

Taylor, J.S., and E.P. Jacobs. Reverse osmosis and Nanofiltration. In *Water Treatment Membrane Processes*, ed. by Mallevialle *et al*. New York: McGraw Hill. 1996.

Technical Applications Bulletin – TAB108. LFC – Low fouling composite membrane technology. California: Hydranautics. 2005.

Todtheide, V., G. Laufenberg, and B. Kunz, Waste water treatment using revere osmosis: real osmotic pressure and chemical functionality as influencing parameters

on the retention of carboxylic acids in multi-component system, *Desalination*, 110, 213-222. 1997.

Tuwiner, S.B. *Diffusion and Membrane Technology*. 1st ed. New York: Reinhold Publishing Corporation. 1962.

Turan, M., Influence of filtration conditions on the performance of nanofiltration and reverse osmosis membranes in dairy wastewater treatment, Desalination, 170, 83-90. 2004.

Van der Bruggen, B., and C. Vandecasteele. Distillation vs. membrane filtration: overview of process evolutions in seawater desalination. *Desalination*, 143, 207-218. 2002.

Van Der Meer, W.G.J., M. Riemersma, and J.C. Van Dijk. Theoretical optimization of spiral-wound and capillary nanofiltration modules, *Desalination*, 113**,** 129-146. 1997.

Van Gauwbergen, D., and J. Baeyens. Assessment of the design parameters for wastewater treatment by reverse osmosis. *Water Sci. Technol.*, 40(4–5), 269-276. 1999.

Van Gauwbergen, D., and J. Baeyens. Modelling reverse osmosis by irreversible thermodynamics. *Sep. Puri. Technol*., 13, 117-128. 1998.

Vedavyasan, C.V. Combating water shortages with innovative uses of membranes, *Desalination*, 132, 345-347. 2000.

Vial, D., and G. Doussau. The use of microfiltration membranes for seawater pre-treatment prior to reverse osmosis membranes, *Desalination*, 153, 141-147. 2002.

Vrouwenvelder, J.S., and D. van der Kooij. Diagnosis, prediction and prevention of biofouling of NF and RO membranes, *Desalination*, 139, 65-71. 2001.

Wiesner, M.R. and S. Chellam. The Promise of Membrane Technology, *Environ. Sci. Tech.*, 33, 360-366. 1999.

Wijmans, J.G., S. Nakao, J.W.A. Van Den Berg, F.R. Troelstra, and C.A. Smolders. Hydrodynamic resistance of concentration polarization boundary layers in ultrafiltration, *J. Membr. Sci.*, 22, 117-135. 1985.

Wilf, M. Design consequences of recent improvements in membrane performance. *Desalination*, 113, 157-163. 1997.

Wilf, M., and K. Klinko. Optimization of seawater RO systems designs, *Desalination*, 138, 299-306. 2001.

Wilf, M., and K. Klinko. Effective new pretreatment for seawater reverse osmosis systems, *Desalination*, 117, 323-331. 1998.

Winfield, B.A. A study of the factors affecting the rate of fouling of reverse osmosis membranes treating secondary sewage effluents, *Water Research*, 13(7), 565-569. 1979.

Winters, H. Control of organic fouling at two seawater reverse osmosis plants, *Desalination*, 66, 319-325. 1987.

Yiantsios, S.G. and A.J. Karabelas. The effect of colloid stability on membrane fouling, *Desalination*, 118, 143-152. 1998.

Zhou, W., L. Song, and K.G. Tay. A numerical study on concentration polarization and system performance of spiral wound RO membrane modules, *J. Membr. Sci.*, 271, 38-46. 2006.

Zhu, X., and M. Elimelech. Colloidal fouling of reverse osmosis membranes: measurements and fouling mechanisms, *Environ. Sci. Tech.*, 31, 3654-3662. 1997.

Zhu, X., and M. Elimelech. Fouling of Reverse Osmosis Membranes by Aluminum Oxide Colloids, *J. Environ. Eng.*, 121, 884-892. 1995.

APPENDIX

Publications from This Research Work

A.1 Published Journal Paper

1. Kwee Guan Tay and Lianfa Song. Differential Pressure in Membrane Channel Caused by Foulant Capture onto Spacers, *Water Environ. Res.*, Accepted for publication. 2006.
2. Tay, K.G., and L. Song. Performance prediction of a long crossflow reverse osmosis membrane channel, *J. Membr. Sci.*, 281, 163–169. 2006.
3. Zhou, W., L. Song, and K.G. Tay. A numerical study on concentration polarization and system performance of spiral wound RO membrane modules, *J. Membr. Sci.*, 271, 38-46. 2006.
4. Tay, K.G., and L. Song. A more effective method for fouling characterization in a full-scale reverse osmosis process, *Desalination*, 177, 95-107. 2005.
5. Tay, K.G., L. Song, S.L. Ong, and W.J. Ng. Nonlinear behavior of permeate flux in full-scale reverse osmosis processes, *J. Environ. Eng.–ASCE*, 131, 1481-1487. 2005.
6. Tay, K.G., L. Song, S.L. Ong, and W.J. Ng. A New Fouling Characterization Method For Effective Detection Of Membrane Fouling In Full-Scale Reverse Osmosis Membrane Processes, *Advances in Asian Environ. Eng.*, 3, 29-36. 2003.

A.2 Overseas Conferences

1. Song, L., K.G Tay, G. Singh. Performance Modeling of Full-scale Desalination Processes with Highly Permeable RO Membranes, International Conference on

Decentralized Water and Wastewater Systems, Fremantle, Western Australia, 9-12 July 2006.

2. Tay, K.G., and L. Song. Quantifying colloidal fouling potential in reverse osmosis processes, 14th KKNN Symposium on Environmental Engineering, Jeju, South Korea. 15–17 June 2005.

3. Tay, K.G., L. Song, S.L. Ong, and W.J. Ng. A Simulation Study of Cleaning Efficiency in Full-Scale RO Processes, Water Environment-Membrane Technology 2004, Seoul, South Korea. 7–10 June 2004.

4. Tay, K.G., L. Song, S.L. Ong, and W.J. Ng. A New Fouling Characterization Method For Effective Detection Of Membrane Fouling In Full-Scale Reverse Osmosis Membrane Processes, 12th KKNN Symposium on Environmental Engineering, Taipei, Taiwan. 26–29 June 2002.

5. Tay, K.G., L. Song, S. L. Ong, W. J. Ng, and J.Y. Hu. Fouling characterization in full-scale reverse osmosis processes, 13th North American Membrane Society Annual Meeting, Long Beach, California, USA. 11–15 May 2002.